1273 J. MYER

DTNSRDC-85/042

RESULTS OF DEBRIS AVOIDANCE MANEUVERS AND FORWARD FOIL BROACHES IN CALM WATER PERFORMED BY THE HYDROFOIL SHIP PCH 1

DAVID W. TAYLOR NAVAL SHIP RESEARCH AND DEVELOPMENT CENTER

Bethesda, Maryland 20084-5000

RESULTS OF DEBRIS AVOIDANCE MANEUVERS AND FORWARD FOIL BROACHES IN CALM WATER PERFORMED BY THE HYDROFOIL SHIP PCH 1

by

William H. Buckley

APPROVED FOR PUBLIC RELEASE; DISTRIBUTION IS UNLIMITED

STRUCTURES DEPARTMENT
RESEARCH AND DEVELOPMENT REPORT

June 1985

DTNSRDC-85/042

MAJOR DTNSRDC ORGANIZATIONAL COMPONENTS

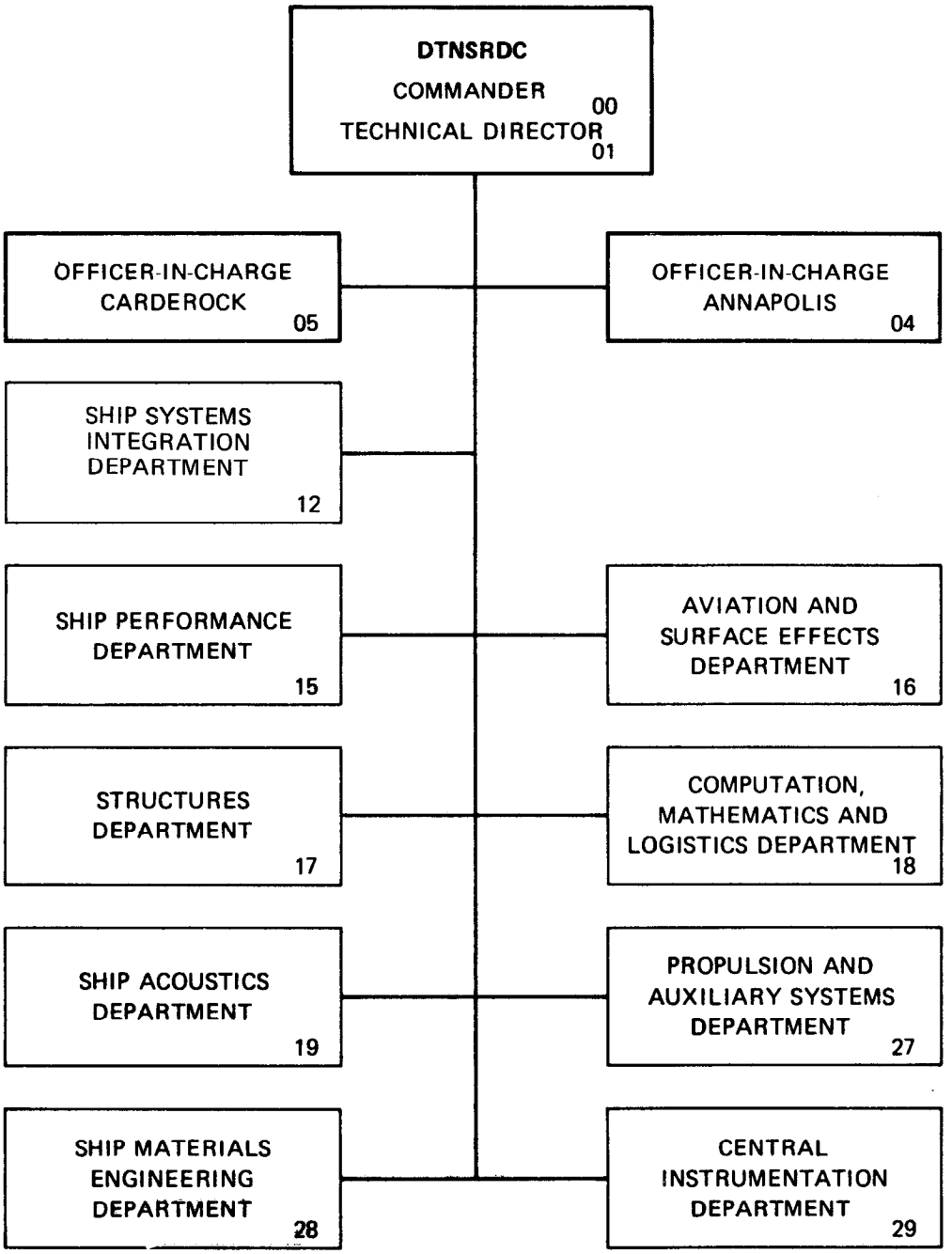

UNCLASSIFIED

SECURITY CLASSIFICATION OF THIS PAGE

REPORT DOCUMENTATION PAGE

1a REPORT SECURITY CLASSIFICATION UNCLASSIFIED	1b RESTRICTIVE MARKINGS
2a SECURITY CLASSIFICATION AUTHORITY	3 DISTRIBUTION / AVAILABILITY OF REPORT APPROVED FOR PUBLIC RELEASE; DISTRIBUTION IS UNLIMITED
2b DECLASSIFICATION / DOWNGRADING SCHEDULE	
4 PERFORMING ORGANIZATION REPORT NUMBER(S) DTNSRDC-85/042	5 MONITORING ORGANIZATION REPORT NUMBER(S)
6a NAME OF PERFORMING ORGANIZATION David W. Taylor Naval Ship R&D Center 6b OFFICE SYMBOL (*If applicable*) Code 1730	7a NAME OF MONITORING ORGANIZATION
6c ADDRESS (*City, State, and ZIP Code*) Bethesda, Maryland 20084-5000	7b ADDRESS (*City, State, and ZIP Code*)
8a NAME OF FUNDING / SPONSORING ORGANIZATION 8b OFFICE SYMBOL (*If applicable*)	9 PROCUREMENT INSTRUMENT IDENTIFICATION NUMBER
8c ADDRESS (*City, State, and ZIP Code*)	10 SOURCE OF FUNDING NUMBERS PROGRAM ELEMENT NO: PROJECT NO: S46-04 TASK NO: S 0354001 WORK UNIT ACCESSION NO:

11 TITLE (*Include Security Classification*)
RESULTS OF DEBRIS AVOIDANCE MANEUVERS AND FORWARD FOIL BROACHES IN CALM WATER PERFORMED BY THE HYDROFOIL SHIP PCH 1

12 PERSONAL AUTHOR(S)
Buckley, William H.

13a TYPE OF REPORT	13b TIME COVERED	14 DATE OF REPORT (*Year, Month, Day*)	15 PAGE COUNT
Final	FROM _____ TO _____	1985 June	113

16 SUPPLEMENTARY NOTATION

17 COSATI CODES		
FIELD	GROUP	SUB-GROUP

18 SUBJECT TERMS (*Continue on reverse if necessary and identify by block number*)
Strut/Foil System Hydrodynamics
Hydrofoil Broaching
Hydrofoil Maneuvers
(Continued on reverse side)

19 ABSTRACT (*Continue on reverse if necessary and identify by block number*)

Calm water trials were conducted using the hydrofoil ship USS HIGH POINT (PCH 1) to determine the effect on foil system loads of both debris avoidance maneuvers and forward foil broaches with symmetric and asymmetric water reentry. Continuous video recordings were made of the hydrodynamic flow over the lower forward strut and foil while local strains were measured in various foil system components.

Debris avoidance maneuvers resulted in forward strut hydrodynamic loadings that approached the maximum attainable steady state loadings determined from model tests of struts having similar airfoil sections. Forward foil broaches-in-turns resulted in asymmetric lift on the forward foil due to the momentary loss of lift on the emergent foil semispan and the subsequent ventilated flow during reentry. A 90° helm broach-in-turn resulted in a persistent asymmetric lift with ventilated flow on one semispan and

(Continued on reverse side)

20 DISTRIBUTION / AVAILABILITY OF ABSTRACT	21 ABSTRACT SECURITY CLASSIFICATION
☒ UNCLASSIFIED/UNLIMITED ☐ SAME AS RPT ☐ DTIC USERS	UNCLASSIFIED
22a NAME OF RESPONSIBLE INDIVIDUAL William H. Buckley	22b TELEPHONE (*Include Area Code*) (202) 227-1719 22c OFFICE SYMBOL Code 1730.6

DD FORM 1473, 84 MAR 83 APR edition may be used until exhausted
All other editions are obsolete

SECURITY CLASSIFICATION OF THIS PAGE
UNCLASSIFIED

(Block 18 continued)

Hydrodynamic Loads
Strut/Foil/Flap Buffet Loads
Transient Cavitation
Transient Ventilation

(Block 19 continued)

fully wetted flow on the other. The bending strain at the lower end of the forward strut reached 85% of the largest value measured during broaches in rough seas. Video camera recordings of hydrodynamic flow over the forward foil revealed a variety of conditions including fully and partially ventilated flow, steady and unsteady cavitated flow, and combinations of these. Transient foil system loadings resulted from cavity shedding on the forward strut and forward foil trailing edge flap. Transient loads also acted on the aft foil following the development of ventilated flow on the forward foil.

TABLE OF CONTENTS

LIST OF FIGURES

LIST OF TABLES

NOTATION AND ABBREVIATIONS

ACS	Automatic Control System
Cy	Side force coefficient
DTNSRDC	David W. Taylor Naval Ship Research and Development Center
EM	Electromagnetic
HYSTU	Hydrofoil Special Trials Unit
V	Velocity
β	Side slip angle
ρ	Density of water
$1/2\ \rho V^2$	Dynamic pressure

ABSTRACT

Calm water trials were conducted using the hydrofoil ship USS HIGH POINT (PCH 1) to determine the effect on foil system loads of both debris avoidance maneuvers and forward foil broaches with symmetric and asymmetric water reentry. Continuous video recordings were made of the hydrodynamic flow over the lower forward strut and foil while local strains were measured in various foil system components.

Debris avoidance maneuvers resulted in forward strut hydrodynamic loadings that approached the maximum attainable steady state loadings determined from model tests of struts having similar foil sections. Forward foil broaches in turns resulted in asymmetric lift on the forward foil due to the momentary loss of lift on the emergent foil semispan and the subsequent ventilated flow during reentry. A 90° helm broach-in-turn resulted in a persistent asymmetric lift with ventilated flow on one semispan and fully wetted flow on the other. The bending strain at the lower end of the forward strut reached 85% of the largest value measured during broaches in rough seas. Video camera recordings of hydrodynamic flow over the forward foil revealed a variety of conditions including fully and partially ventilated flow, steady and unsteady cavitated flow, and combinations of these. Transient foil system loadings resulted from cavity shedding on the forward strut and forward foil trailing edge flap. Transient loads also acted on the aft foil following the development of ventilated flow on the forward foil.

ADMINISTRATIVE INFORMATION

The work described herein was performed by the Ship Structures Division of the David W. Taylor Naval Ship Research and Development Center (DTNSRDC), Code 173 of the Structures Department. This project was initiated under the sponsorship of the Naval Sea Systems Command, Code 0322, with funding provided under Project S46-04. It was completed under the sponsorship of the Naval Sea Systems Command with funding provided under Task Area S 0354001. Technical direction was provided by John R. Meyer, DTNSRDC Code 1233, and overall management by James Schuler, NAVSEA 05R12.

INTRODUCTION

The hydrofoil ship HIGH POINT (PCH 1) entered service in 1963 and has been employed intermittently in structural loads research since 1966. In its original configuration (MOD 0), it was used to obtain data on foil system loads in rough water. Based upon these data, it was apparent that the foil system load criteria originally employed in design adequately defined design load magnitudes in most cases, although these criteria were not well related to the operating conditions that

produced the loads. The original criteria for forward strut lateral bending loads, however, could be exceeded during recovery from a forward foil broach - that is, recovery from a momentary loss of foil lift caused when the foil emerged from the water. In addition, helmsman-induced loads had not been investigated to determine if extreme directional maneuvers could produce high loads on the foil system.

As a result of these considerations, a program of calm and rough water loads research was initiated when the MOD 1 version of HIGH POINT was put into service in 1973. This report summarizes results of the calm water trials program in which foil system loads were measured during rapid helm displacements and during artificially induced broaches in turns. The broaches-in-turns were intended to determine, through concurrent foil load measurements and hydrodynamic flow observations, whether asymmetric forward foil lift loads occurring during rough water broaches could be caused by ventilated flow acting on only one semispan of the foil during the recovery phase of a broach. Such a finding would account in part for the large lateral bending moments measured on MOD 0 at the lower end of the forward strut during rough water broach recoveries.

Service experience with more recent hydrofoil ship designs has shown that foil system service loads can result in significant fatigue and flaw growth problems. As a result, it also became an objective of the trials to identify the origin and magnitude of unsteady loads observed during periods of locally ventilated or cavitated flow. Such loads could then be considered in establishment of fatigue load spectra for new foil systems.

DESCRIPTION OF USS HIGH POINT (PCH 1, MOD 1)

HIGH POINT (Figure 1) is a canard configuration hydrofoil ship of approximately 122 long tons displacement. The foil system of MOD 1 is a fully submerged type of relatively modern design. Propulsion is furnished by two 3100-hp Bristol Proteus gas turbines, each driving two tandem mounted propellers installed in nacelles below the aft strut-to-foil intersection.

Foilborne stabilization is accomplished by the automatic control system (ACS) described and shown schematically in Appendix A. Flap-type control surfaces on the forward and aft foils stabilize the ship in pitch and heave while the aft surfaces also stabilize it in roll. Heading is controlled by differential driving of the aft flaps with helm commands so as to produce a proportional roll angle. Roll angle and yaw rate sensors then control the displacement of the all-moveable forward strut so as to produce a coordinated turn. To stabilize height, the ACS compares the

filtered output of the bow-mounted height sensors with the preselected setting of the height command control lever to maintain the average foil system depth at the desired value.

LOAD SENSING AND RELATED INSTRUMENTATION

HIGH POINT's structural load instrumentation consists primarily of strain gages installed on various elements of the foil system* as shown schematically in Figure 2. Most of the foil strain gages were installed internally in the foils and at the upper end of the forward strut when HIGH POINT was changed from the original MOD 0 to the present MOD 1 configuration. Generally, these strain gages, which sense shear and bending moment, were calibrated by application of point loads at two chordwise and two or more spanwise locations. From the resulting data, load calibration equations were developed by methods similar to those used in Appendix B. Except for the forward strut gages, a relatively high percentage of the internal gages failed before the calm water trials began. As a result, either the original calibration equations could no longer be used or, in the forward foil port semispan, no strain measurements were available at all.

Before the calm water trials, a number of new external strain gages were added to HIGH POINT to provide a more complete survey of loads as part of the program to develop general foil system criteria. These installations included gages to measure lateral bending strains at the lower end of the forward strut, lateral bending strains at the upper end of the aft struts, spanwise bending strains in the center portion of the aft foil, strains in all flap control linkages, and strains in the tiller arm, which controls rotation of the forward strut. Except for those in the aft struts and the aft foil center section, all of the new gages were load calibrated.

Because of the interest in hydrodynamic flow conditions during abrupt maneuvers, video cameras were mounted outboard of the forward hull and outboard of the port aft hull area. They permitted viewing of local flow conditions during the various turns and broaches. A time code was displayed on the video tape of the port, forward camera so that the strain measurements could be correlated with hydrodynamic flow conditions in data analysis. For the starboard forward and port aft cameras,

---

*Detailed information regarding strain gage installations and load calibrations is available in the DTNSRDC Code 1204 Advanced Ship Data Bank.

observed flap position changes were used to time correlate flow and load measurements.

TEST OBJECTIVES AND PROCEDURES

Two types of foilborne tests were performed: debris avoidance maneuvers and forward foil broaches. The trials were conducted by the Hydrofoil Special Trials Unit (HYSTU)* in Puget Sound under trials agenda number 75-H-P329A on 10 October 1975.

SEA CONDITIONS

The seaway was calm and free of swell with a local wind of 3 knots.

DEBRIS AVOIDANCE MANEUVERS

This type of maneuver was expected to result in maximum helmsman-induced loadings on the foil system. It corresponds to an operational situation in which the helmsman, while in a tight turn, reverses the helm abruptly to avoid debris or other objects in the path of the ship. It normally can be expected to produce large loads on directional control surfaces. The helm displacement procedure was as follows:

> The helmsman stabilized the ship on a straight course with 6-ft foil depth set at the speed indicated in the test agenda (Table 1). He then rapidly moved the helm to the position indicated on the table, holding it until the real-time data observer advised that enough steady-state turning data had been obtained. He then rapidly shifted to equal and opposite helm and held it until sufficient data had been recorded. Following this, he stabilized on a straight course before proceeding with the next maneuver.

Movies of the debris avoidance maneuver were taken from a stationary chase boat during conditions a) through h) of Table 1 as the ship flew by (see Figure 3). Hull-mounted video cameras were operated during all test maneuvers to record the hydrodynamic flow over the forward foil, port and starboard semispans, and over the aft foil port tip. For the starboard semispan and the aft foil tip, data recording time had to be shared on a single video tape.

---

*The HYSTU is at the Puget Sound Naval Shipyard, Bremerton, Washington.

TABLE 1 - TEST AGENDA FOR DEBRIS AVOIDANCE MANEUVERS
(TAPE PT 1237, LOG 75P-08)

Maneuver	Speed (knots)	Helm Command*		Actual Time (hr:min:sec)	
		Direction	Degrees	On	Off
a)	36	Right	45	10:55:30	
	36	Left	45		10:55:53
b)	36	Right	90	10:59:45	
	36	Left	90		11:04:10
c)	36	Right	135	11:03:36	
	36	Left	135		11:04:10
d)	36	Right	180**	11:08:32	
	36	Left	180**		11:08:55
e)	45	Right	45	11:17:56	
	45	Left	45		11:18:20
f)	45	Right	90	11:21:03	
	45	Left	90		11:21:26
g)	45	Right	135	11:23:41	
	45	Left	135		11:24:10
h)	45	Right	180**	11:26:56	
	45	Left	180**		11:27:20
a)	Repeat	Right	45	11:12:14	
		Left	45		11:12:39

*0.3 seconds or less for helm reversals.

**Full helm displacement.

FORWARD FOIL BROACHES

This test condition was intended (1) to produce forward foil asymmetric lift loads associated with ventilated hydrodynamic flow on one semispan and unventilated flow on the other semispan and (2) to allow observed flow conditions to be compared with concurrent foil system load measurements. The procedure employed in the test agenda (Table 2) was as follows:

> Using the Automatic Control System (ACS) "Test Box," the helmsman produced forward foil broaches by stepping the forward flap down in less than 1.0 s. All steps were inserted during steady-state straight ahead or turning conditions. Immediately following the broach, he removed the test signal and allowed steady foilborne conditions to reestablish. The ship was landed, if necessary, to prevent a second broach. Forward foil broach conditions were approached prudently so that the proper amplitude of the test box input could be determined, the optimum initial foil depth set, and the ability of the ship to recover satisfactorily from the broaches determined.

TABLE 2 - TEST AGENDA FOR STRAIGHTAWAY BROACHES AND BROACHES IN TURNS (TAPE PT 1237, LOG 75P-08)

Maneuver	Speed (knots)	Initial Helm Displacement		Actual Time (hr:min:sec)	
		Direction	Degrees	On	Off
a)	36	Center	0	11:31:38	11:31:54
b)	45	Center	0	11:36:28	11:36:40
		(Repeat Run)	0	12:01:22	12:01:34
c)	36	Right	30	11:40:35	11:40:54
d)	36	Left	60	11:44:22	11:44:36
e)	36	Right	90	11:48:12	11:48:27
f)	36	Left	30	11:57:30	11:57:40

Movies of the broaches were taken from a stationary chase boat during conditions a) through e) of Table 2 as the ship flew by. Hull-mounted video cameras

were operating during all of the broaches to record the hydrodynamic flow conditions over the forward foil, port and starboard semispans, and over the aft foil port tip. Data recording of the starboard semispan and the aft foil tip was time shared on a single video tape.

TRIALS DATA

Two general types of data are presented for each of the basic test conditions. These are: (1) time-history variations of selected foil system and ship motion parameters and (2) concurrent photographs of the hydrodynamic flow over the forward foil strut. For the debris avoidance maneuvers, local trends during buildup to full helm displacement are presented to show which component loadings were significant compared to design loadings. The photographic data presented do not include pictures of the port aft tip because spray from the forward strut and foil frequently obscured this area during broaches and because distinctive cavitated and ventilated flow patterns were generally lacking during debris avoidance maneuvers. The ship's weight and center of gravity during the trials are given in Table 3.

DEBRIS AVOIDANCE MANEUVERS

Ship Motion and Control Data

The response of HIGH POINT during a full displacement maneuver is shown pictorially in Figure 3 and in terms of motion and control parameters in Figure 4. As shown in Figure 4, helm commands were abrupt, approaching a desired 0.3 s for full equal and opposite helm displacement. Rudder (i.e., forward strut) and flap displacements generally occurred at a slower rate than helm displacement, while yaw rate lagged roll angle by about 0.5 s, which had a significant affect on resultant rudder displacements, as discussed below.

Foil System Transient Strain

Transient load, motion, acceleration and strain data for the full helm displacement maneuver at 45 knots are presented in Figure 5. Pitch attitude remained effectively constant during the maneuvers, but some settling in heave occurred upon entry into the initial turn. This was followed by an upward motion of the ship during and after helm reversal, as evidenced in the ACS Height trace (P2102). Lateral acceleration increments were relatively large during helm displacements and approached 0.5 g in the pilot house at the time of helm reversal. This results from the rapid changes in roll angle and from the roll motion tending to occur about a point below the water surface.

TABLE 3 - RECORD OF ONBOARD LOADS ON HIGH POINT (PCH 1) MOD 1 IN CALM WATER TRIALS

		Quantity	Weight (lb)	Longitudinal Center of Gravity (Ft Aft of Forward Perpendicular)
Basic Displacement Weight Less Fuel, Dated 17 March 1975 Includes Assumed Loads		*	247,075	61.26
Loads:	Assumed	(Actual)	(Difference)	
Provisions: Dry	615 lb	500	- 115	22.0
Refrigerator	200 lb	200		28.8
Freezer	500 lb	300	- 200	28.8
General Stores	450 lb			14.0
Ammunition	150 lb			41.8
Pyro & Flares	397 lb			23.9
Lube Oil Tanks	85 Gal	68	- 126	97.5
H.W. Tank	25 Gal			19.2
F.W. Tank	212 Gal			18.8
Hyd Oil Reserve (Skydrol)	-	55	+ 490	97.5
Ship's Crew	20 Men	16	- 896	47.5
Trials Crew	6 Men	7	+ 224	48.6
Fuel Total	Start	4487	30,512	65.29
	Finish	2958	20,115	65.67
Additional Weight:				
Correction to Estimated Weight			+ 220	-123.08
Diving Gear & OBA			400	55.0
Foil Camera System			150	77.5
TV Monitor System			350	40.7
Electronic Test Equip.			500	47.0
Predicted Displacement Weight	Start	124.3	278,584	62.17
	Finish	119.7	268,187	61.71

*Basic displacement weight less fuel.

Foil System Load and Strain Data Trends

Data indicating load buildup trends for progressively larger helm displacements are presented in Figure 6 through 18. The buildup parameter is expressed as the measured strain divided by a derived limit strain which is calculated in Appendix C for each component strain gage location. This limit strain corresponds to the maximum loading anticipated in service as derived from the original component design loads. In general the peak strains experienced by HIGH POINT's foil system during calm water debris avoidance maneuvers are significantly less than the maximum values anticipated in service. The upper forward strut bending strains (shown in Figure 7), come closest to the derived limit bending strains (approximately 75% of the limit value). A contributing factor to these high bending strains is a steady bending moment at 0° helm displacement, which is believed to be due to asymmetric foil lift associated with manufacturing tolerances. Figures 10 through 18 present peak strains for the first and second data peaks that occur at the time of helm reversal as identified in Figure 5. The peak forward strut hydrodynamic side loading shown in Figure 19 has been estimated from the forward strut lateral shear measurement, the calibration for which is discussed in Appendix B. The measured shear load is assumed to act uniformly over the submerged part of the forward strut. The submerged depth was determined from depth markings painted on the leading edge of the strut and from the instantaneous spray root of the free water surface as recorded on video tape. The rudder actuator pressure required by the full helm maneuver at 45 knots is close to full system pressure, but well below the limit pressure employed in structural design. Figures 20 and 21 present transient peak hydrodynamic loadings on the port and starboard outboard panels, respectively, of the aft foil. Since these loadings are based on the output of only one shear bridge, they are identified as apparent loadings, i.e. loadings whose values are subject to large tolerance limits. Figure 22 presents flap cavitation boundaries as determined from video tapes and by the output of strain gages on the forward flap control linkages. The boundaries are strongly influenced by forward speed as would be expected. At 45 knots, full cavitation begins at a flap deflection angle of approximately 1.5° and buffeting at an angle of approximately 4°. At 36 knots these increase to 7.0° and 11.5°, respectively.

It can be seen in Figure 5 that at 45 knots buffet loads in the forward flap control linkage are somewhat greater near the onset of buffeting than at large flap deflections.

Photographic Studies

Flow patterns on the port forward foil semispan and the port side of the forward strut are shown in Figures 23 and 24 for steady turns at 36 and 45 knots, respectively. Selected areas of the port semispan have an experimental coating, which appears as lighter or darker panels on the foil and which, at 45 knots, resulted in some local cavitation at the seams between panels.

The steady trim deflection of the forward flap increases with helm angle, so that flap cavitation and, in some cases, vapor cavity shedding increase with helm displacement.

Flow patterns for submerged forward foil and strut areas are shown in Figures 25 and 26 for full helm displacement at 36 and 45 knots during the maneuver. At the time of transition from full starboard to full port helm, cavitation and cavity shedding could be seen on the port side of the forward strut. In Figure 5, the upper strut bending strain gage bridge (P4803) is shown to have responded to the buffet loads during the time interval in which cavity shedding is evident in Figure 26. Steady sheet cavitation is also evident at the outboard leading edge of the port semispan during the time interval in which roll velocity is maximum. This condition is presumably due to the increase in local angle of attack induced by roll velocity.

An apparent anomally existed during the 45-knot debris avoidance maneuver with respect to forward flap trim deflections. In Figure 5 the flap trim deflection (P2707) is about 14° at the time of hard over helm deflection to starboard, but only about 8° in the full helm turn to port which followed. This is also reflected in the flap cavitation patterns of Figure 26. The reason for this result is not apparent.

FORWARD FOIL BROACHES

Forward foil broaches were performed with the ship flying straight ahead at 0° helm displacement so as to provide a base line for subsequent load and motion responses associated with broaches in turns. The data presented in all cases provide time-varying load and motion parameters measured during individual broaches, together with photographs of the associated transient local flow over the port and starboard sides of the forward foil and strut. The individual photographs presented were selected primarily to show local cavitation and ventilation patterns as the foil broached and then recovered. As a result, the number of photographs shown here, as well as the time increments between them, are not the same from one test condition to another.

In order to help assure static directional stability during broaches, the pitch attitude of the ship was sent initially at 1° to 2° bow up so that the after foil and lower portion of the aft struts would remain submerged while the forward foil broached. With the exception of the 90° helm broach-in-turn, the loss in lift of the forward foil upon broaching was abrupt enough that the ship immediately lost flying height and descended until hull impact occurred.

The traces of ACS height (P2102) presented in Figures 27 through 31 are marked for reference as to "foil emergence" and "hull-level impact" based upon the simplifying assumption that the hull was level at all times which, in general, was not the case. Since the ACS height sensors are located only slightly ahead of the forward foil, this discrepancy did not affect the accuracy of the foil emergence boundary very much. It did affect the hull impact boundary, however, whenever the attitude of the ship was bow up at the time of impact. No effort was made to introduce an attitude correction since the time correlated trace of vertical acceleration also provides an indication of hull impact. In general, the slope of each ACS height trace shows an abrupt change at the time the hull-mounted accelerometers indicated water impact.

Because of the adverse effects of aerated flow on the output of the forward foil mounted electromagnetic (EM) speed log and the relatively long time required for its recovery, the values of ship speed shown in Figures 27 through 31 following forward foil broaching are of questionable accuracy, except possibly the broach in turn at 90° helm displacement, where the photos of Figure 36 suggest that the forward foil remained submerged at the location of the EM log.

Straightaway Broach at 36 Knots

Ship motion, control system displacements, and strain gage response parameters versus time are presented in Figure 27. Forward foil broaching, as indicated by the pilot house vertical acceleration trace, was initiated at 11:31:43.0 (hr:min:sec). This is further confirmed by the photographic data of Figure 32, which shows the flow venting at the tip of the foil at 11:31:42.96. Hull impact is indicated by the vertical acceleration trace (P6202) to have started at 11:31:45.3. The roll angle trace of Figure 27 shows that the ship remained level until hull impact, at which time it rolled slightly (1°) to starboard. The lower forward strut bending bridge (P4810) indicates a small bending moment due to asymmetric lift at the time the forward foil broached and later just after hull impact. The forward foil

starboard bending gage (P4405) shows an abrupt loss of lift occurring at the time of forward foil broaching. This is followed by a gradual return to the 1 g steady flight value with full forward flap deflection. Figure 32 at 11:31:45.46 shows that even at a foil submergence of 10.8 ft, flow over the foil was vented; this accounts for the persistence of only 1 g lift at full flap deflection.

The aft strut and foil strain gage traces indicated large fluctuating loads following forward foil broaching. The aft foil bending strain gages indicate an apparent buildup in lift load beginning approximately 1 s after forward foil broaching, while later they indicate a relatively abrupt decrease in foil lift at the time of hull impact.

Straightaway Broach at 45 Knots

Ship motion, control system displacements, and strain response parameters versus time are presented in Figure 28. Concurrent photographic data are in Figure 33. Forward foil broaching began at 11:36:32.1, hull impact at 11:36:34.8. Venting of the foil again occurred initially at the port tip despite the level attitude of the ship. Roll angle was held constant during the broach even after hull impact. In contrast to results from the broach at 36 knots, here the pilot house vertical acceleration indicates a more abrupt and sustained loss of forward foil lift at the time of broaching. During the interval between forward foil broaching and hull impact, the aft foil was again subject to substantial load fluctuations. An abrupt loss of lift again occurred at the time of hull impact. Just before hull impact, rudder deflection and rudder torque built up appreciably with rudder torque reaching a momentary peak corresponding to the full output of the steering actuator. Shortly after hull impact the lower forward strut bending bridge (P4810) indicated an abrupt but low-level increment of asymmetric lift on the forward foil. The forward flap linkages indicate buffeting of the flaps immediately after the elevator step deflection which was introduced to cause broaching. The buffeting subsided just before broaching and did not occur again during the recovery.

Broach-in-Turn at 36 Knots with 30° Starboard Helm

The lower forward strut bending bridge (P4810) of Figure 29 indicates that broaching of the port tip began at 11:40:43.7, which is further confirmed by the video camera views of the port tip shown in Figure 34. The loss of forward foil lift was somewhat less abrupt than in the straight-away broaches at 36 and 45 knots,

although the cumulative lift loss and the resultant ship motion were virtually the same. Hull impact occurred at 11:40:46.25 as indicated by the pilot house vertical acceleration trace (P6202). The lower forward strut bending bridge (P4810) shows that asymmetric lift existed for about 0.7 s, which in turn suggests that the starboard (downhill) semispan experienced fully vented flow about 0.7 s after the port (uphill) semispan. The trace of forward flap deflection and ACS height are virtually the same as those from the straightaway broach at 36 knots despite the slight lag in venting of the starboard semispan. The aft foil strain gages (P4204, P4214, P4114, and P4104) indicate substantial load fluctuations following forward foil broaching. Hull impact is again associated with a momentary but distinct decrease in aft foil lift.

The photographic data of Figure 34 clearly shows initial broaching of the forward foil port semispan. As in the straightaway broaches venting of the foil occurs first at the flaps, which are full down, and then proceeds to envelop the entire upper surface of the foil. In this case, the tip of the starboard (downhill) semispan did not vent before the root section of the foil, apparently due to the 3° roll angle during the broach.

Broach-in-Turn at 36 Knots with 60° Port Helm

The lower forward strut bending bridge output (P4810) of Figure 30 indicates that broaching of the starboard (uphill) semispan began at 11:44:30.3. This is confirmed by the starboard semispan bending bridge (P4405), which indicates a nearly complete loss of lift during the broach, as well as by the video camera views of Figure 35. The start of the port semispan broach cannot be determined easily from the available strain gage bridge outputs, but Figure 35 shows that ventilated flow occurred at the inboard flap and foil root at 11:44:30.63. The flow over the port semispan after this (see Figure 35 at 11:44:32.0, for example) was a mixture of ventilated and cavitated flow, with ventilated flow at both foil root and foil tip and cavitated flow in between. The output of P4810 beginning at 11:44:31 suggests that the venting of this semispan was not complete since the lower strut bending moment did not reflect symmetrical lift on the foil as had been the case in the 30° helm broach in turn. At 11:44:32, however, the output of P4810 dropped, indicating more nearly symmetrical lift. Figure 35 shows that this time (11:44:32.0) corresponds to the appearance of ventilated flow over the tip area of the port semispan.

The output of the aft foil strain gages (P4204, P4214, P4114, and P4104) again reflects transient loadings due to forward foil broaching (see Figure 30). Broaching of the forward foil starboard semispan at 11:44:31.06 is again followed in about 1 s by an abrupt change in the output of the starboard, aft, inboard bending bridge (P4114).

Broach-in-Turn at 36 Knots with 90° Starboard Helm

The lower forward strut bending bridge (P4810) trace of Figure 31 indicates that forward foil broaching began at 11:48:21 which is also evident in the views of the forward foil port semispan shown in Figure 36. The change in ACS height of Figure 31, which began with forward flap deflection at 11:48:19.8 and continued through initial forward foil broaching, is very similar to that which occurred during the previous broaches. However, the ensuing behavior was quite different. The forward foil remained at shallow submergence for approximately 3.5 s after the initial broach. In addition, the roll angle trace (P2014) shows that, at the time of the initial broach, the roll angle associated with the initial steady turn began to decrease steadily. Approximately 2.5 s later the roll angle began to change much more rapidly in the same direction. The pilot house vertical acceleration trace (P6202) indicates fairly minor hull impact at 11:48:26. Because of the ship's bow-up attitude of approximately 4°, the "hull-level impact" line shown next to the ACS height trace failed to indicate the impact that occurred at this time.

The starboard forward foil bending trace (P4405) and the lower forward strut bending bridge trace (P4810) indicate that lift on the down hill semispan of the forward foil never fell below the initial 1 g steady flight value during the broaching sequence. The views of the flow over the starboard semispan presented in Figure 36 show that, while venting of the starboard flap occurred briefly, the rest of the foil did not vent at any time. A relatively large area of cavitation did appear, however, near the leading edge of the outboard half of the semispan. The apparent reduction in foil lift shown by P4810 and P4405 between 11:48:21.9 and 11:48:22.9 corresponds closely to the interval of port flap venting evident in Figure 36. A subsequent decrease in lift is apparent between 11:48:24.4 and 11:48:25.0. It can be correlated with the relatively abrupt decrease in forward flap deflection shown in the forward flap angle trace (P2702) starting at 11:48:24.3 A low level buffet load in the starboard semispan is evident in the foil bending bridge (P4405) from approximately 11:48:25.1 to 11:48:25.9, which corresponds to the interval during which cavities were being

shed from the starboard semispan as shown in Figure 36. The port aft foil bending gages (P4214 and P4201) indicate an increase in foil lift approximately 1 s after broaching of the forward foil port semispan as in the previous broaches. At this time, however, the starboard outboard strain gage bridge shows only a slight increase while the inboard bridge (P4114) shows no increase. The time of broaching of the forward foil starboard semispan was not indicated in Figure 31 because, as mentioned above, this semispan did not broach. The trace of forward strut position (P2701) shows that the strut was hard over, nose left from 11:48:24.7 to 11:48:28 and, further, that the rudder torque (P4812) was slightly above maximum actuator output (3000 psi hydraulic pressure) from approximately 11:48:25.2 to 11:48:26.8.

DISCUSSION

HELM-INDUCED LOADS

The debris avoidance maneuver of Figure 4 resulted in a momentary hydrodynamic loading of the forward strut that approached maximum attainable side force for the submergence involved, as evidenced by the cavity shedding in Figures 25 and 26. (See also Figures 7 and 8 of Rothblum et al.* for correlation of strut cavity shedding with maximum side force coefficient.) The sequence of events that results in this condition can be explained upon examination of the automatic control system schematic presented in Figure A-1 of Appendix A. The rudder servo is driven by the output of the roll angle gyro ($K_{\phi R}$) and the yaw rate gyro (K_{RR}) with gains as shown in Table A-1. Referring to the initial full-helm steady turn data of Figure 4, the roll angle of 18° calls for a strut rotation of 1.34 x 18° = 26.1° nose right in a right hand turn. The yaw rate of 8.5°/s calls for a strut rotation of -2.0 x 8.5° = -17° nose left. The net nose right strut deflection is 9.1°, which is close to the measured initial strut deflection angle of 8.6° reported in Figure 26 at 11:27:09.6.

At this strut angle the ship is performing a coordinated turn. The side force on the strut can be seen in Figure 5 (P4801) to be very small. At the time of maximum forward strut lateral shear, 11:27:10.6, the roll angle is 1.8° while the yaw rate is 5.0°/s. The ACS command strut angle is (1.45 x 1.8°) - (2.0 x 5.0°) = -7.4° (nose left); the actual position is -3.9° due to a slight lag between the command and actual positions. Despite this lag we find the strut turned from its

*Rothblum, R.S., D.A. Meyer and G.M. Wilburn, "Ventilation, Cavitation and Other Characteristics of High Speed Surface-Piercing Struts," Report NSRDC 3023, July 1969.

initial position of 8.5° nose right to 3.9° nose left. However, the yaw rate has only changed from 8.5°/s bow right to 5.0° bow right, thus causing an appreciable buildup of side force acting to port. Figure 4 shows that in this particular case yaw rate lags roll angle by about 0.5 s, which causes the ACS to call momentarily for more nose left strut deflection than it would if the maneuver were performed slowly.

Figure 37 shows the hydrodynamic loading on the forward strut at the time of maximum side load as given in Figure 18 superimposed on strut model test data taken from Rothblum et al.* In Figure 37 the model strut loadings correspond to cases where the plots of side force coefficient (Cy) versus side slip angle (β) have a clearly defined ventilation- or cavitation-limited maximum. The peak loading shown corresponds to Cy_{max} x dynamic pressure ($1/2\ \rho V^2$). Two of the model test struts had hydrodynamic sections similar to that of HIGH POINT. As Figure 37 shows, the full scale loadings agree generally with the model data at corresponding speeds, and hence near-surface cavitation numbers. Since the full scale strut did not ventilate, the maximum attainable loading was presumably somewhat higher than the model test value. The aspect ratio shown corresponds to the ratio of strut submergence to strut chord, which on HIGH POINT is approximately one. Although Rothblum et al.* showed that aspect ratio substantially affected initial slope of the curves of Cy versus β, it affected maximum attainable hydrodynamic loading substantially less. They also showed a significant buffet load on the model struts near maximum loading due to cavitation cavity shedding just prior to strut ventilation. This buffet load is also evident in the HIGH POINT upper forward strut bending bridge (P4803) during the brief time interval that cavity shedding occurred (Figures 25 and 26).

Thus it is evident that debris avoidance maneuvers can produce maximum attainable hydrodynamic loadings on the forward strut of a canard configuration hydrofoil ship like HIGH POINT with its steerable forward strut. This finding, it should be noted, will be influenced by the particular characteristics of the automatic control system.

BROACH-INDUCED LOADS

It is generally apparent from the data of Figures 29, 30, 31, 34, 35, and 36 that ventilated flow over one semispan only of the forward foil can produce sizeable

---

*Rothblum, R.S., D.A. Meyer and G.M. Wilburn, "Ventilation, Cavitation and Other Characteristics of High Speed Surface-Piercing Struts," Report NSRDC 3023, July 1969.

bending moments at the lower end of the forward strut. The significance of these bending moments can be assessed by comparing the maximum lower forward strut bending bridge strain (P4810) measured in the present tests to the highest value measured at any time during rough water trials. These values are as follows:

TABLE 4 - COMPARISON OF BROACH-INDUCED LOADS ON FORWARD STRUT IN CALM AND ROUGH WATER TRIALS

Conditions of Broach	Peak Lower Forward Strut Bending Strain (P4810) (in/in x 10^6)	Percent of Maximum Observed Rough Water Bending Strain (P4810)*
Straightaway Broach at 36 Knots	300	18%
Straightaway Broach at 45 Knots	200	12%
30° Helm Broach-in-Turn at 36 Knots	700	42%
60° Helm Broach-in-Turn at 36 Knots	1000	61%
90° Helm Broach-in-Turn at 36 Knots	1400	85%
*1650 (10^{-6} in/in) measured in head seas in sea state 5 immediately after a forward foil broach.		

Since, the peak bending strain measured in rough water resulted from a forward foil broach, and since the maximum bending moments measured in these trials closely approached the peak rough water value, it is reasonable to conclude that maximum lower forward strut bending moments encountered in rough water result largely from asymmetric venting of the forward foil.

Further insight into the nature of forward foil asymmetric lift generation can be gained by correlating the flow conditions observed on the foil with the bending moments measured at the lower end of the forward strut (P4810). Before doing this, however, it is instructive to compare the curves of lower forward strut bending strains versus time during each of the broaches. Figures 27 and 28 (P4810) show that the straightaway broaches resulted in almost no net change in bending moment at the time of broaching. Nevertheless, the net loss of foil lift was abrupt during foil emergence and, as can be seen in the ACS height traces (P2102) of Figures 27 and 28,

an appreciable sink speed was built up. Since the ensuing sink speed of about 6.3 ft/s was nearly constant, it can be concluded that the foil produced approximately 1 g lift (roughly 1370 lb/ft^2) during the interval when the foil was fully vented with flap down. The associated positive angle of attack induced by the sink speed, neglecting pitch attitude change, was approximately [6.3/(36 x 1.690] x 57.3°/radian = 6° during the 36-knot broach and 4.7° during the 45-knot broach. A small increment in lower strut bending strain is evident in the straightaway broaches after hull impact, presumably because of a momentary asymmetric lift at the time vented flow ceased to exist.

The bending moment increments of Figure 38, which are associated with the 30° and 60° helm displacement trials, were caused by the existence of vented flow on the uphill semispan before it occurred on the downhill semispan. The bending moment increments are of opposite sign since these broaches were induced while turning in opposite directions. In the case of the 60° helm broach in turn (ship roll angle ≈ 6°), a significant increment of bending moment persisted for about 1 s after the initial broach. The sink speed after forward foil broach was again uniform but at a slightly lower value, i.e. 5.6 ft/s as compared with 6.3 ft/s in the prior broaches, which suggests that the time-integrated loss of lift during the period of foil emergence was somewhat less here than in the prior broaches.

Figure 38 shows that the 90° helm broach-in-turn produced substantially different behavior. The bending moment at the lower end of the forward strut was higher and persisted for a much longer period than in the previous broaches. In addition, the ACS height trace (P2102) of Figure 31 shows that the net loss of lift at foil emergence was small (with the forward flap full down) so that the sink speed for about 3 s after the broach remained effectively zero. The sink speed at the end of this interval can be seen in Figure 31 to have developed when the forward flap deflection was decreased by the automatic control system from 13° to approximately 3° trailing edge down.

The variation of lower forward strut bending strain (P4810) shown in Figure 31 from 11:48:20 to 11:48:23.2 is a measure of forward foil asymmetric lift. It directly indicates the effect on foil lift of the port and starboard semispan hydrodynamic flow (Figure 36) during this same time period. Trace P4810 reaches an initial peak at 11:48:21.7, at which time Figure 36 shows the port semispan to be fully vented and the starboard semispan unvented but with starboard flap venting incipient. The lower strut bending strain then begins to decrease to a minimum

at 11:48:22.2. Figure 36 shows that while the port semispan vent remains unchanged, the flap on the starboard semispan has become fully vented.

During this broach-in-turn, ACS trace height decreases from about 2.0 to 1.3 ft, indicating that total forward foil lift is less than that required for level flight. Beginning at 11:48:22.2, the bending strain trend reverses until it reaches a new peak at 11:48:23.2, which is appreciably greater than the first peak. The port semispan remains fully vented during this interval (not shown in Figure 36 beyond 11:48:23.04) but the flap vent on the starboard semispan can be seen to disappear until 11:48:23.26, when Figure 36 shows that it is completely gone. A large area of cavitation has developed over the outboard portion of the semispan. It is apparently due to the positive angle of attack associated with the 3.5° bow-up pitch attitude of the ship, the sink speed being effectively zero at this time. It is apparent that venting of the flap from 11:48:21.85 to 11:48:23.14 substantially reduced lift on the starboard semispan. Figure 36 shows that the flap vent appeared at an average foil depth of 1.6 ft and a flap trailing edge down deflection of 20.5°. It then disappeared completely at an average foil depth of 2.7 ft and a flap trailing edge down deflection of 15.4° In contrast to the straightaway broaches, where venting of the complete foil was very persistant, it appears that venting of only the flap can be eliminated by a relatively modest increase in foil submergence and decrease in flap deflection angle.

In addition to providing information relative to the flow conditions which can occur during a forward foil broach, these trials have provided quantitative measures of attainable foil lift loads under these same flow conditions. Unfortunately the earlier loss of strain gage channels in the forward and aft foils preclude use of foil load calibrations which otherwise would have provided direct load measurements. Even so, certain estimates of foil lift are possible. For fully vented operation with flaps down and a high angle of attack ($\approx$ 5° to 6°), which occurred just after the straightaway broaches, the constant sink speeds suggest that average forward foil lift was approximately equal to the nominal 1 g foil loading of 1370/ lb/ft^2. The maximum attainable lift with fully wetted flow cannot be estimated because a steady lift condition corresponding to operation with flaps fully down and a high angle of attack was not experienced. The highest semispan bending strains (P4405) were measured during the 90° helm broach-in-turn with the foil in low submergence. In terms of factors of lift, the bending strain reached 1.75 times the steady 1 g

value from 11:48:23 to 11:48:24. This corresponds to an apparent foil loading of 1375 x 1.75 = 2400 lb/ft^2. Flap deflection and ship pitch attitude were both changing during this time. At 11:48:23 the flap angle was 17.5° trailing edge down, pitch angle 2.4° bow up and foil submergence 2.7 ft. At 11:48:24, the flap angle was 13.3°, pitch angle 3.7°, and submergence 2.9 ft.

It is of interest to note that during this interval, tiller arm strain (see Figure 31, P4812) remained close to the initial steady state value of 90° starboard helm. This indicates that despite substantial asymmetric lift on the foil the drag on the port and starboard semispans was not substantially different. Just prior to this time, a large increment in tiller arm loading is evident due to the decrease in drag on the port semispan as it broached the surface. The subsequent buildup of rudder torque to a level exceeding peak actuator output (11:48:26) cannot be readily attributed to a single cause. Photographs of flow behind the forward strut presented in Figure 36 for 11:48:23.26 to 11:48:26.18 suggest that the strut was vented during this time. The side force on the strut during this interval, as indicated by the lateral shear gage (P4801), acts to starboard even though the strut has turned nose left. The side force is thus opposite to that which would be expected in unvented flow but consistent with the existence of vented flow at low to moderate side slip angles. (Note: The sudden decrease in tiller arm load (P4812) at 11:48:27.3 may be related to the disappearance of the vent. This possibility could normally be checked by examining photos of the flow as viewed from the starboard side of the strut; however, spray of undetermined origin obscured the strut at this time.)

UNSTEADY LOADS

The unsteady loads measured during these trials are of two general types: those due to vapor cavity shedding and those due to flow interference effects. Three components in particular were subject to cavitation cavity shedding loads - the forward strut, the forward flaps, and the forward foil outboard leading edge area. In general, the responses to these buffet loads were small percentages of the limit strains associated with the particular component. If fatigue loading is considered, the buffet loads on the forward flaps are perhaps the most significant, because they can be experienced under any operating condition that calls for flap deflections corresponding to the buffet boundary defined in Figure 22. Where steady flight requires flap trim deflections of 4° to 6°, as has been noted in some cases in service, only a few additional degree of flap deflection will result in continuous

buffeting. Such incremental deflections can occur typically in large helm displacement steady turns and in moderate to severe sea states. The resulting buffet loads act on flap control linkages, flap skin panels, flap hinge fittings and bearings, and the foil rear spars to which the hinge fittings are attached.

The largest unsteady loads measured were those on the aft foil center section immediately following foward foil broaches. As discussed above these loads appear to result from the effects of vented flow from the forward foil as it passes the aft foil. The strain fluctuations in the aft foil center section and the aft struts are large enough, for example, that they can be easily identified during rough water broaches experienced in other trials when the general level of fluctuating loads itself was quite high (see Figure 39). Since such large, unsteady loads appear to occur only during forward foil broaches, they are encountered infrequently. It is implicit from these observations that downwash effects on the aft foil center section due to forward foil flap activity in rough water may be important from a fatigue loading point of view. Review of HIGH POINT aft foil strain gage data from rough water operation confirms that the fluctuating load activity of the foil center section is significantly greater than that of the aft foil tips as is the case, for example, in Figure 39.

CONCLUSIONS

1. Debris avoidance maneuvers resulted in relatively large forward strut hydrodynamic loadings at the time of helm reversal. Vapor cavity shedding on the strut during the full helm displacement maneuver suggested that the peak loading approached the maximum attainable value. This loading was estimated to be approximately 1200 lb/ft^2 at both 36 and 45 knots, which is consistent with maximum strut loading obtained from model test data for similar strut hydrodynamic sections.

2. Flap cavitation and buffet boundaries were defined as a function of ship speed and forward flap deflection angle. Both boundaries were found to be strong functions of ship speed. At 45 knots the spread between onset of cavitation and the onset of flap buffeting was approximately 2.5° of flap displacement.

3. Calm water boraches-in-turns successfully reproduced the forward foil asymmetric lift conditions that are believed to cause the large forward strut bending moments measured during broaches in rough water. The maximum lower strut bending strain measured in these trials attained 85% of the maximum value measured in

rough water trials. Photographic data revealed that the maximum asymmetric lift condition resulted from vented flow over one foil semispan and wetted flow over the other with the forward flap full down. Because of the loss of lift at the time of emergence of the uphill semispan, the subsequent sink speed at the forward foil resulted in a positive angle of attack acting in combination with the full flap down displacement.

4. Broaches were performed at ship roll angles of 0°, 3°, 6°, and 9°. Substantially different flow conditions were produced on the downhill semispans for the two highest roll angles. At 0° roll, venting occurred simultaneously on each semispan, with the vent developing first near the tips of the foil. At 3° roll the downhill as well as the uphill semispan vented, but slightly later. At 6° roll, the downhill semispan experienced a mixture of vented and cavitated flow, whereas at 9° roll it vented momentarily only over the flap. In the latter case, cavitation along the leading edge of the downhill semispan reached the point of vapor cavity shedding. In general, the maximum value of lower strut bending moment was a direct function of the roll angle at which the broach was performed, the highest bending moment being associated with the broach at 9° roll.

5. Following emergence of the forward foil in the 0° roll (i.e., straightaway) broaches, constant sink speed at essentially constant ship pitch attitude was observed. From this, one may conclude that foil lift in the fully vented flow condition with the flap full down was approximately equal to the nominal 1 g foil loading of 1370 lb/ft^2. Venting of the foil following emergence was found to persist to submergence levels at which spray due to hull impact obscured the view of the foil.

6. Relatively large, unsteady lift loads acted on the aft foil center section. They appeared to result from the development of vented flow on the forward foil during broaches.

7. Tiller arm torques exceeded full actuator output during the recovery phase of the broach performed at 9° roll. Strut venting may have been a contributing factor to the large torque encountered at this time, but this could not be established conclusively with the available data.

ACKNOWLEDGMENTS

The author wishes to thank Messrs. Daniel Gill, Gregory Schudel, and Andrew Davis for their assistance in data analysis and figure preparation for this report. The trials, the strain gage instrumentations, and the data acquisition were conducted by Hydrofoil Special Trials Unit (HYSTU), the ship's company of HIGH POINT, and the HYSTU Support Group of the Boeing Company. The trials were planned and structured under the supervision and encouragement of Mr. William C. O'Neill, then Deputy Technical Manager of the Advanced Hydrofoil Systems Office, DTNSRDC. Preparation of the final report was undertaken under the direction of Mr. John R. Meyer, Manager of Technology Development, Hydrofoil Group, Ship Systems Integration Department, DTNSRDC.

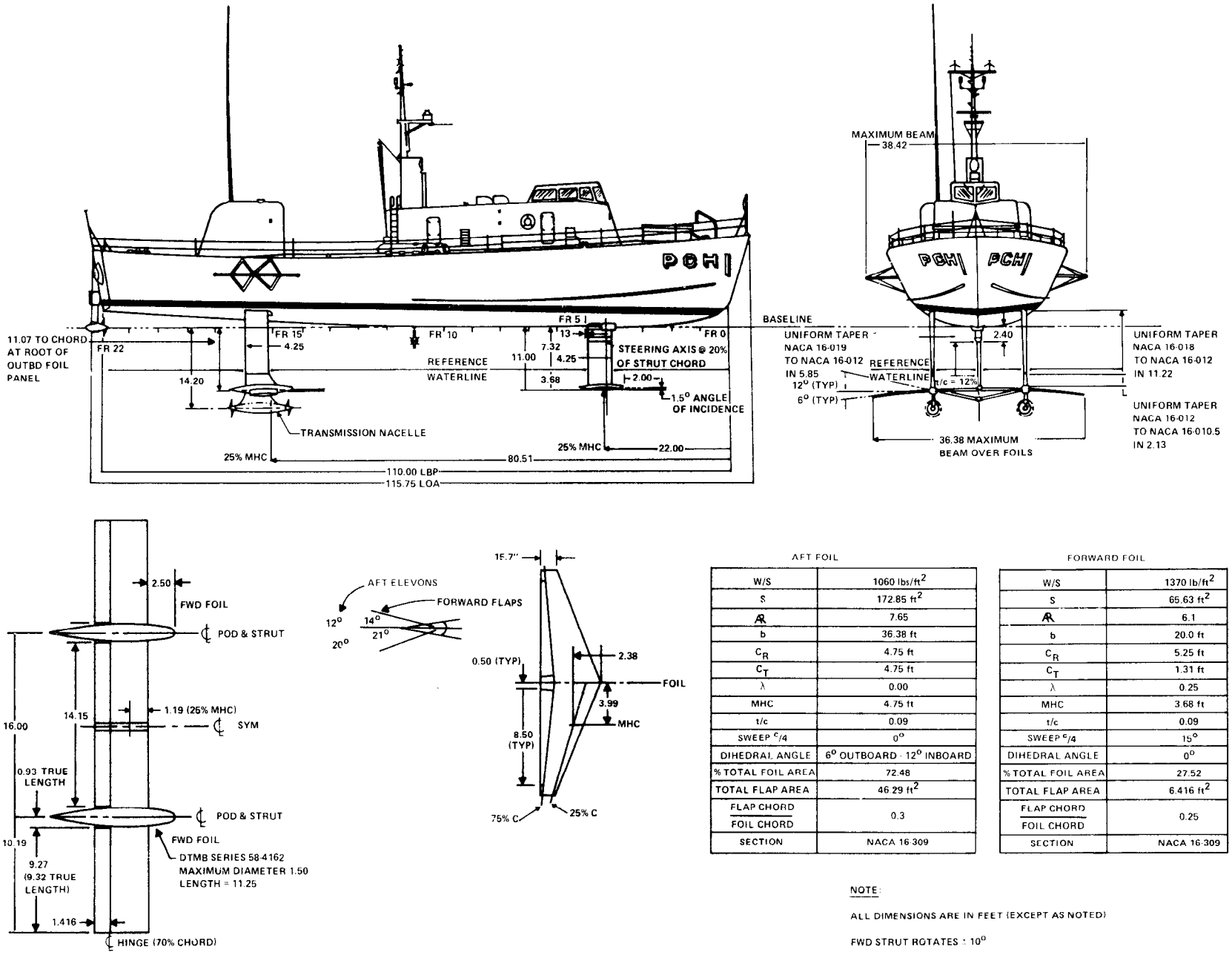

AFT FOIL

W/S	1060 lbs/ft^2
S	172.85 ft^2
AR	7.65
b	36.38 ft
C_R	4.75 ft
C_T	4.75 ft
λ	0.00
MHC	4.75 ft
t/c	0.09
SWEEP $^C/_4$	0°
DIHEDRAL ANGLE	6° OUTBOARD - 12° INBOARD
% TOTAL FOIL AREA	72.48
TOTAL FLAP AREA	46.29 ft^2
FLAP CHORD / FOIL CHORD	0.3
SECTION	NACA 16-309

FORWARD FOIL

W/S	1370 lb/ft^2
S	65.63 ft^2
AR	6.1
b	20.0 ft
C_R	5.25 ft
C_T	1.31 ft
λ	0.25
MHC	3.68 ft
t/c	0.09
SWEEP $^C/_4$	15°
DIHEDRAL ANGLE	0°
% TOTAL FOIL AREA	27.52
TOTAL FLAP AREA	6.416 ft^2
FLAP CHORD / FOIL CHORD	0.25
SECTION	NACA 16-309

NOTE:

ALL DIMENSIONS ARE IN FEET (EXCEPT AS NOTED)

FWD STRUT ROTATES ± 10°

Figure 1 - PCH 1 MOD 1 Principal Dimensions and Foil System Arrangement

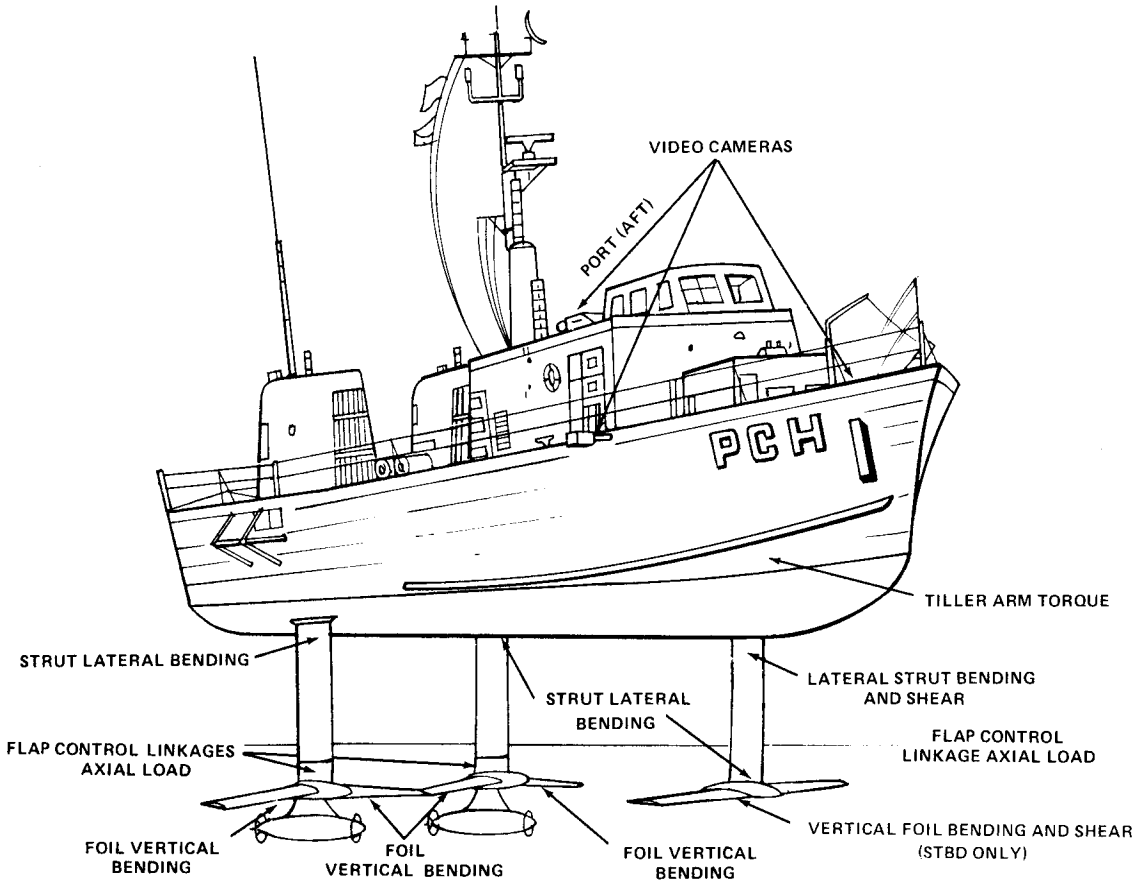

Figure 2 - PCH 1 MOD 1 Structural Load Instrumentation for Calm Water Trials

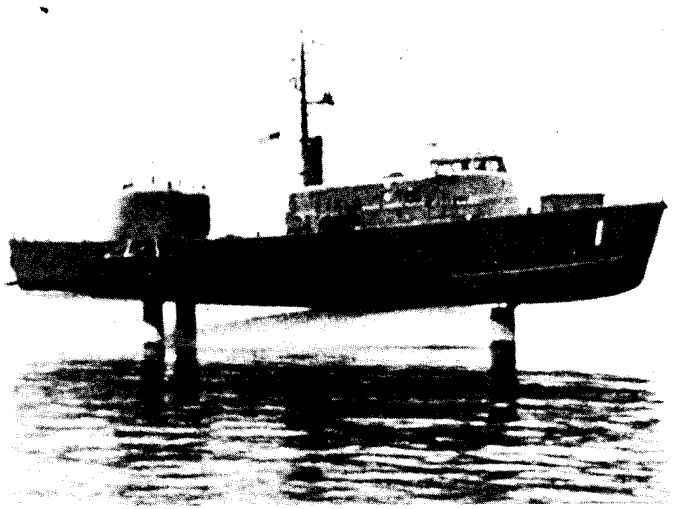

STRAIGHT AND LEVEL FLIGHT

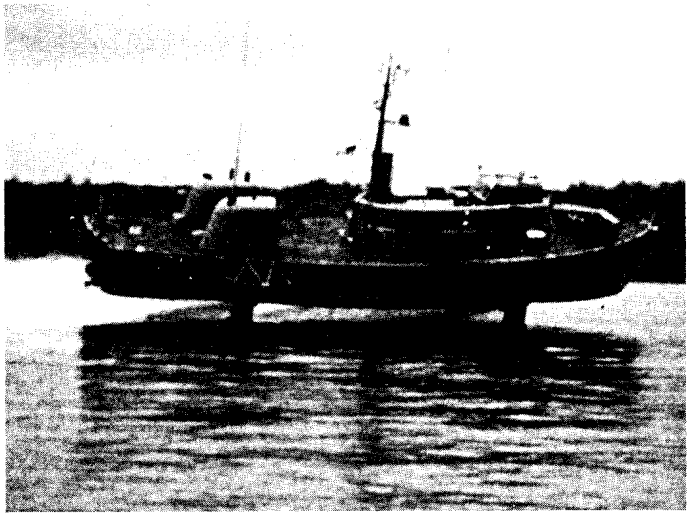

INITIAL STARBOARD TURN

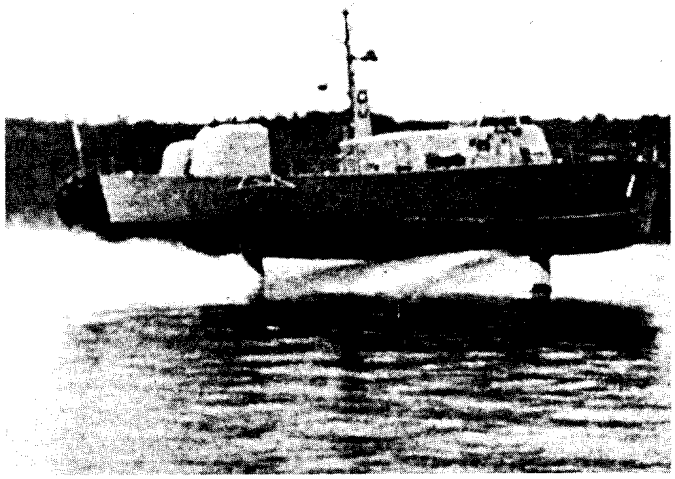

TRANSITION TO EQUAL AND OPPOSITE PORT TURN

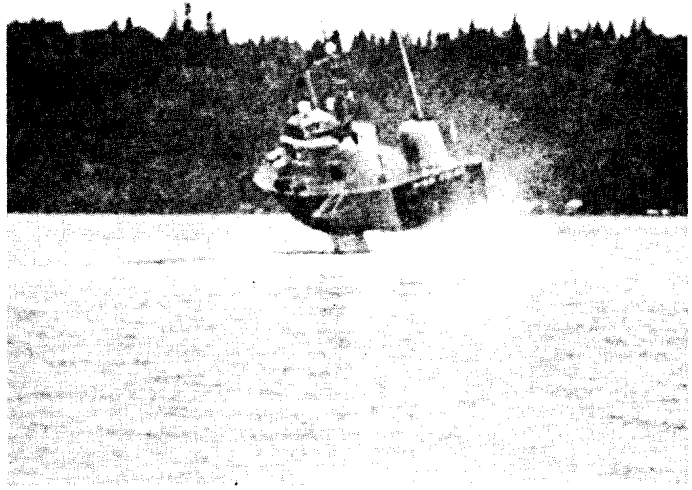

PORT TURN

Figure 3 - Overall View of PCH 1 MOD 1 Performing a Debris Avoidance Maneuver

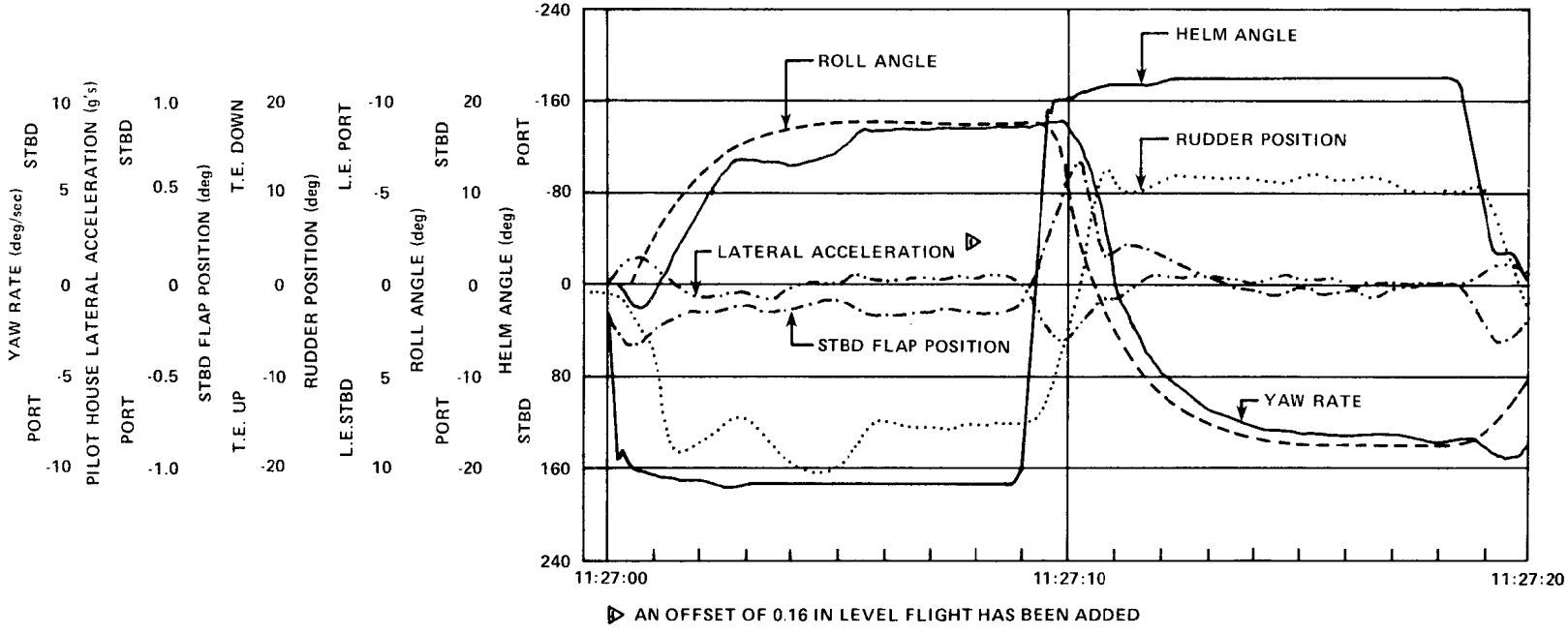

Figure 4 - Debris Avoidance Maneuver Motion and Control Parameters at 45 Knots with 180° Helm Displacement

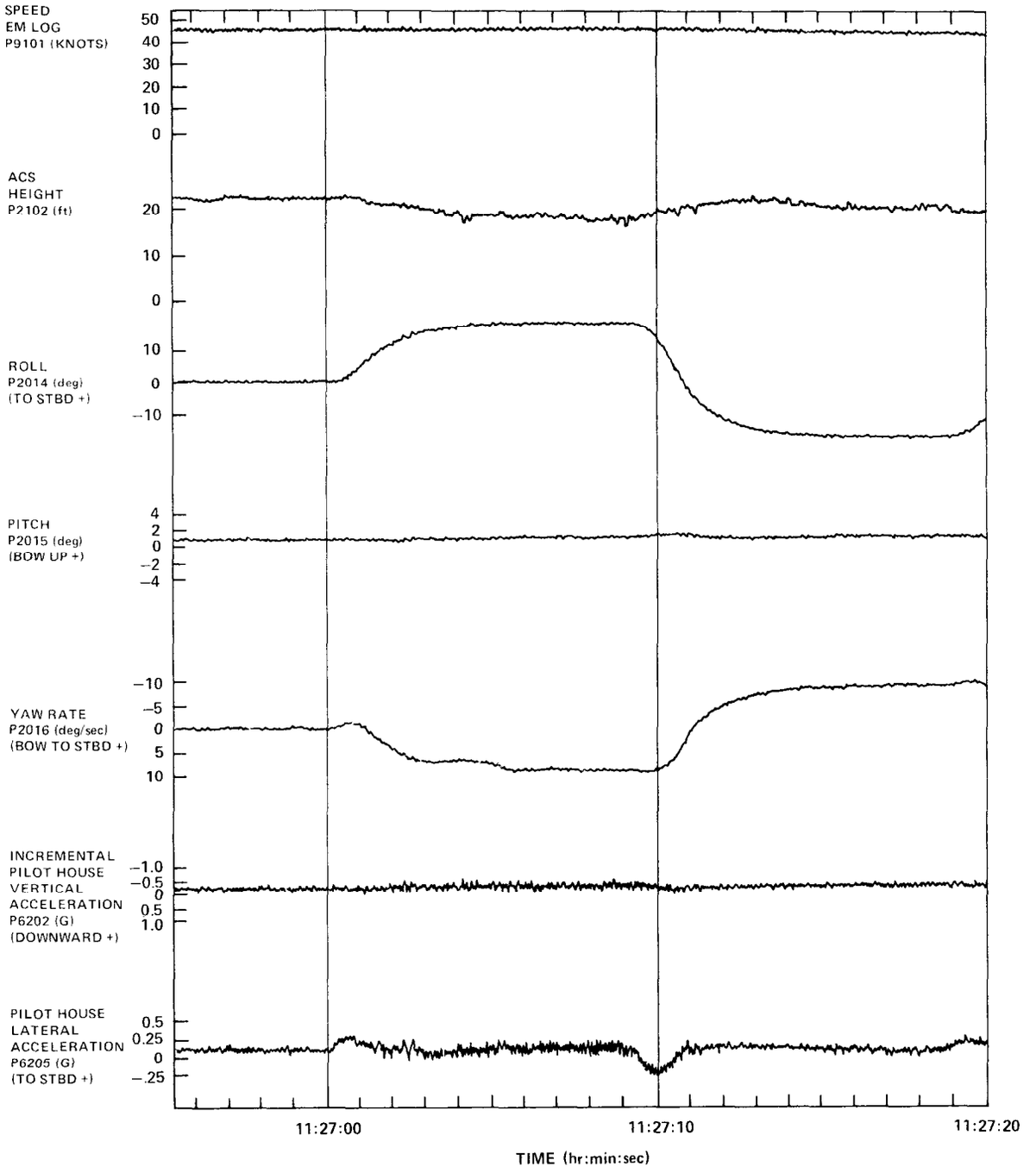

Figure 5 - Data Traces--Debris Avoidance Maneuver at 45 Knots with 180° Helm Displacement

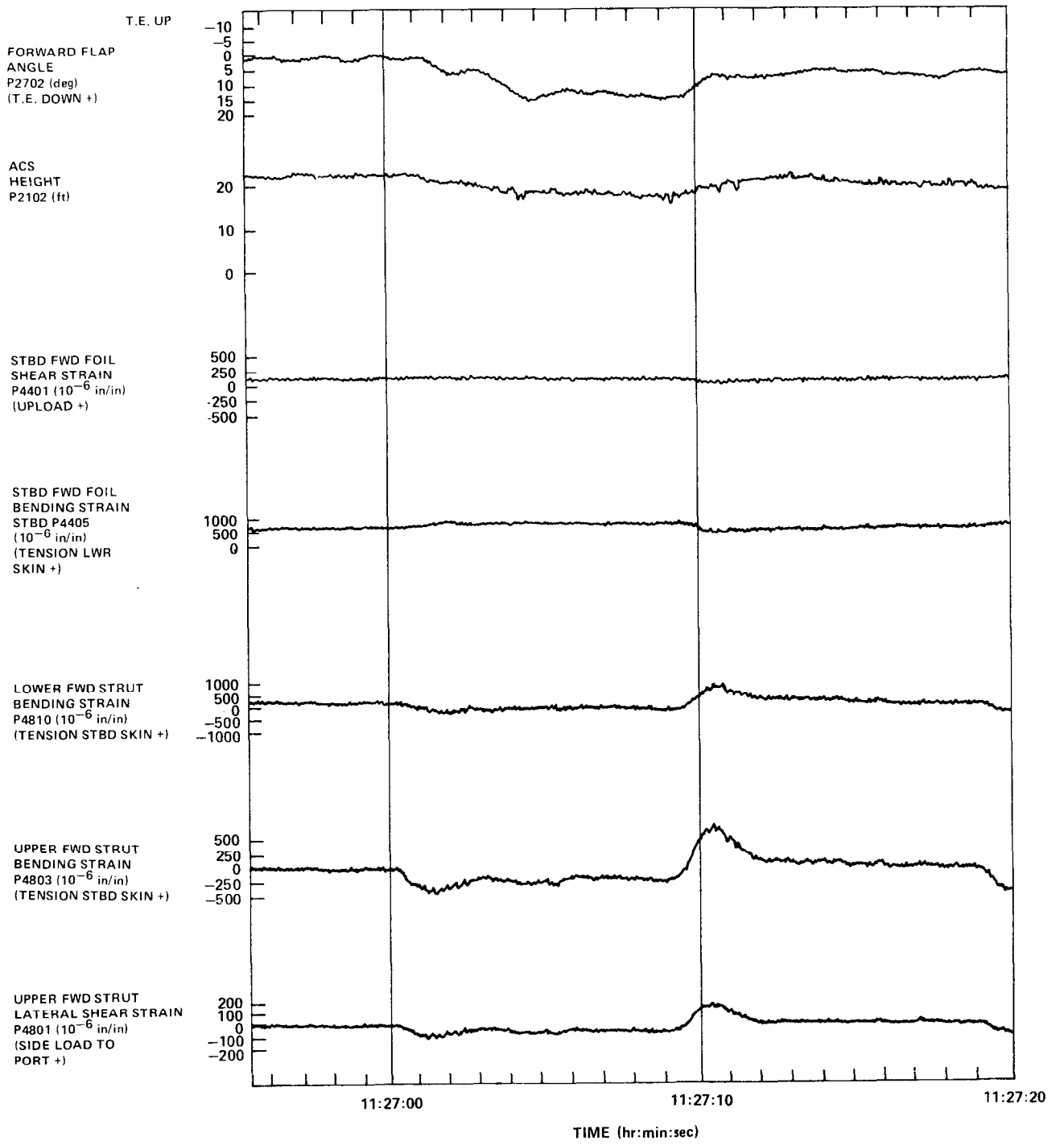

Figure 5 (Continued)

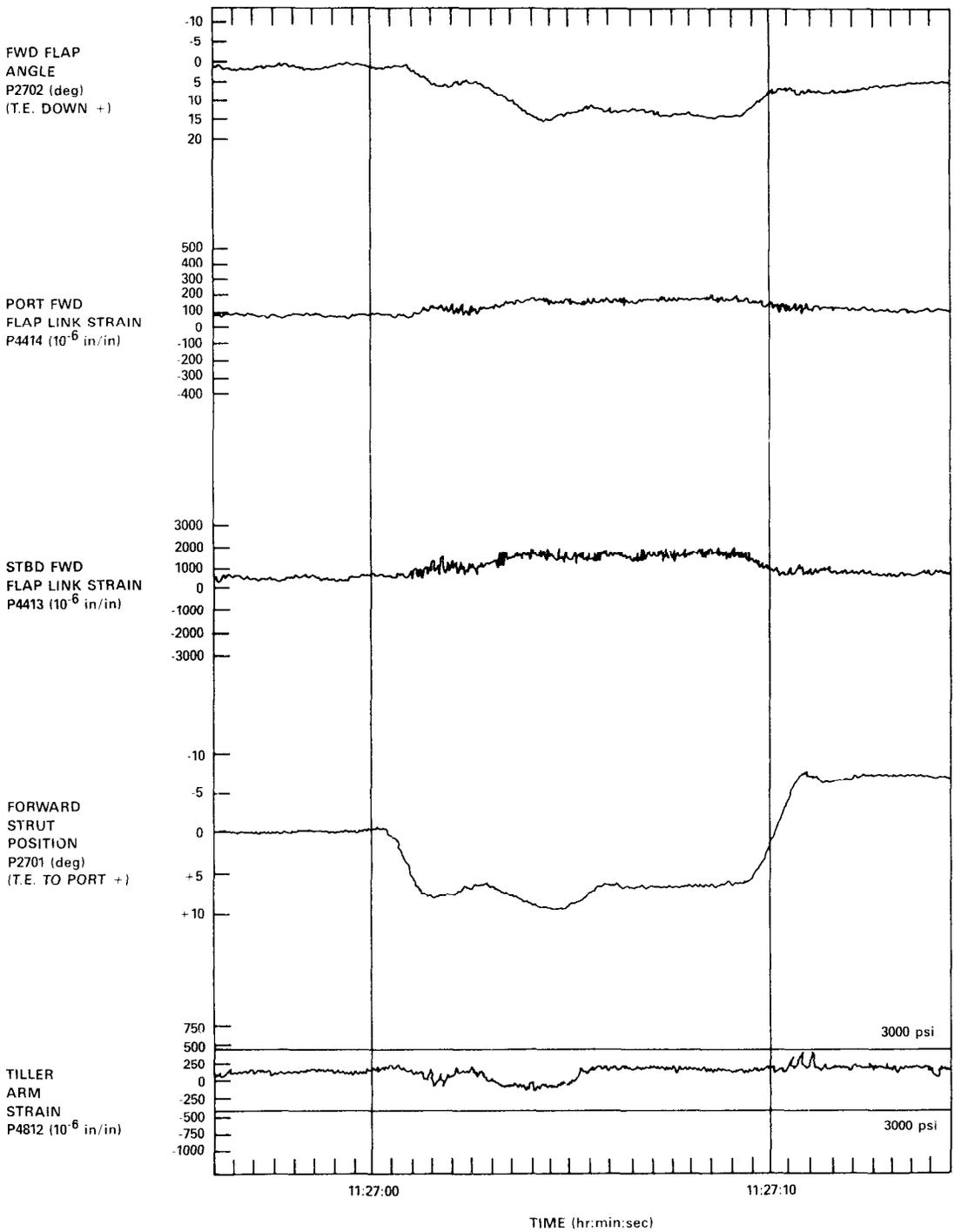

Figure 5 (Continued)

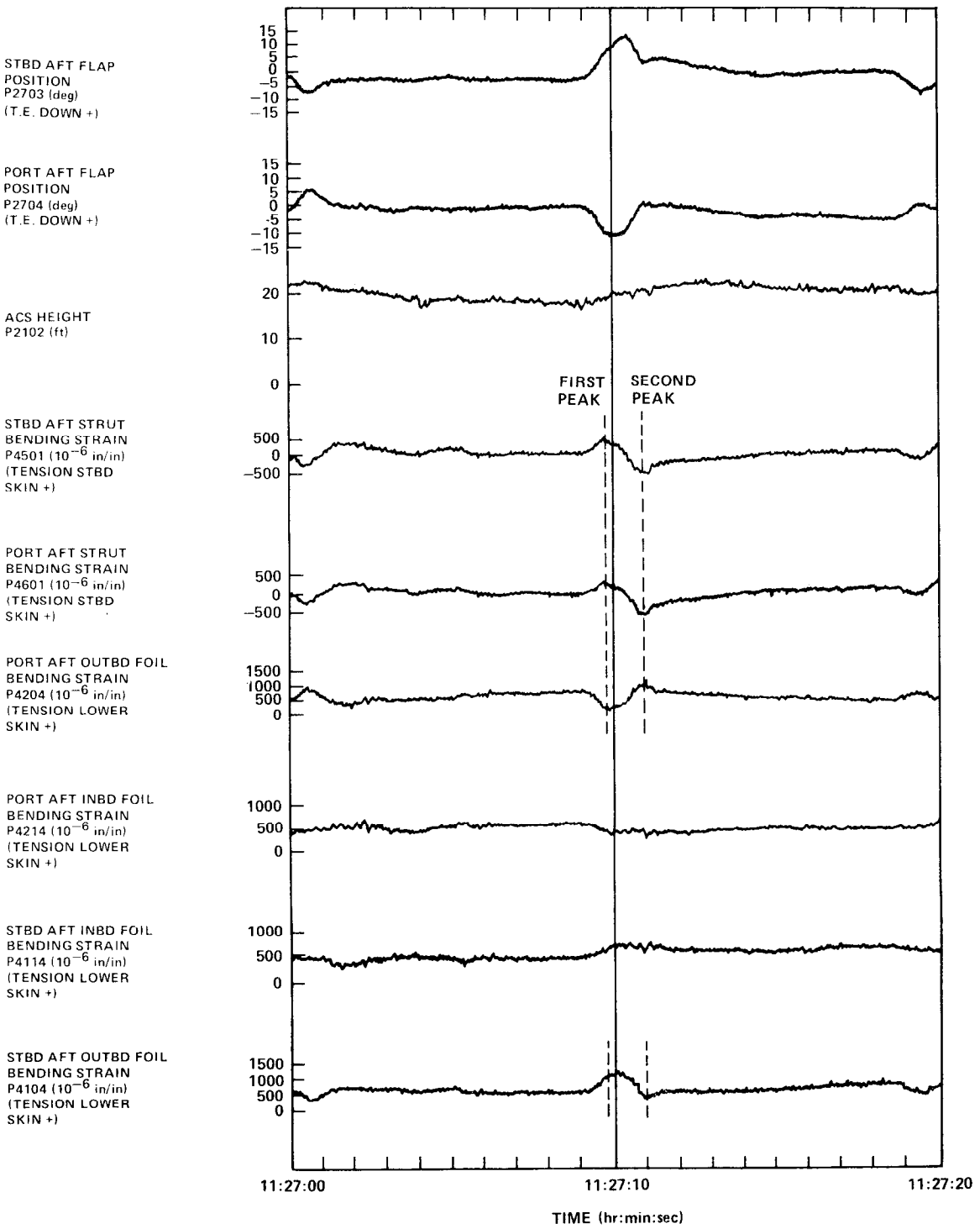

Figure 5 (Continued)

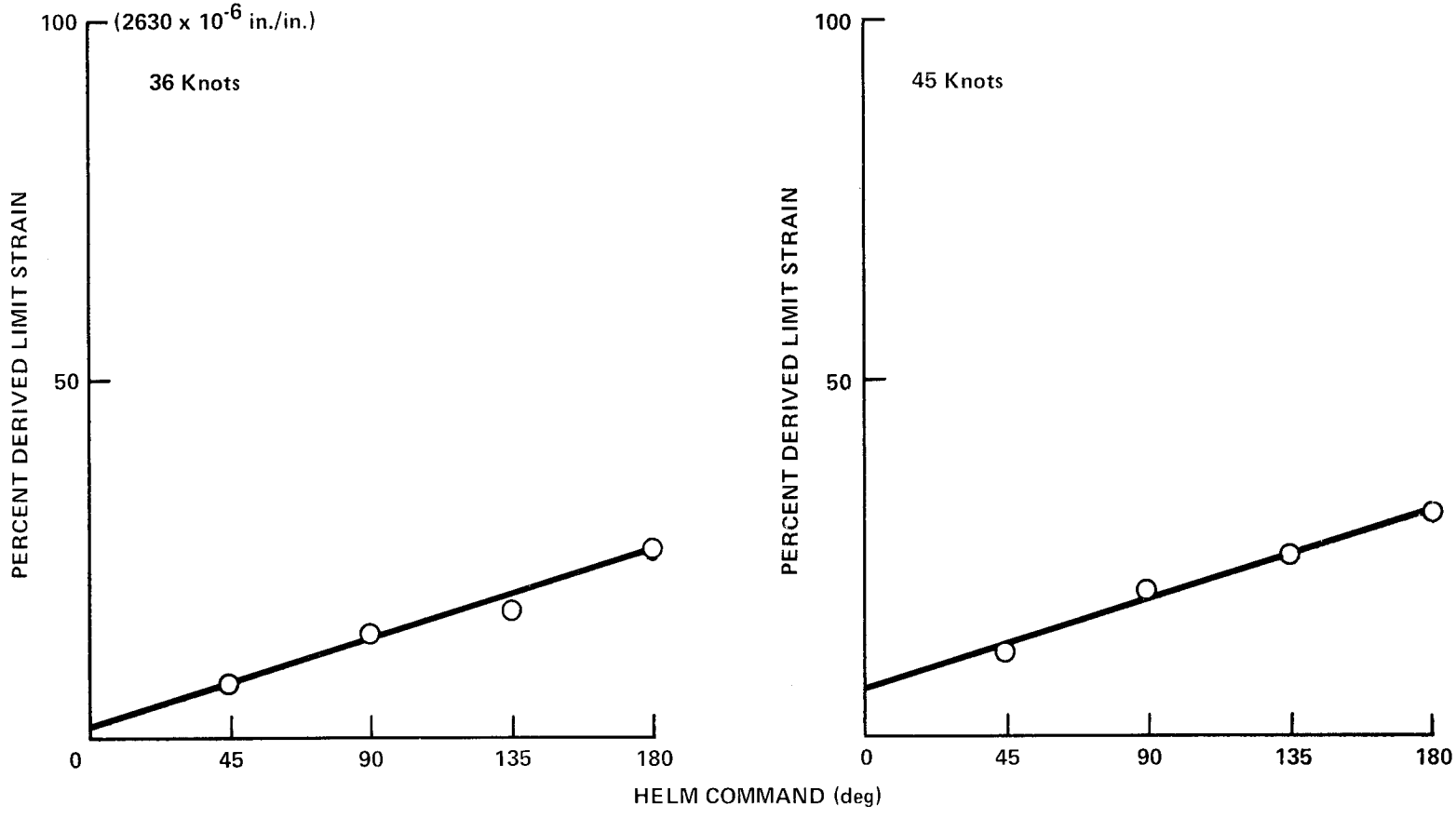

Figure 6 - Maximum Lower Forward Strut Bending Strain (P4810) versus Helm Command During Debris Avoidance Maneuvers

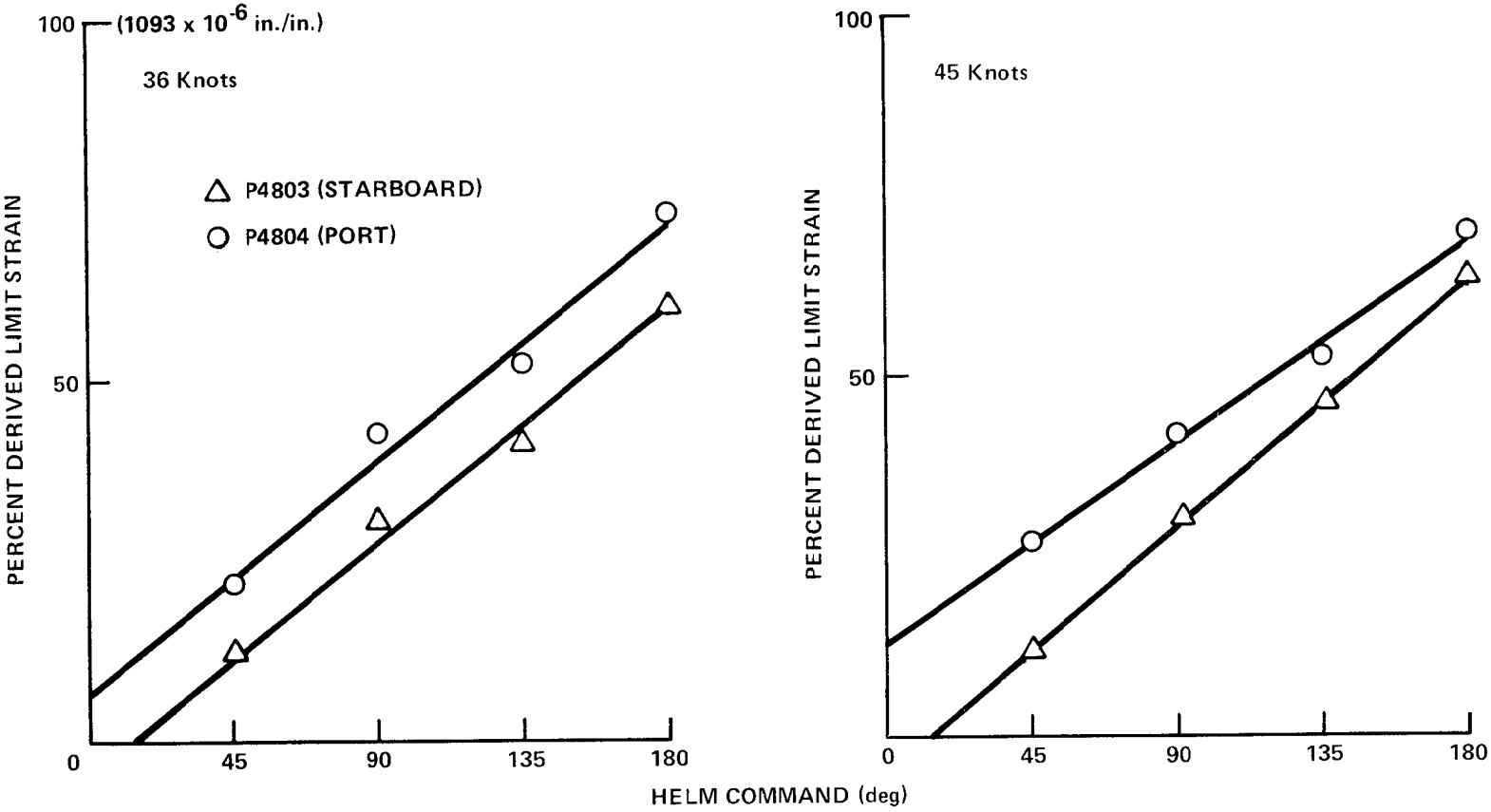

Figure 7 - Maximum Upper Forward Strut Bending Strain (P4803, P4804) versus Helm Command During Debris Avoidance Maneuvers

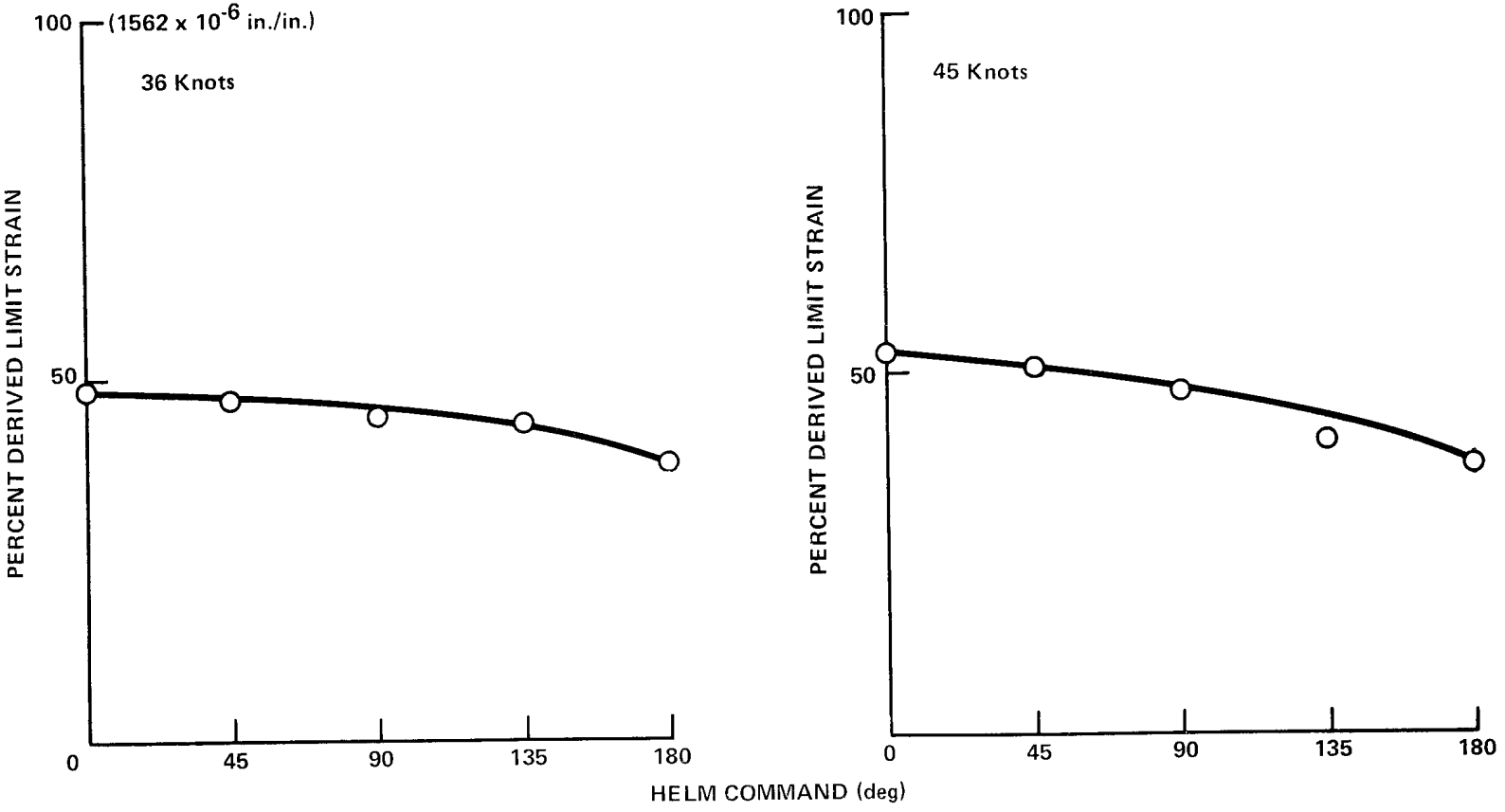

Figure 8 - Maximum Forward Foil Bending Strain, Starboard Semispan, (P4405) versus Helm Command During Debris Avoidance Maneuvers

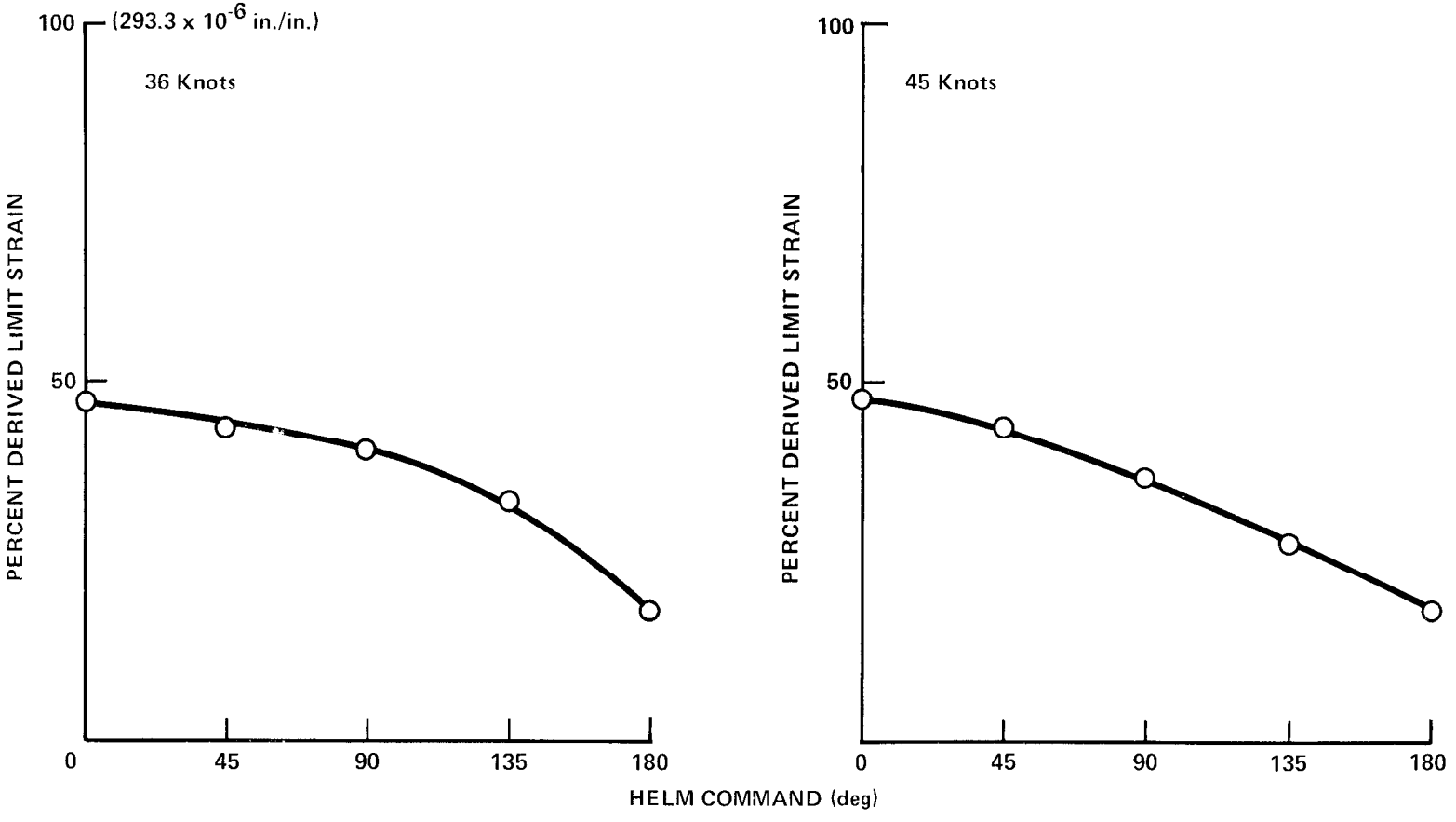

Figure 9 - Maximum Forward Foil Shear Strain, Starboard Semispan, (P4401) versus Helm Command During Debris Avoidance Maneuvers

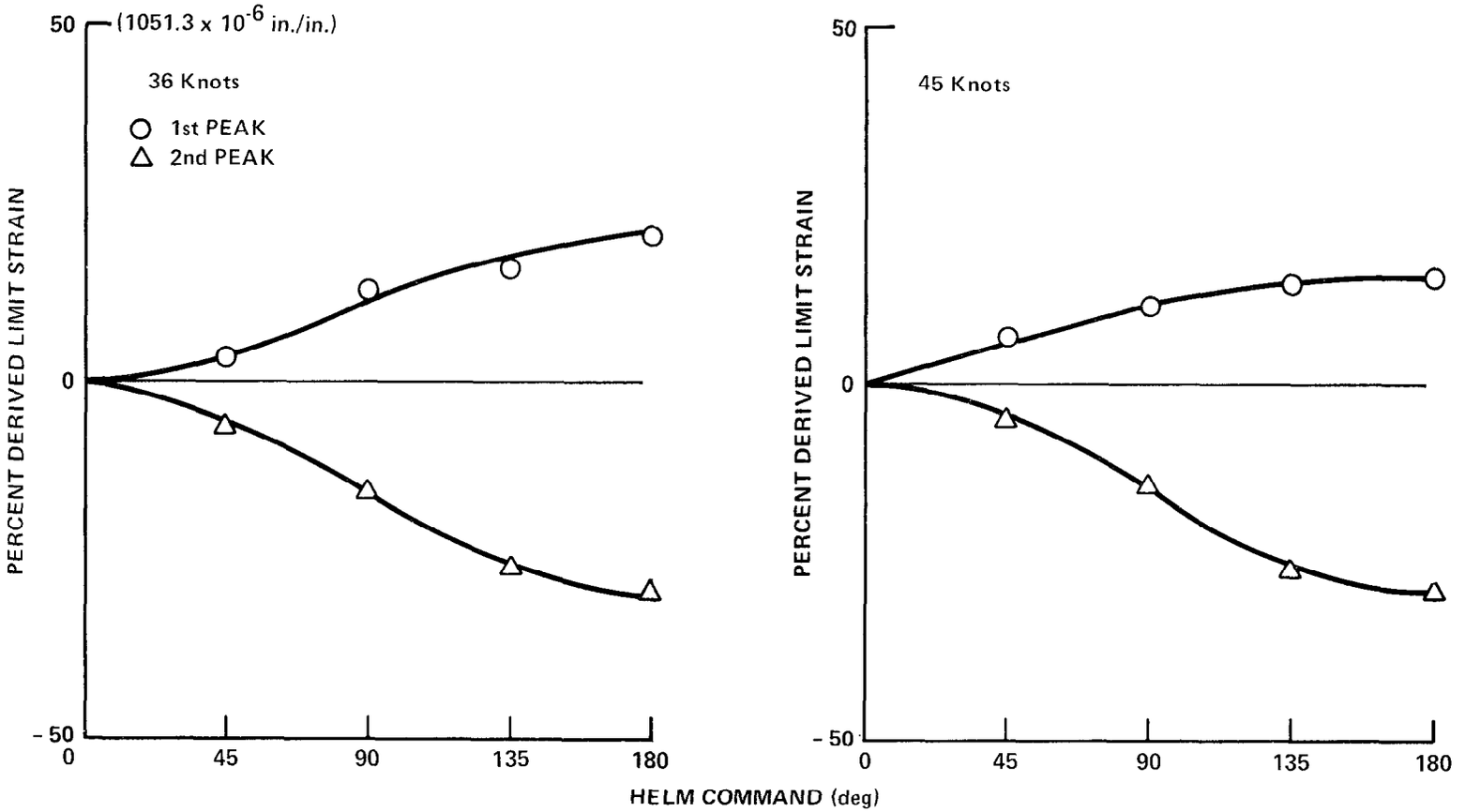

Figure 10 - Maximum Port Aft Strut Bending, Upper End, (P4601) versus Helm Command During Debris Avoidance Maneuvers

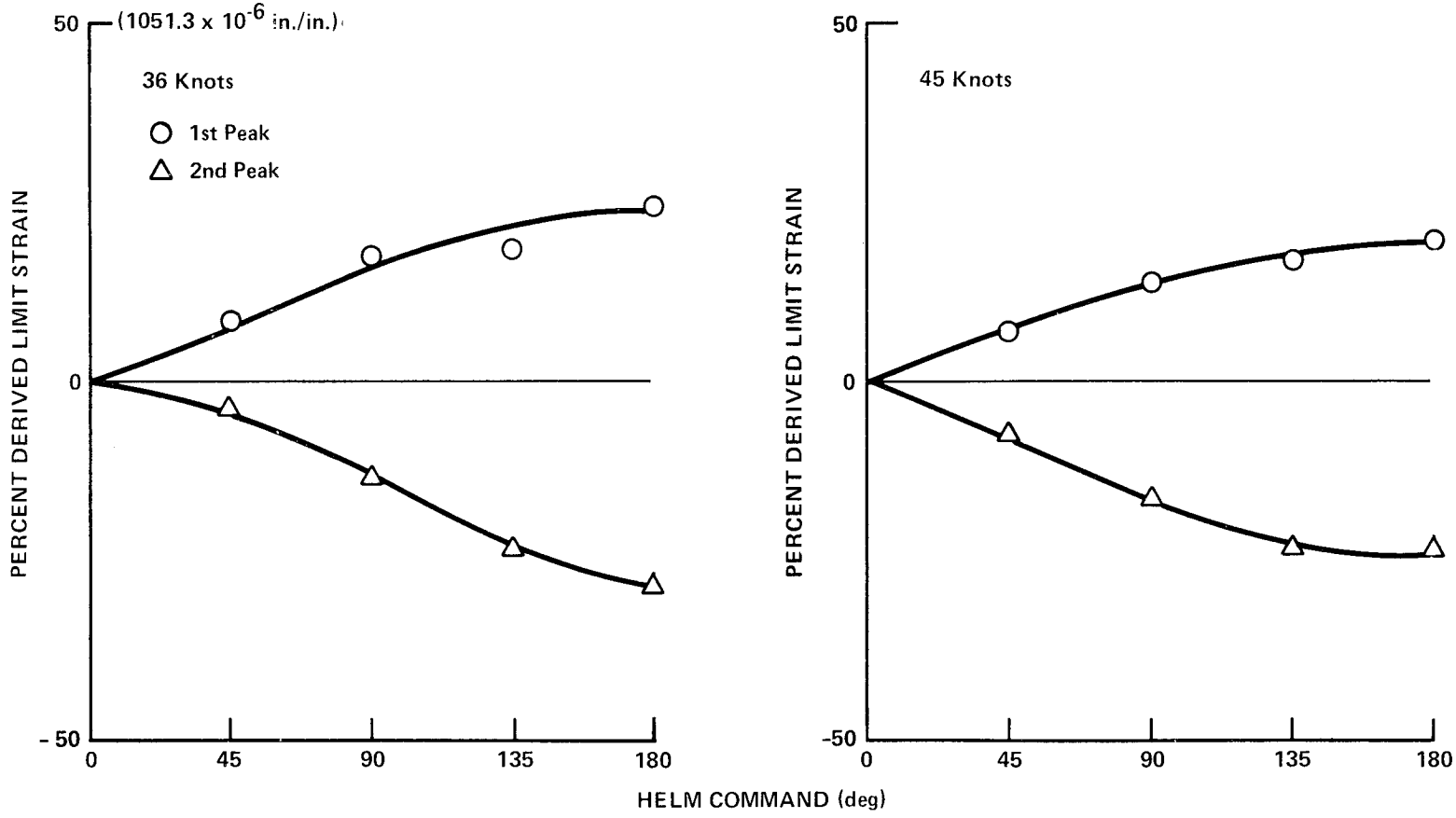

Figure 11 - Maximum Starboard Aft Strut Bending, Upper End, (P4501) versus Helm Command During Debris Avoidance Maneuvers

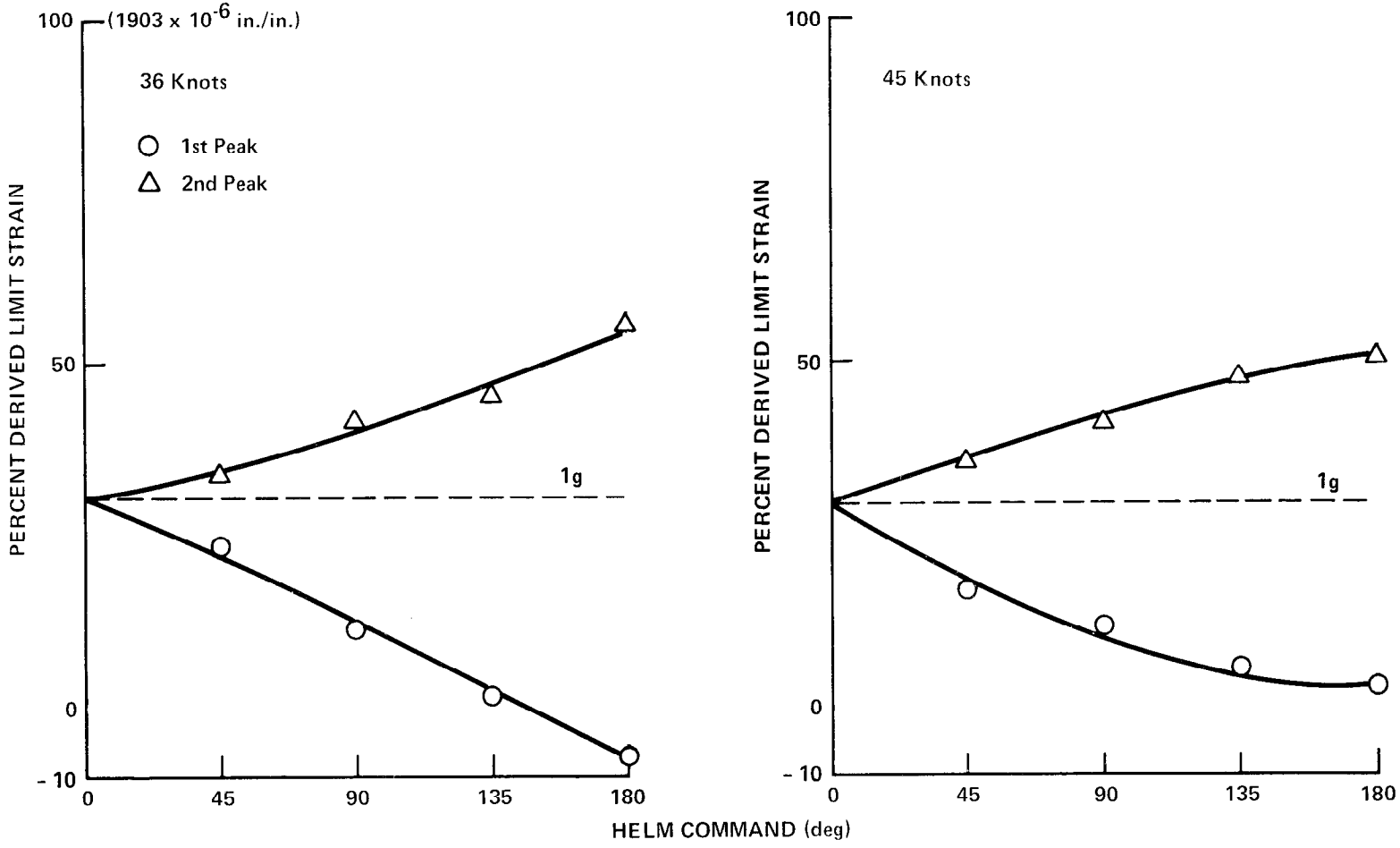

Figure 12 - Maximum Aft Foil Bending Strain, Port Outboard Span, (P4204) versus Helm Command During Debris Avoidance Maneuvers

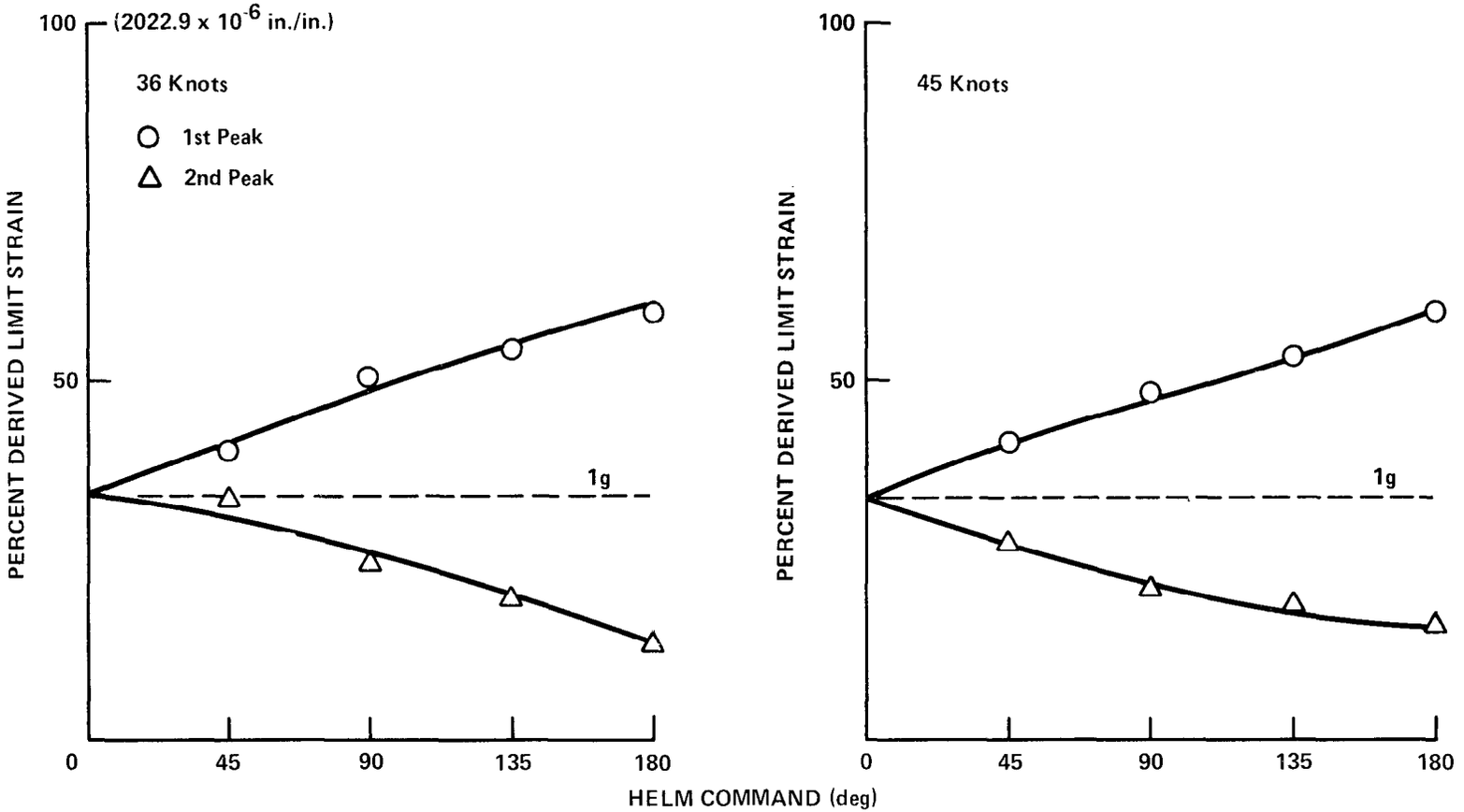

Figure 13 - Maximum Aft Foil Bending Strain, Starboard Outboard Span, (P4104) versus Helm Command During Debris Avoidance Maneuvers

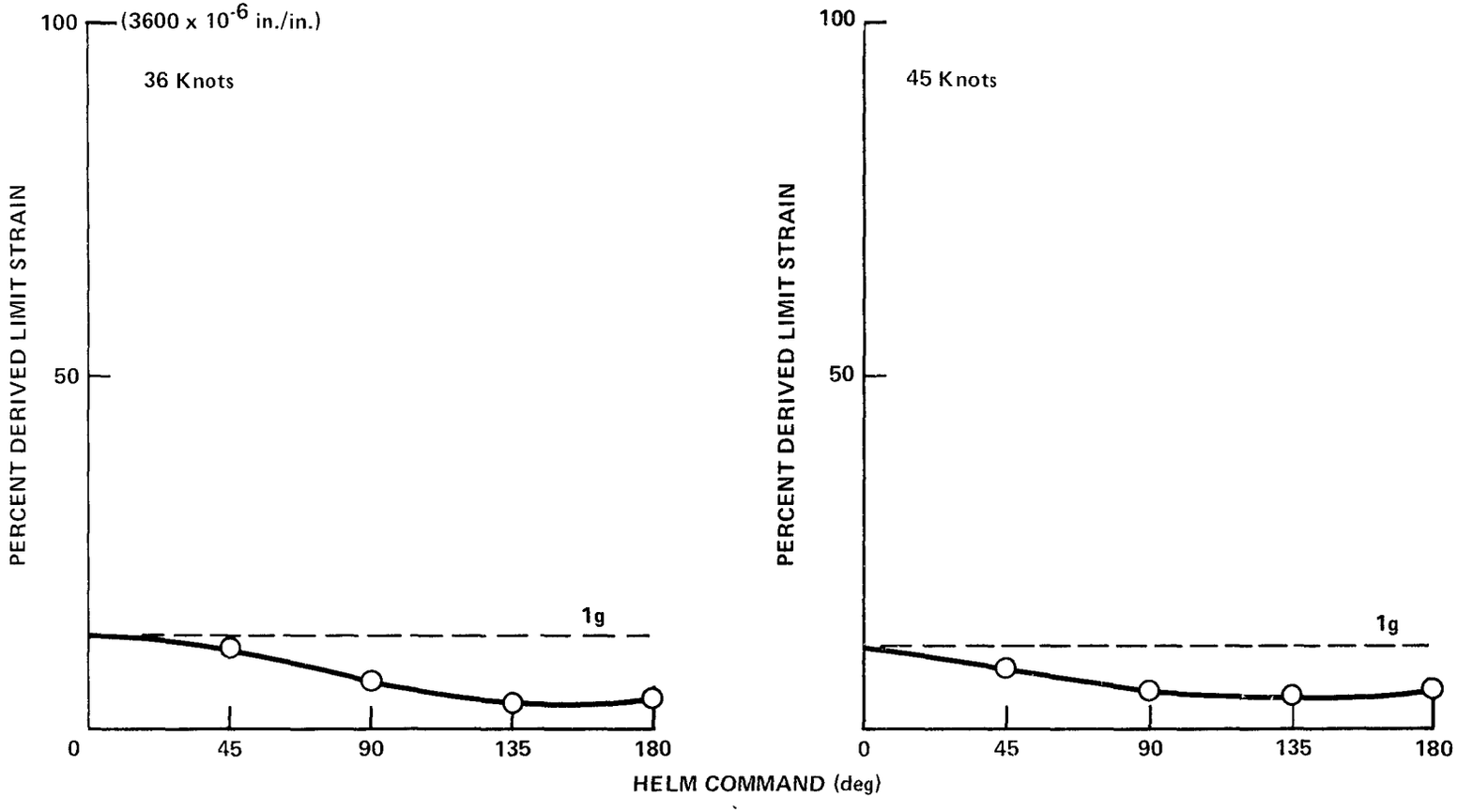

Figure 14 - Maximum Aft Foil Bending Strain, Port Inboard Span, (P4214) versus Helm Command During Debris Avoidance Maneuvers

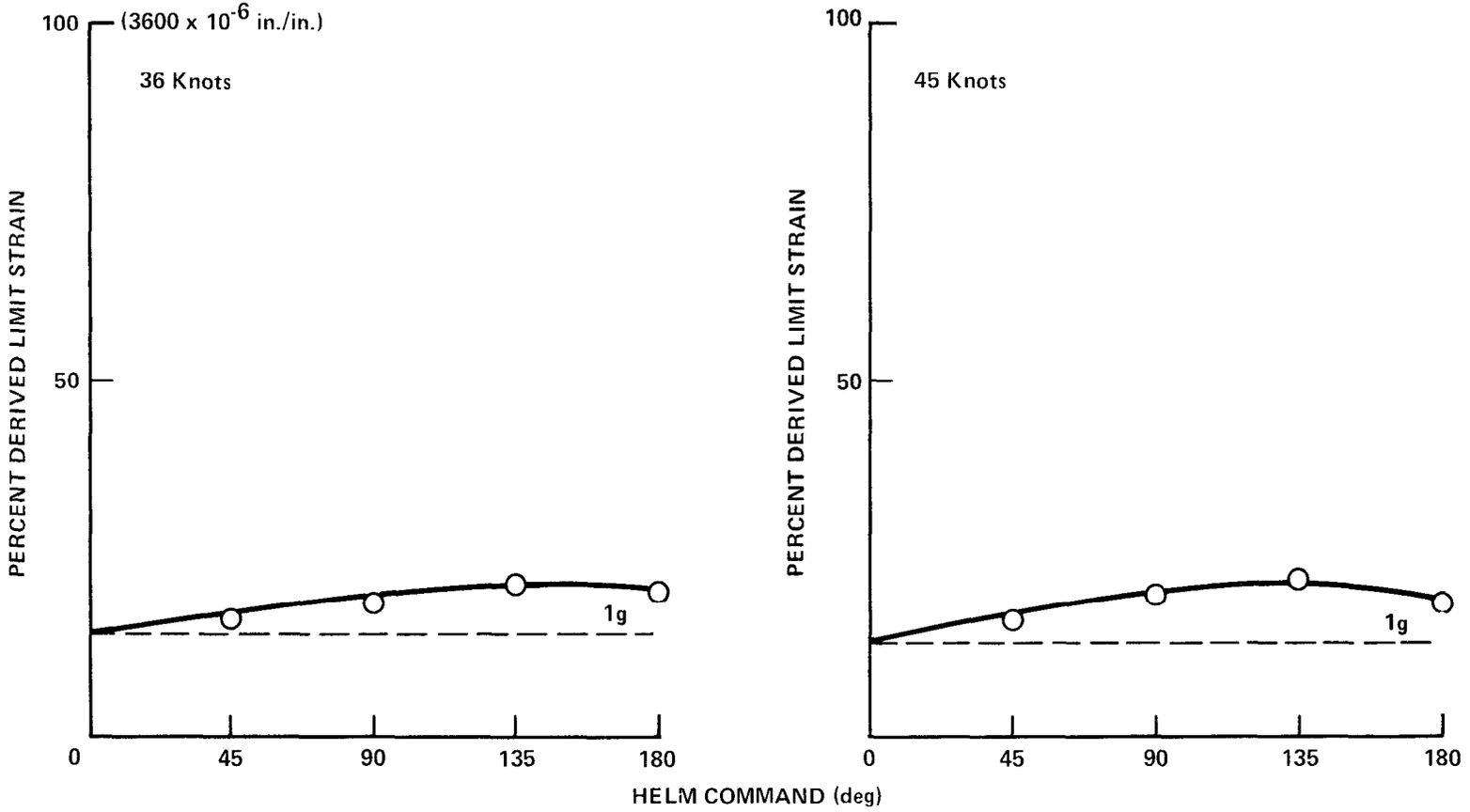

Figure 15 - Maximum Aft Foil Bending Strain, Starboard Inboard Span, (P4114) versus Helm Command During Debris Avoidance Maneuvers

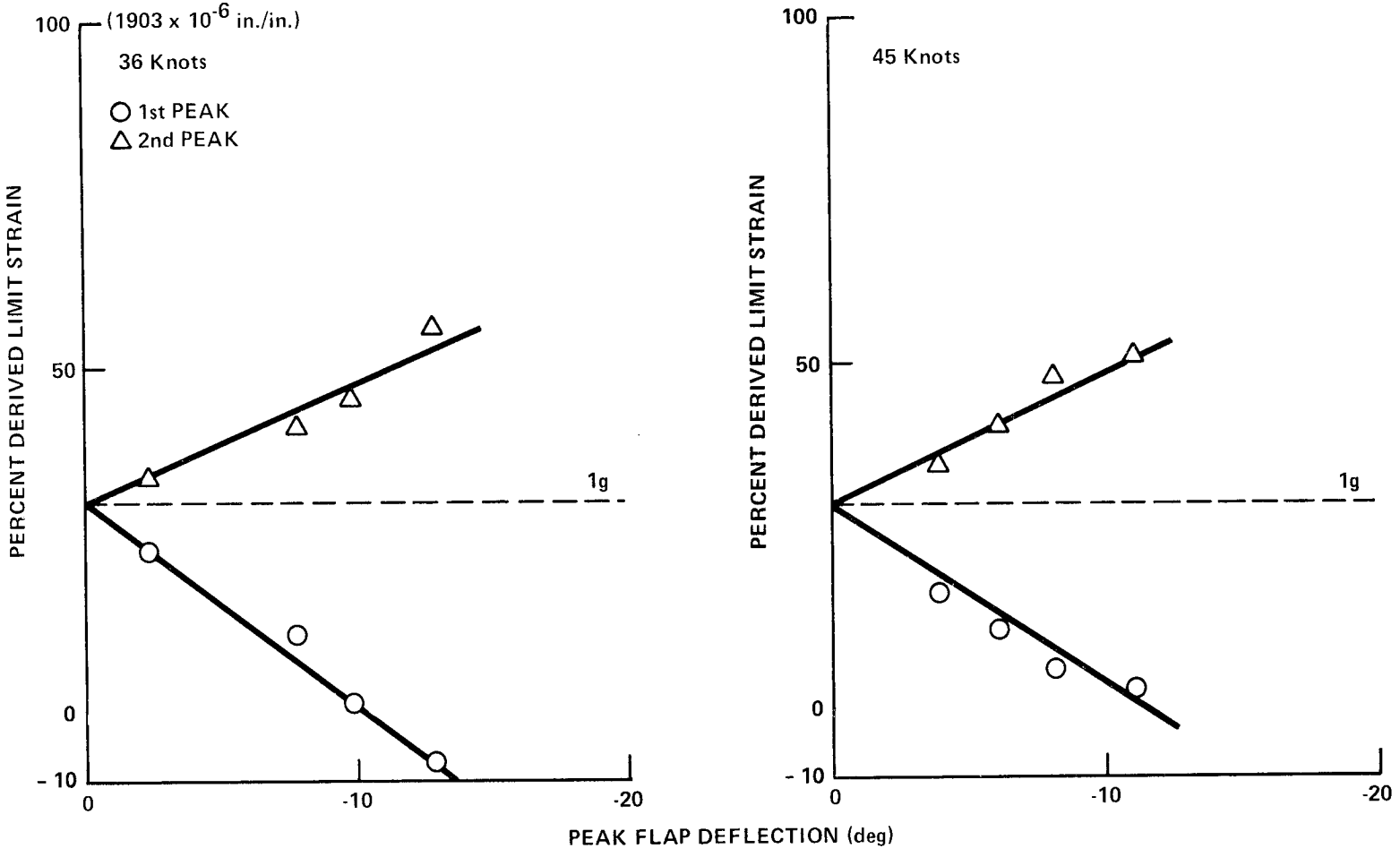

Figure 16 - Maximum Aft Foil Bending Strain, Port Outboard Span, (P4204) versus Maximum Port Flap Deflection During Debris Avoidance Maneuvers

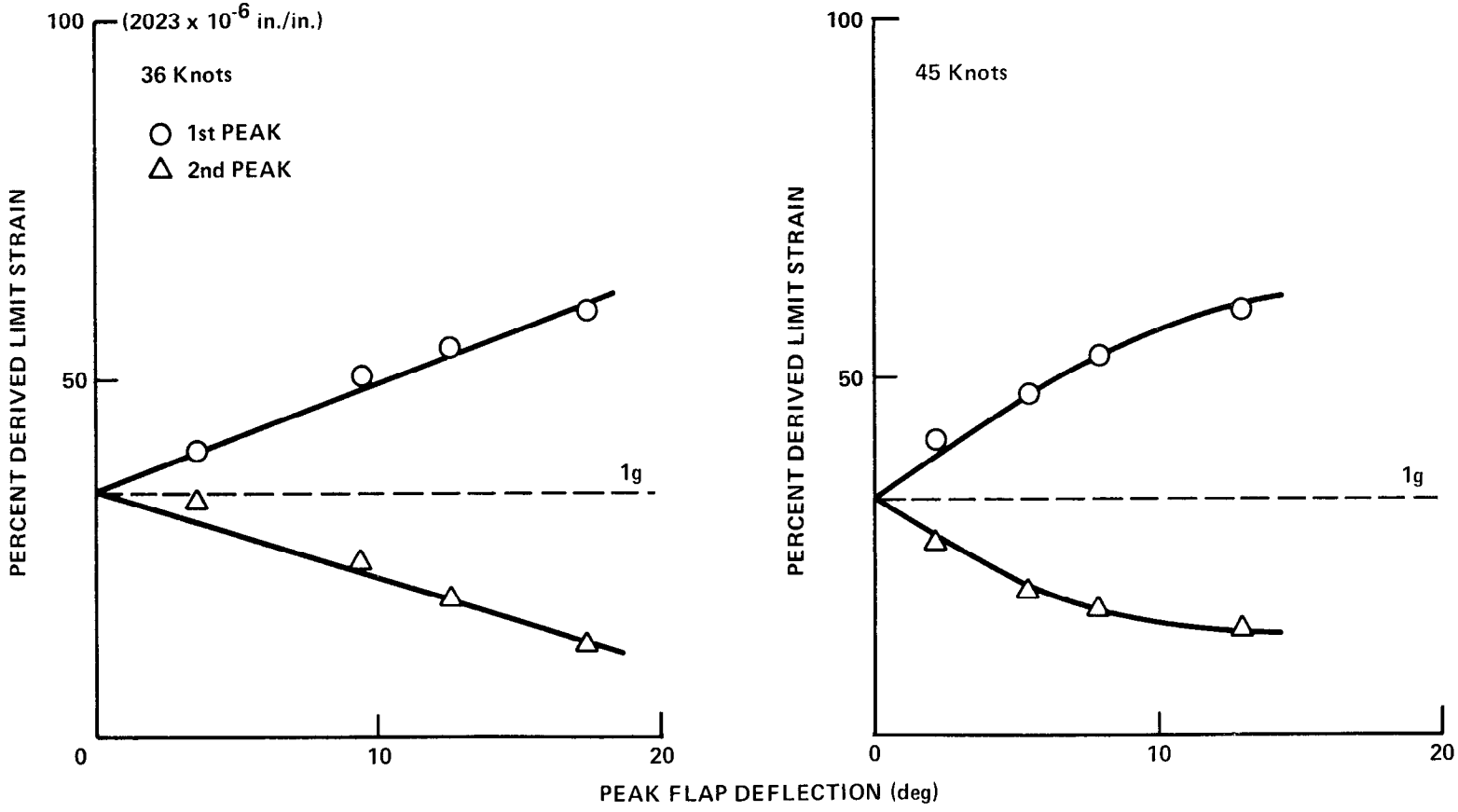

Figure 17 - Maximum Aft Foil Bending Strain, Starboard Outboard Span, (P4104) versus Maximum Starboard Flap Deflection During Debris Avoidance Maneuvers

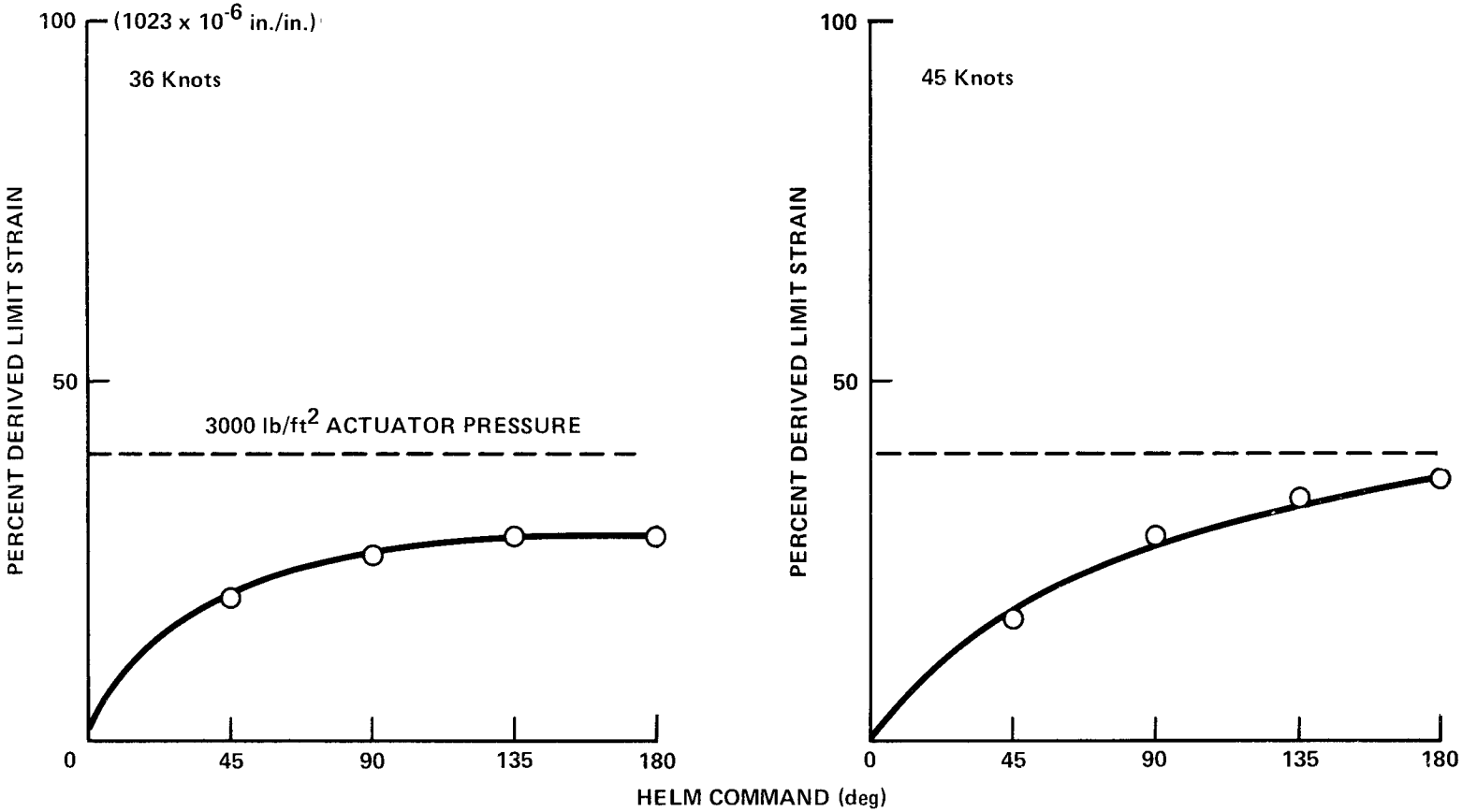

Figure 18 - Maximum Tiller Arm Bending Strain (P4812) versus Helm Command During Debris Avoidance Maneuvers

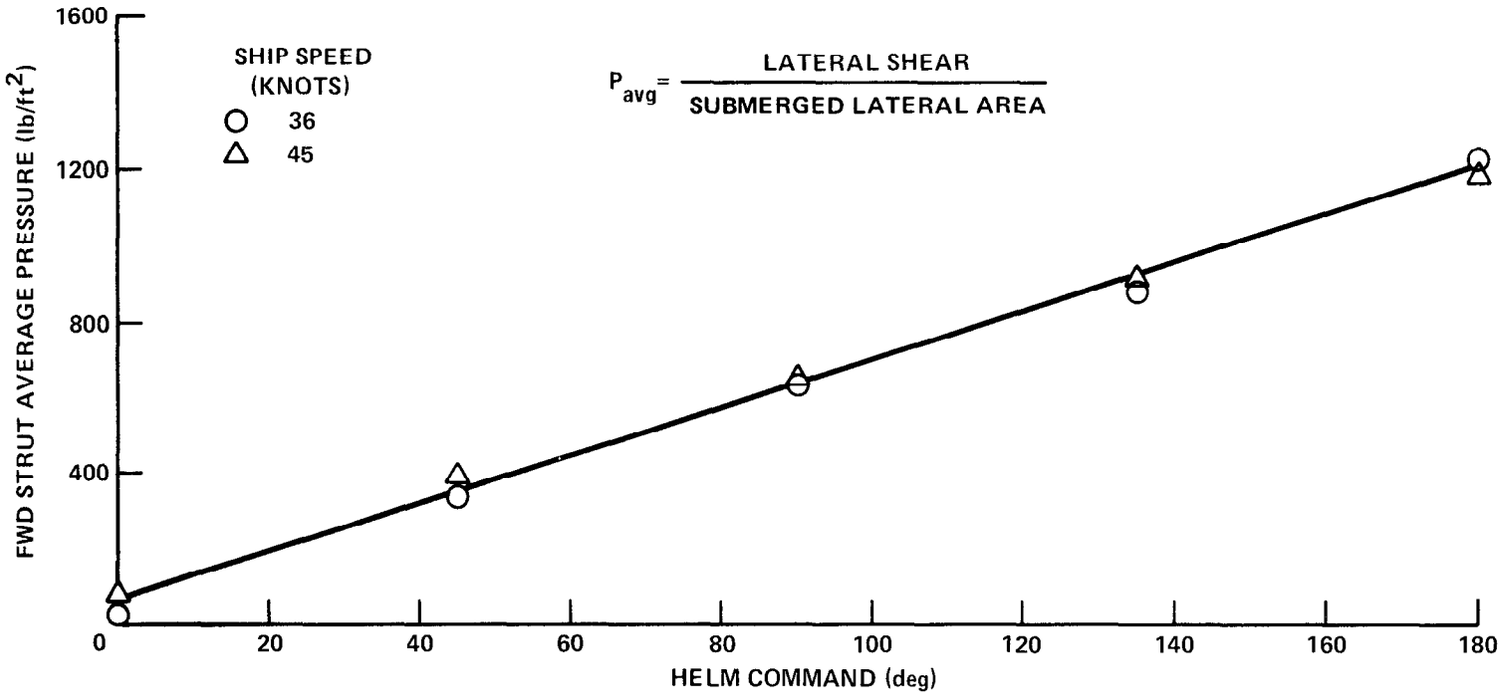

Figure 19 - Maximum Forward Strut Hydrodynamic Loading versus Helm Command During Debris Avoidance Maneuvers

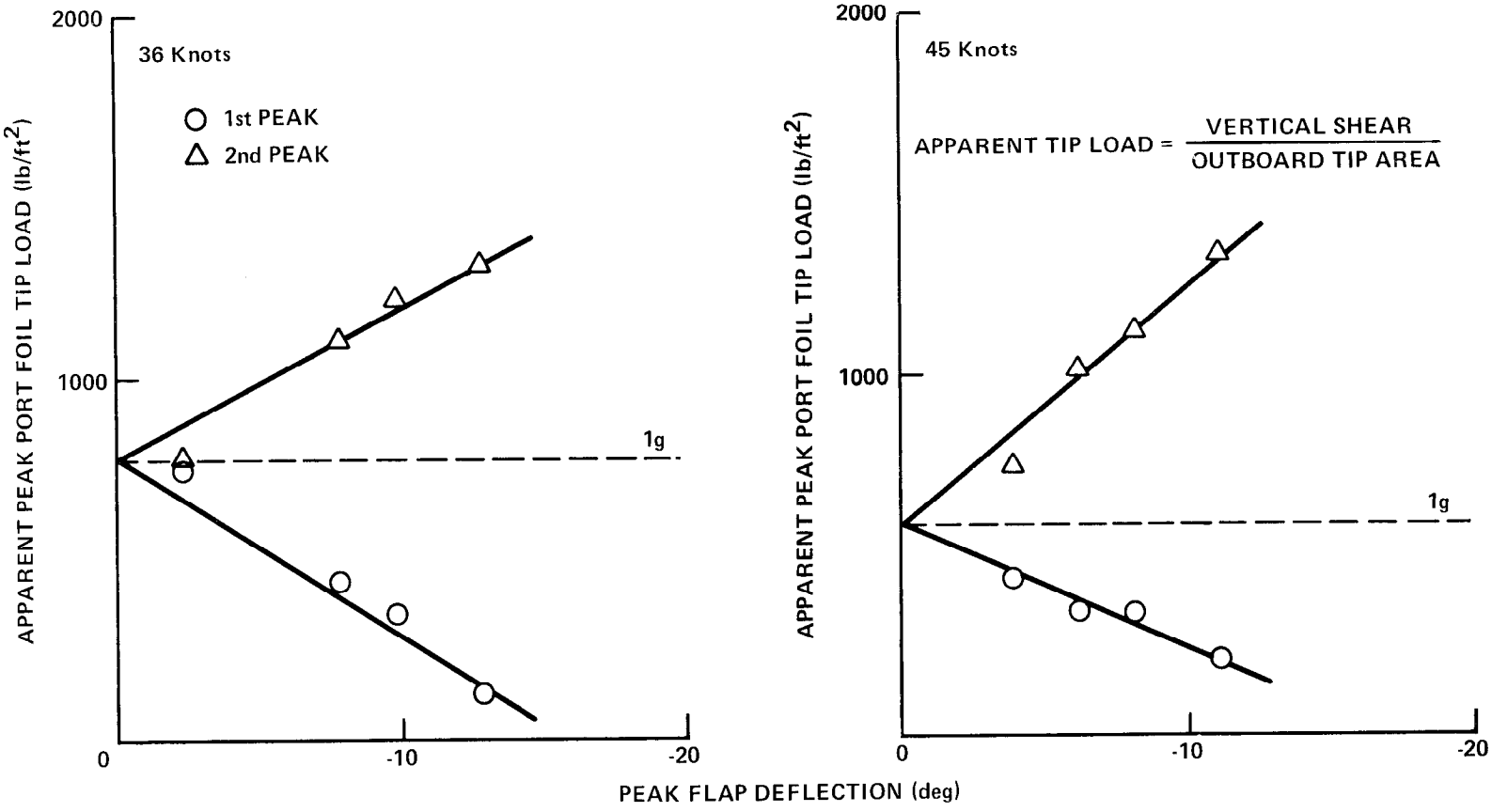

Figure 20 - Apparent Maximum Aft Foil Hydrodynamic Loading, Port Outboard Span, versus Port Flap Deflection During Debris Avoidance Maneuvers

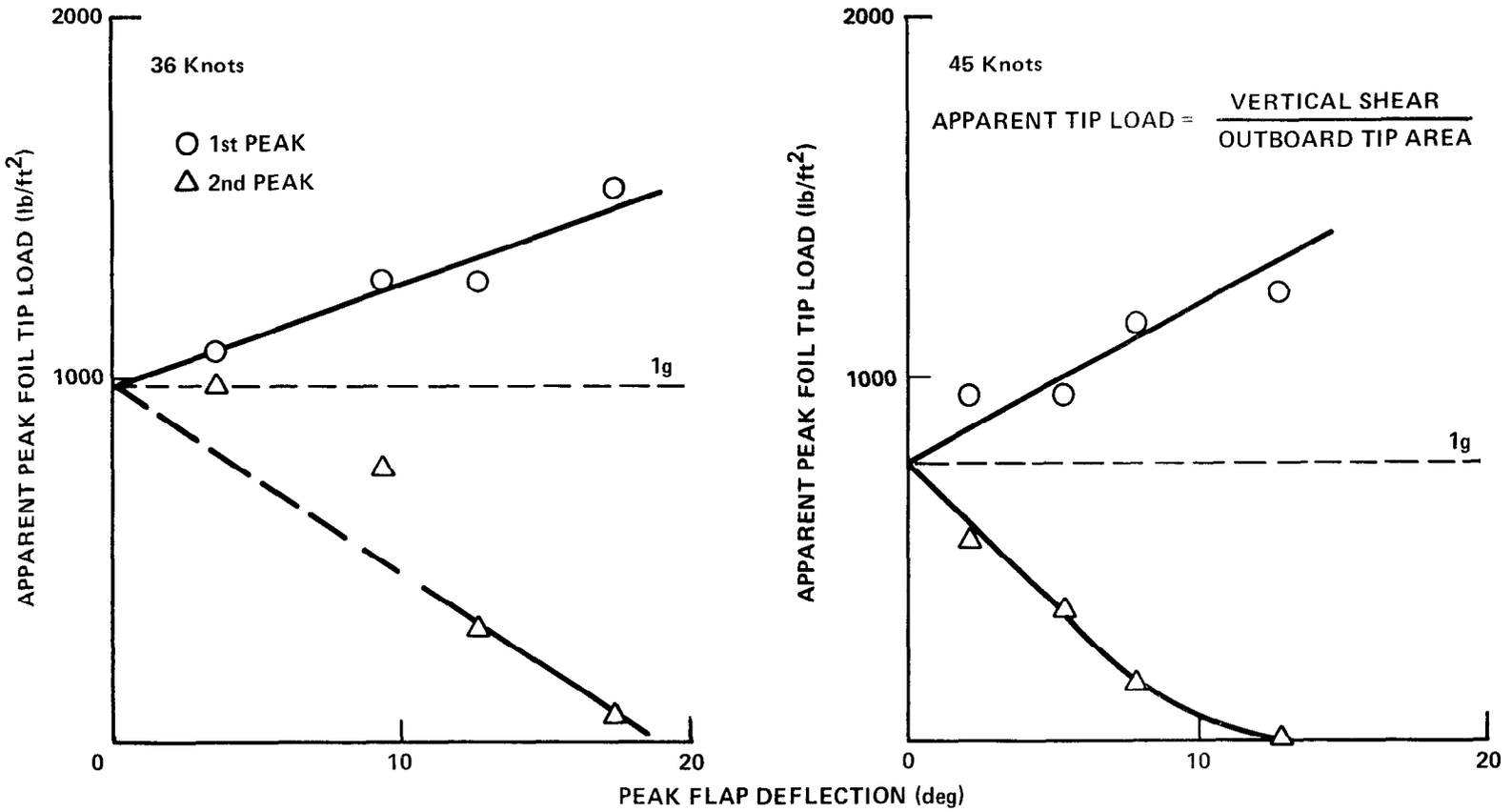

Figure 21 - Apparent Maximum Aft Foil Hydrodynamic Loading, Starboard Outboard Span, versus Starboard Flap Deflection During Debris Avoidance Maneuvers

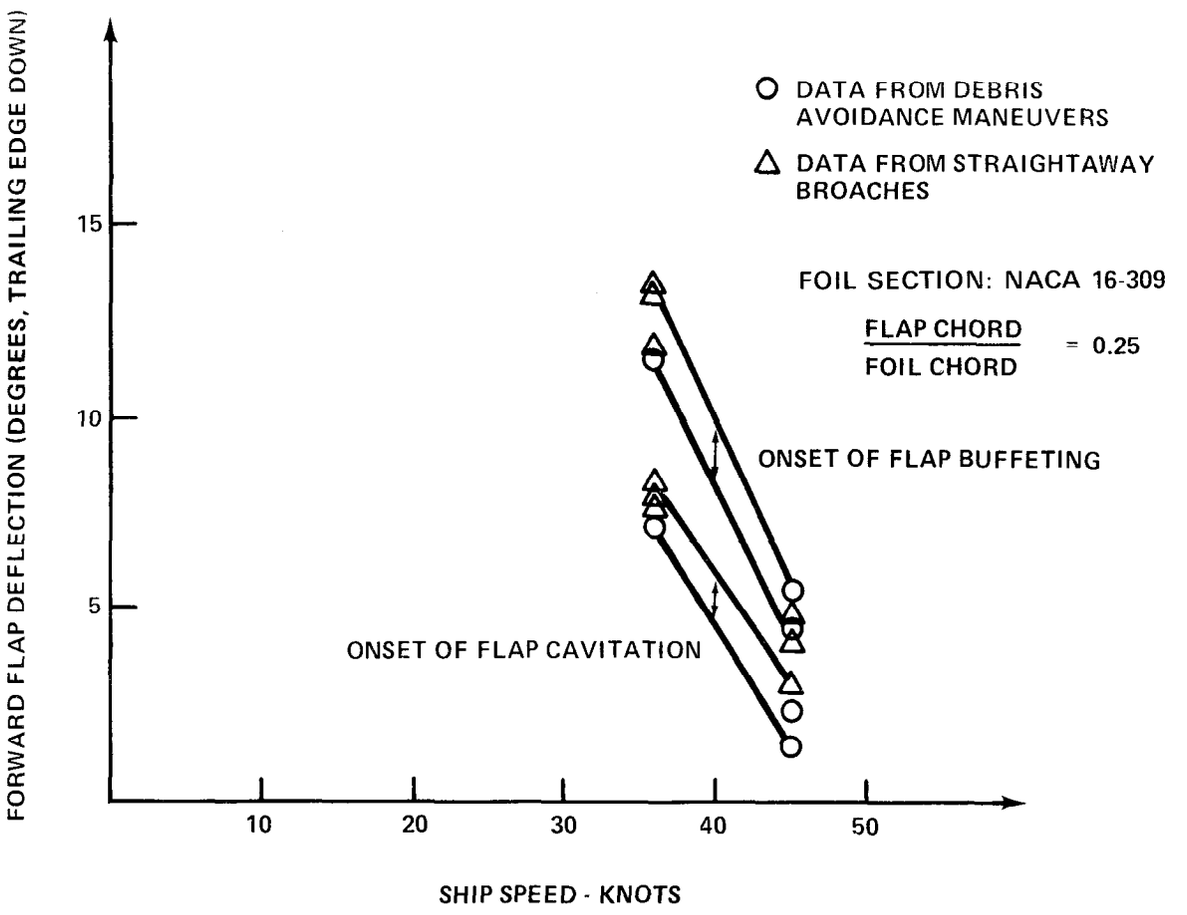

Figure 22 - Forward Flap Deflection for Onset of Cavitation and Buffeting versus Ship's Speed

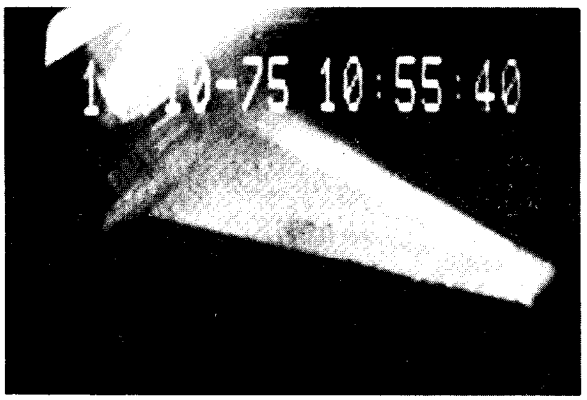

10:55:40.0
STRUT ANGLE = 2.9°
FLAP ANGLE = 2.8°

PORT SEMI SPAN
HELM ANGLE = 45°
ROLL ANGLE = 4.70°

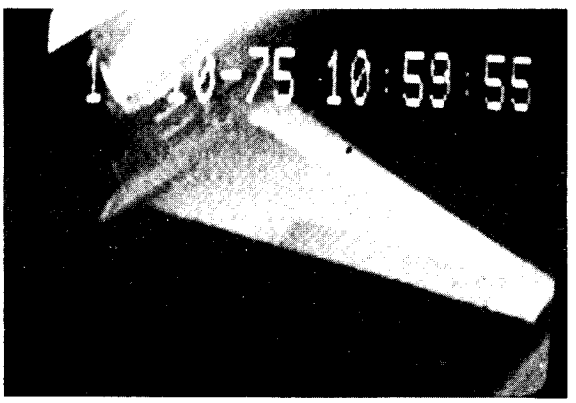

10:59:55.96
STRUT ANGLE = 5.4°
FLAP ANGLE = 5.6°

PORT SEMI SPAN
HELM ANGLE = 90°
ROLL ANGLE = 9.13°

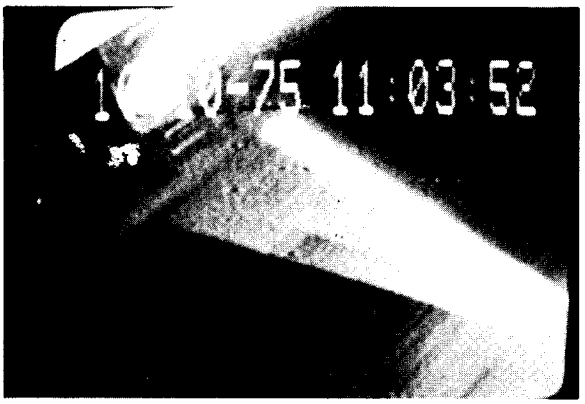

11:03:52.0
STRUT ANGLE = 7.0°
FLAP ANGLE = 9.7°

PORT SEMI SPAN
HELM ANGLE = 135°
ROLL ANGLE = 14.2°

11:08:43.60
STRUT ANGLE = 9.7°
FLAP ANGLE = 13.5°

PORT SEMI SPAN
HELM ANGLE = 180°
ROLL ANGLE = 18.3°

Figure 23 - Forward Foil Flow--Steady Starboard Turns at 36 Knots for Helm Angles of 45°, 90°, 135°, and 180°

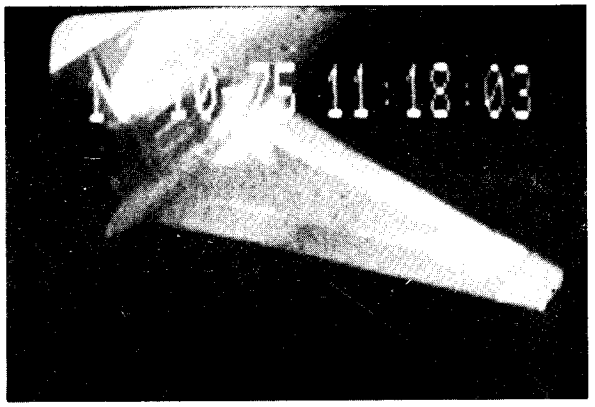

11:18:03.0
STRUT ANGLE = 2.3°
FLAP ANGLE = 1.7°

PORT SEMI SPAN
HELM ANGLE = 45°
ROLL ANGLE = 4.70°

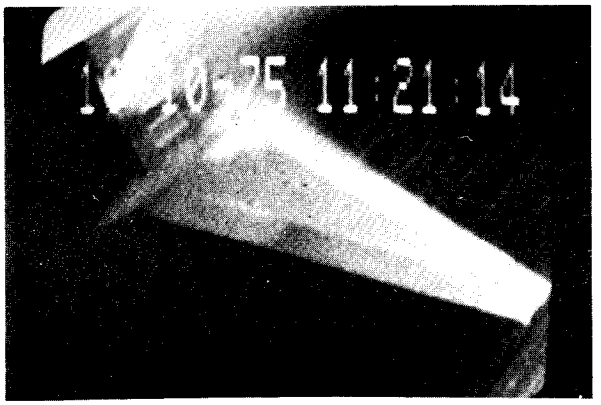

11:21:14.0
STRUT ANGLE = 4.7°
FLAP ANGLE = 3.0°

PORT SEMI SPAN
HELM ANGLE = 90°
ROLL ANGLE = 8.87°

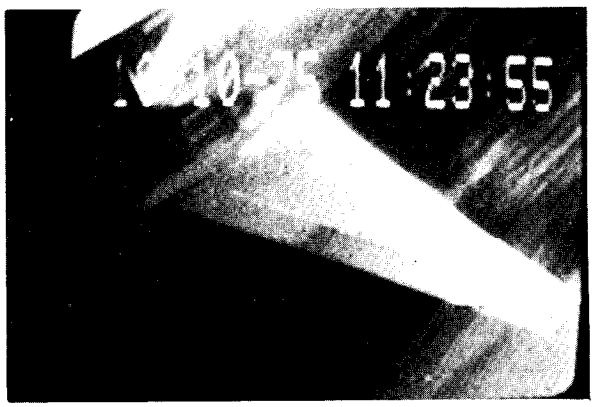

11:23:55.16
STRUT ANGLE = 6.5°
FLAP ANGLE = 5.7°

PORT SEMI SPAN
HELM ANGLE = 135°
ROLL ANGLE = 13.97°

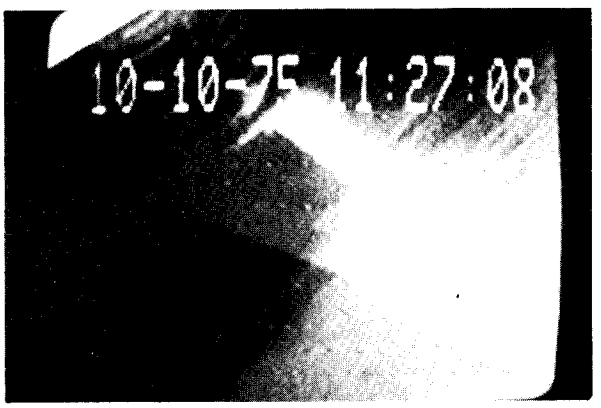

11:27:08.0
STRUT ANGLE = 10.7°
FLAP ANGLE = 13.8°

PORT SEMI SPAN
HELM ANGLE = 180°
ROLL ANGLE = 18.27°

Figure 24 - Forward Foil Flow--Steady Starboard Turns at 45 Knots for Helm Angles of 45°, 90°, 135°, and 180°

11:08:43.84
STRUT ANGLE = 9.3°
FLAP ANGLE = 13.8°

PORT SEMI SPAN
ROLL ANGLE = 17.5°

11:08:44.04
STRUT ANGLE = 7.1°
FLAP ANGLE = 13.8°

PORT SEMI SPAN
ROLL ANGLE = 16.4°

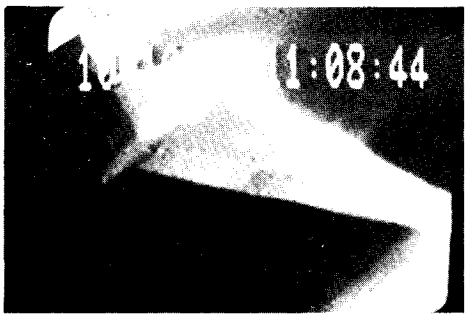

11:08:44.16
STRUT ANGLE = 5.6°
FLAP ANGLE = 13.2°

PORT SEMI SPAN
ROLE ANGLE = 15.1°

11:08:44.28
STRUT ANGLE = 3.1°
FLAP ANGLE = 12.6°

PORT SEMI SPAN
ROLL ANGLE = 13.7°

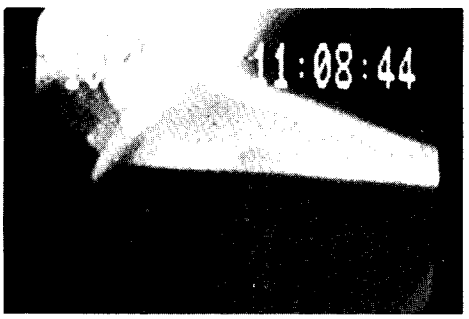

11:08:44:80
STRUT ANGLE = −5.0°
FLAP ANGLE = 9.7°

PORT SEMI SPAN
ROLL ANGLE = 5.4°

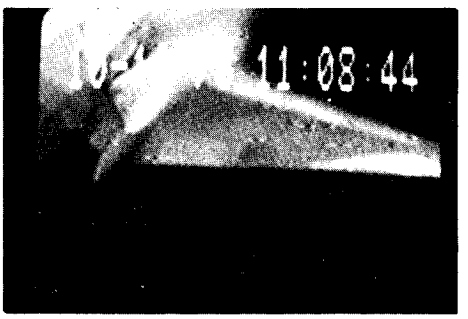

11:08:44.96
STRUT ANGLE = −7.2°
FLAP ANGLE = 9.3°

PORT SEMI SPAN
ROLL ANGLE = 1.2°

Figure 25 - Forward Foil Flow--Debris Avoidance Maneuver, Initial 180° Starboard Helm 36 Knots

11:08:45.12
STRUT ANGLE = −12.4°
FLAP ANGLE = 8.2°

PORT SEMI SPAN
ROLL ANGLE = 2.0°

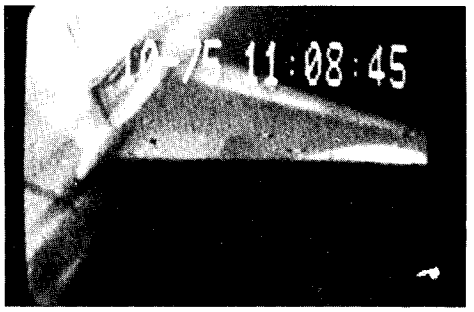

11:08:45.38
STRUT ANGLE = −9.7°
FLAP ANGLE = 7.9°

PORT SEMI SPAN
ROLL ANGLE = −5.6°

11:08:45.54
STRUT ANGLE = −10.2°
FLAP ANGLE = 7.8°

PORT SEMI SPAN
ROLE ANGLE = −7.0°

Figure 25 (Continued)

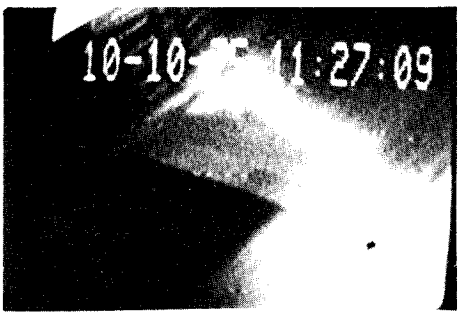

11:27:09.60
STRUT ANGLE = 8.6°
FLAP ANGLE = 13.5°

PORT SEMI SPAN
ROLL ANGLE = 16.5°

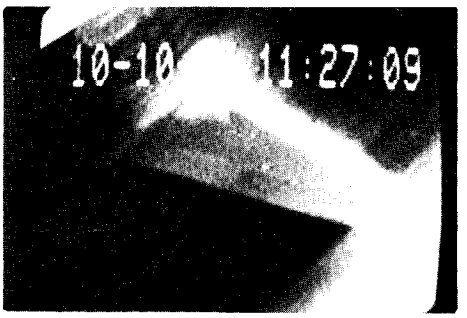

11:27:09.76
STRUT ANGLE = 7.4°
FLAP ANGLE = 11.7°

PORT SEMI SPAN
ROLL ANGLE = 15.5°

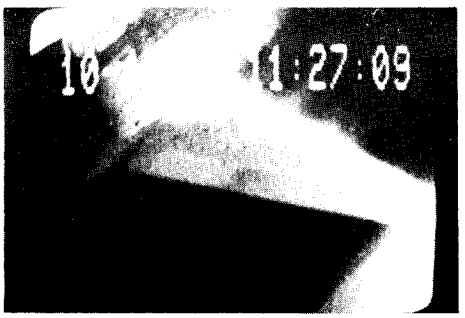

11:27:09.92
STRUT ANGLE = 5.6°
FLAP ANGLE = 10.6°

PORT SEMI SPAN
ROLE ANGLE = 14.2°

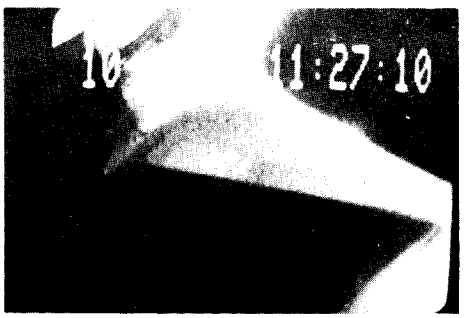

11:27:10.09
STRUT ANGLE = 3.4°
FLAP ANGLE = 9.7°

PORT SEMI SPAN
ROLL ANGLE = 11.0°

11:27:10.17
STRUT ANGLE = 1.9°
FLAP ANGLE = 8.7°

PORT SEMI SPAN
ROLL ANGLE = 10.0°

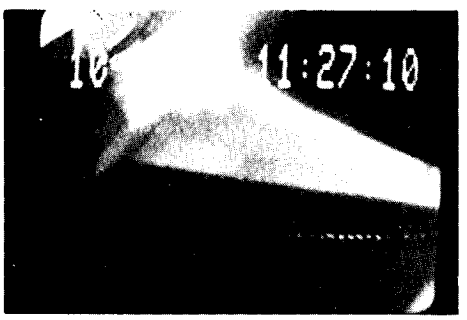

11:27:10.24
STRUT ANGLE = 0.2°
FLAP ANGLE = 8.3°

PORT SEMI SPAN
ROLL ANGLE = 8.5°

Figure 26 - Forward Foil Flow--Debris Avoidance Maneuver, Initial 180° Starboard Helm, 45 Knots

11:27:10.32
STRUT ANGLE = −0.2°
FLAP ANGLE = 8.5°

PORT SEMI SPAN
ROLL ANGLE = 7.25°

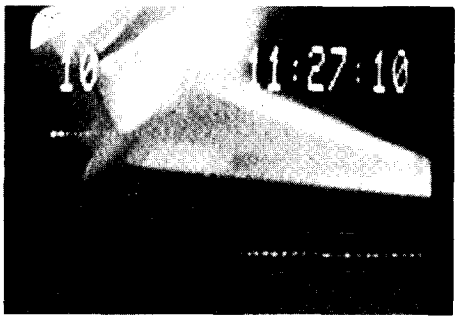

11:27:10.40
STRUT ANGLE = −2.5°
FLAP ANGLE = 8.0°

PORT SEMI SPAN
ROLL ANGLE = 6.1°

11:27:10.60
STRUT ANGLE = −3.9°
FLAP ANGLE = 7.6°

PORT SEMI SPAN
ROLL ANGLE = 1.75°

11:27:10.80
STRUT ANGLE = −6.7°
FLAP ANGLE = 7.6°

PORT SEMI SPAN
ROLL ANGLE = −2.4°

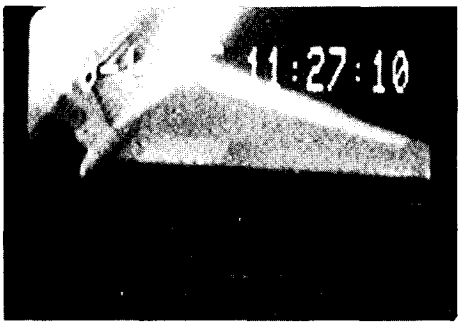

11:27:10.96
STRUT ANGLE = −7.6°
FLAP ANGLE = 7.9°

PORT SEMI SPAN
ROLL ANGLE = −4.2°

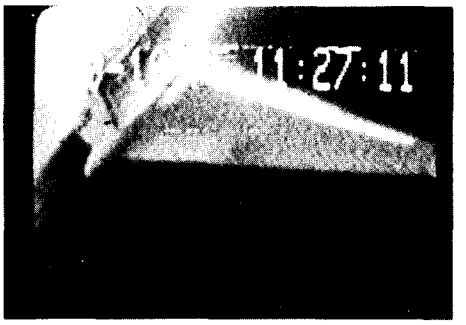

11:27:11.11
STRUT ANGLE = −7.3°
FLAP ANGLE = 8.2°

PORT SEMI SPAN
ROLL ANGLE = −5.8°

Figure 26 (Continued)

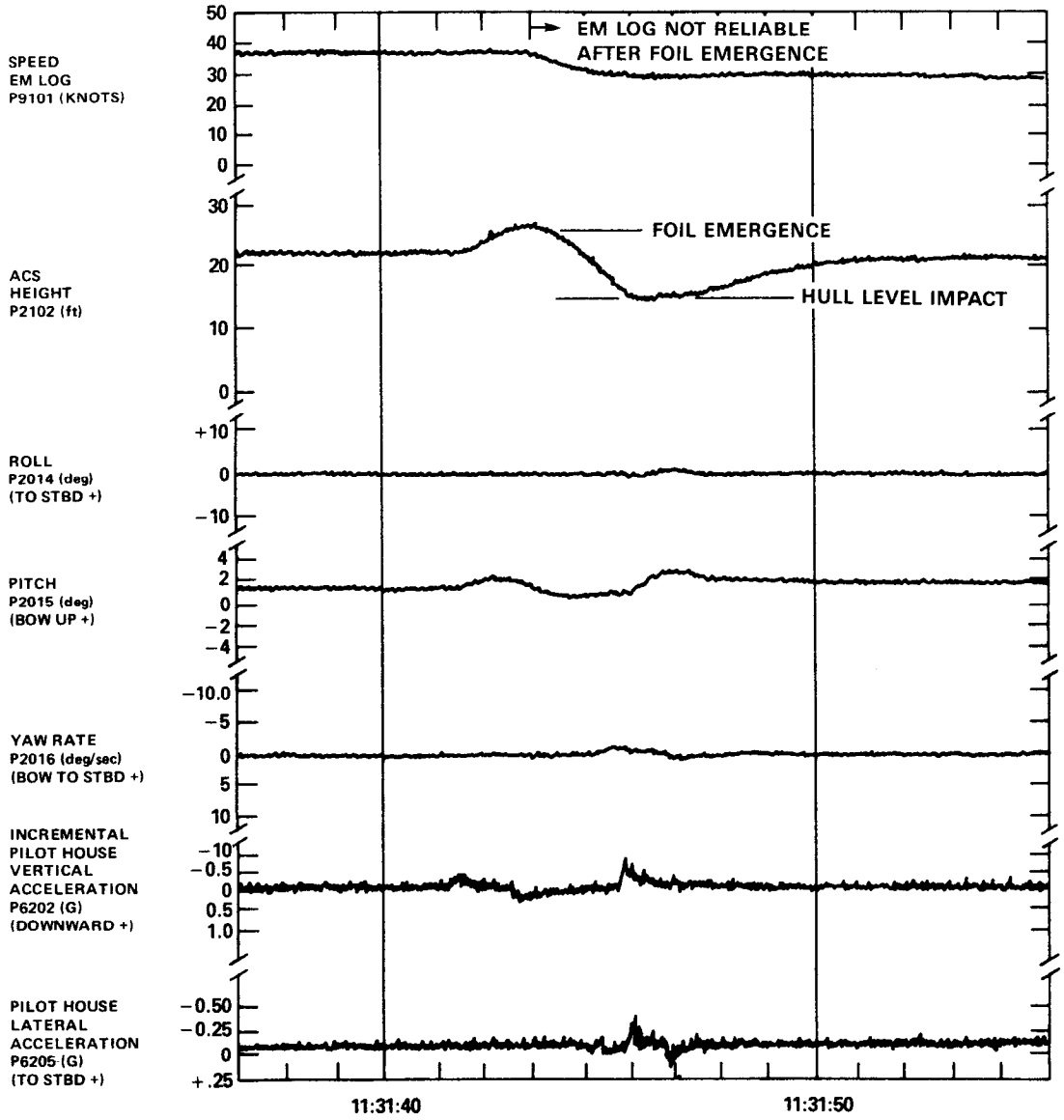

Figure 27 - Data Traces--Straightaway Broach at 36 Knots, 0° Helm

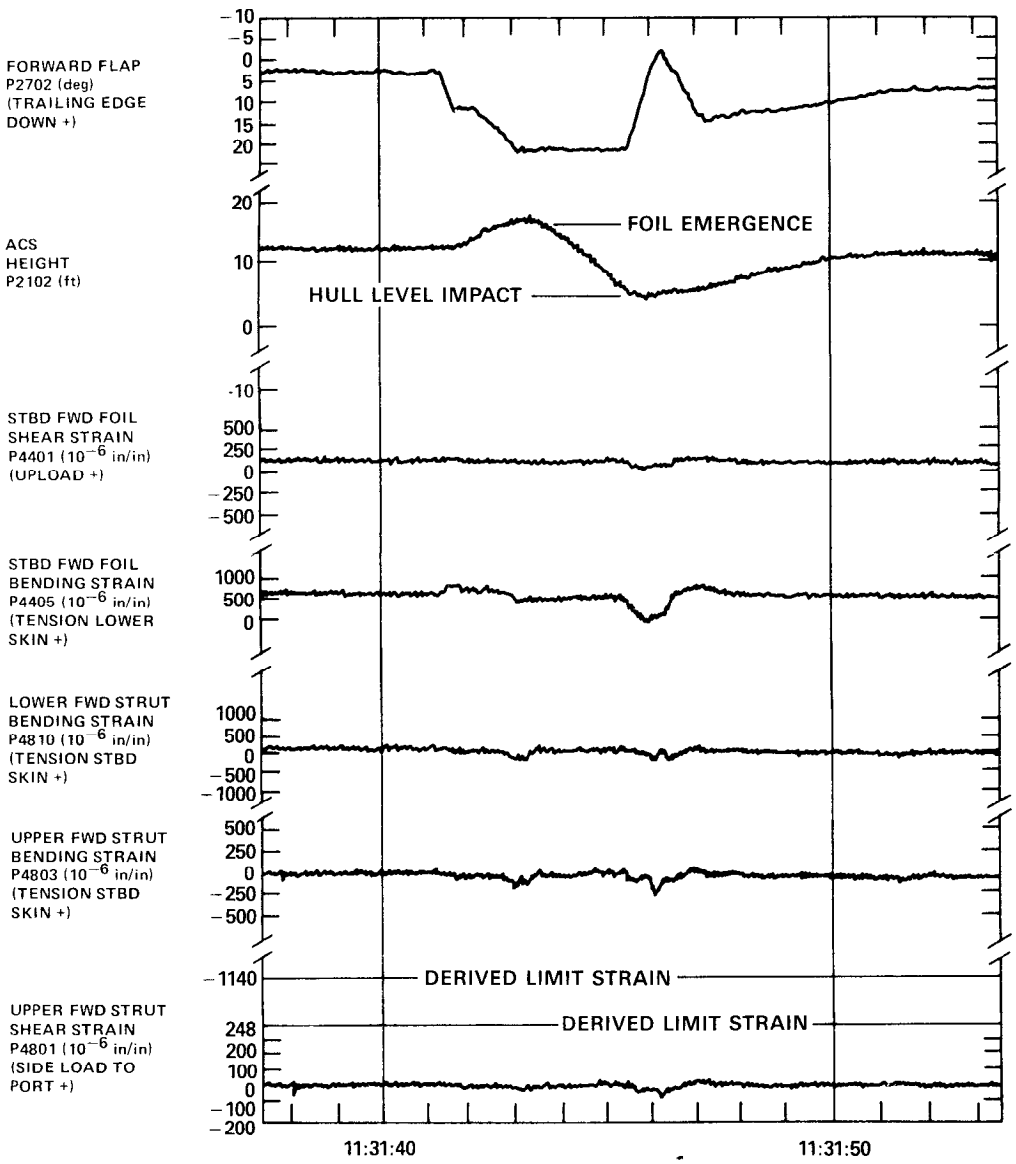

Figure 27 (Continued)

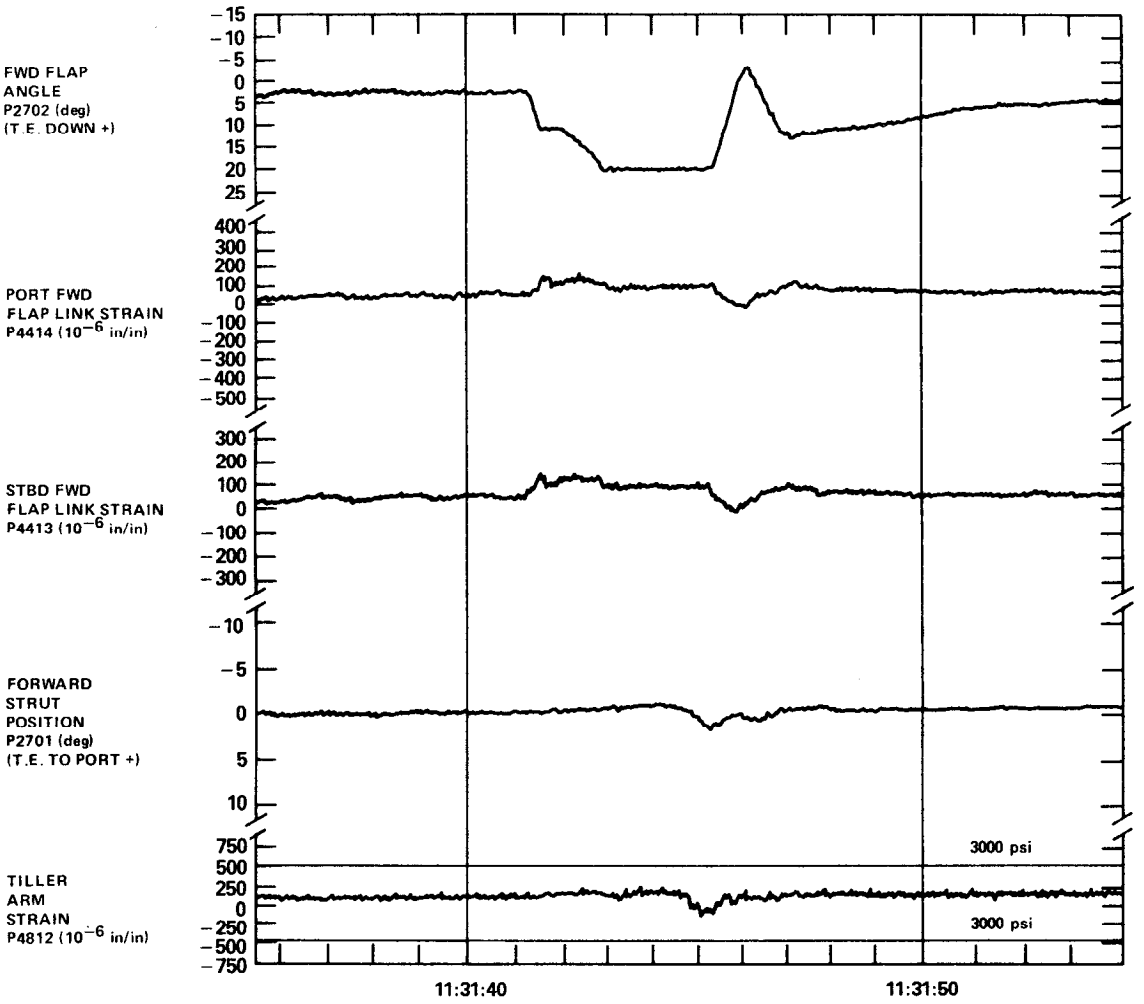

Figure 27 (Continued)

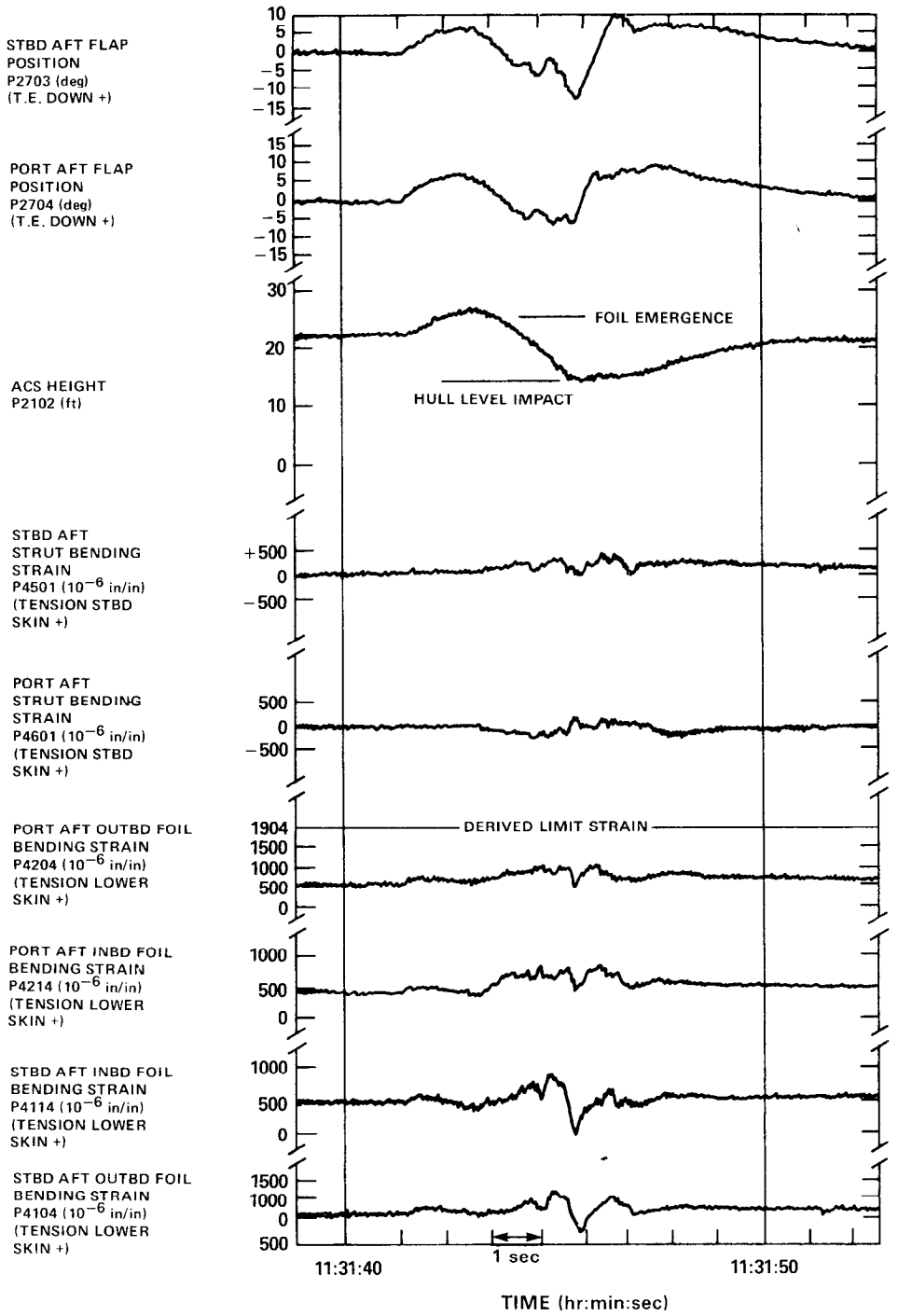

Figure 27 (Continued)

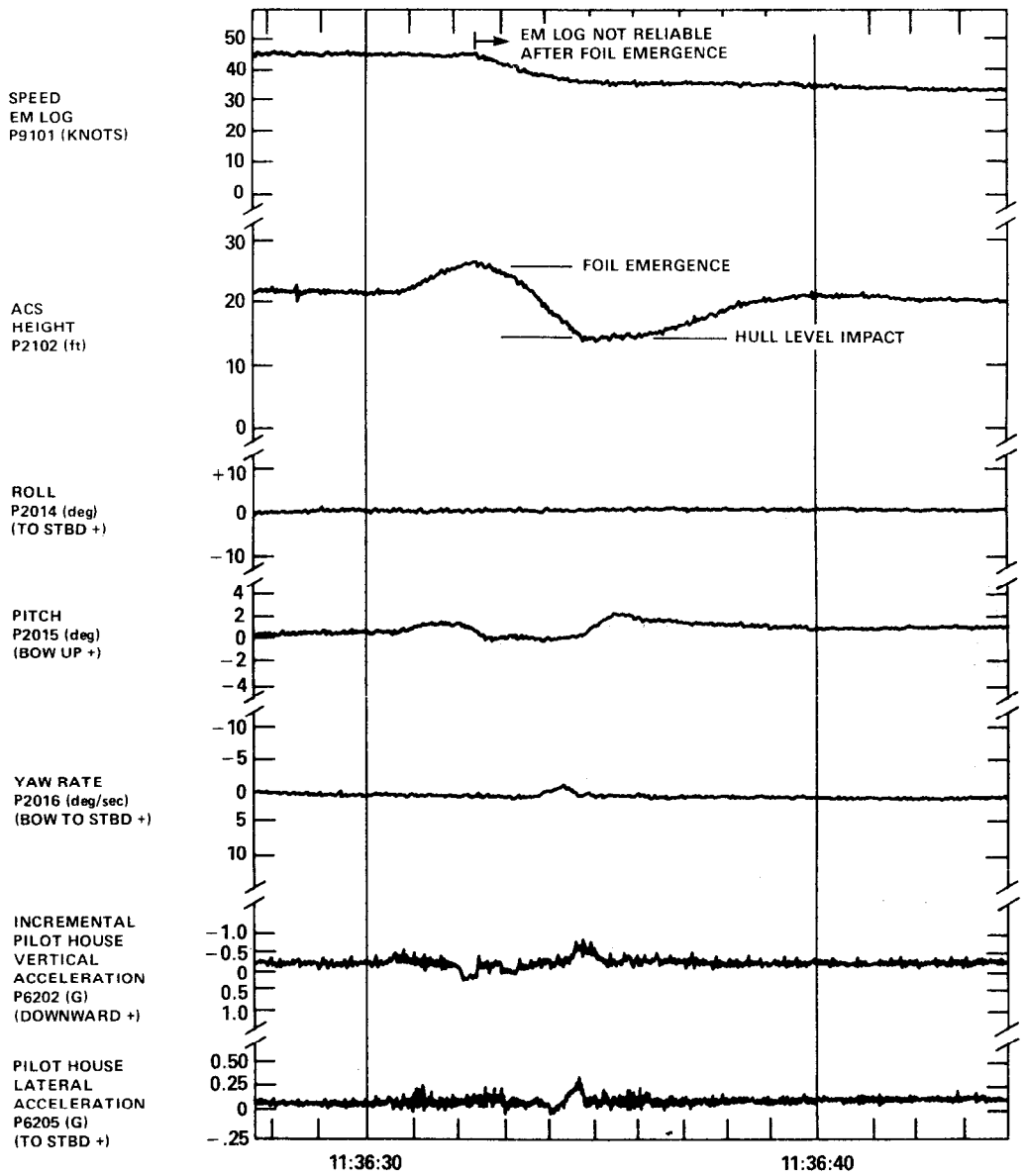

Figure 28 - Data Traces--Straightaway Broach at 45 Knots, 0° Helm

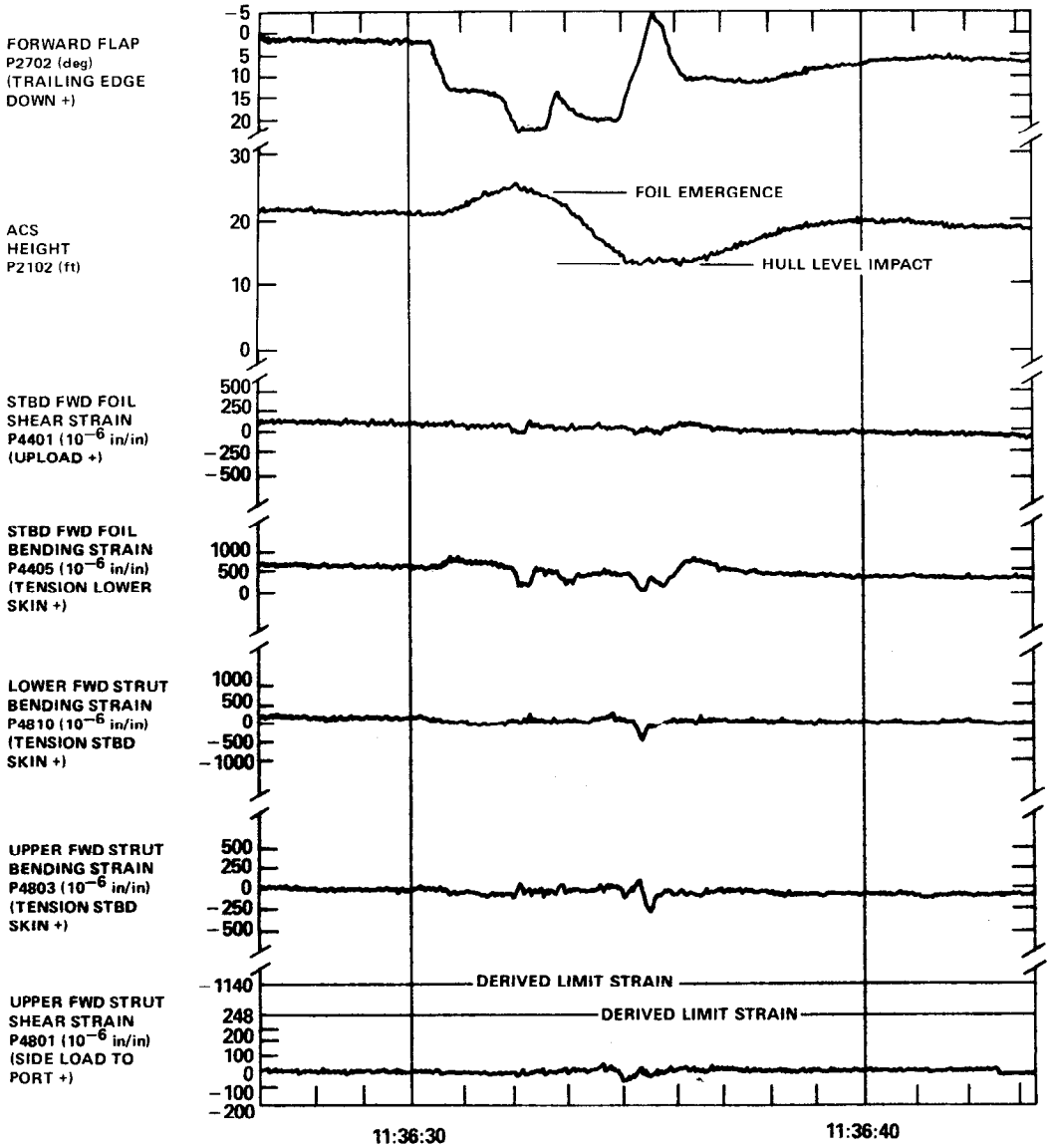

Figure 28 (Continued)

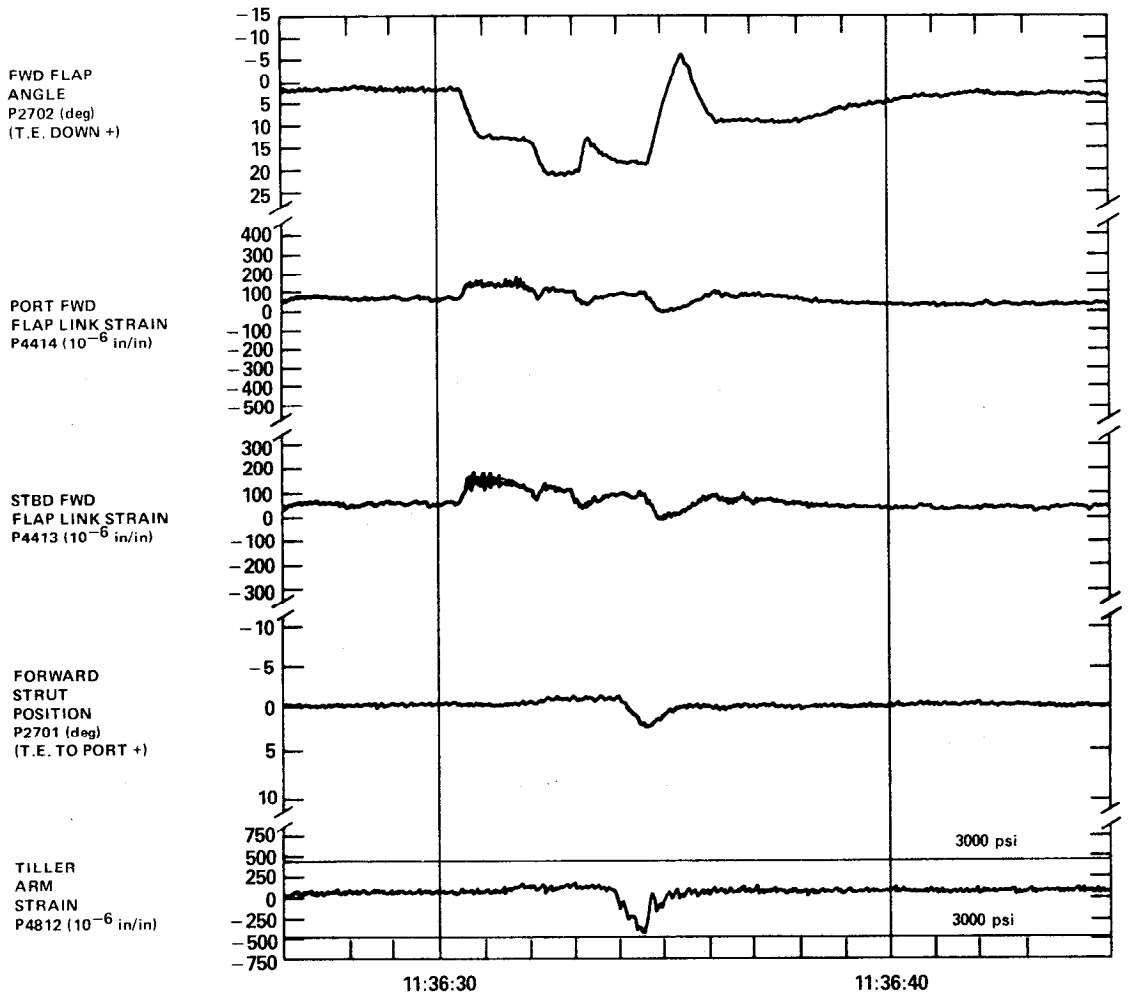

Figure 28 (Continued)

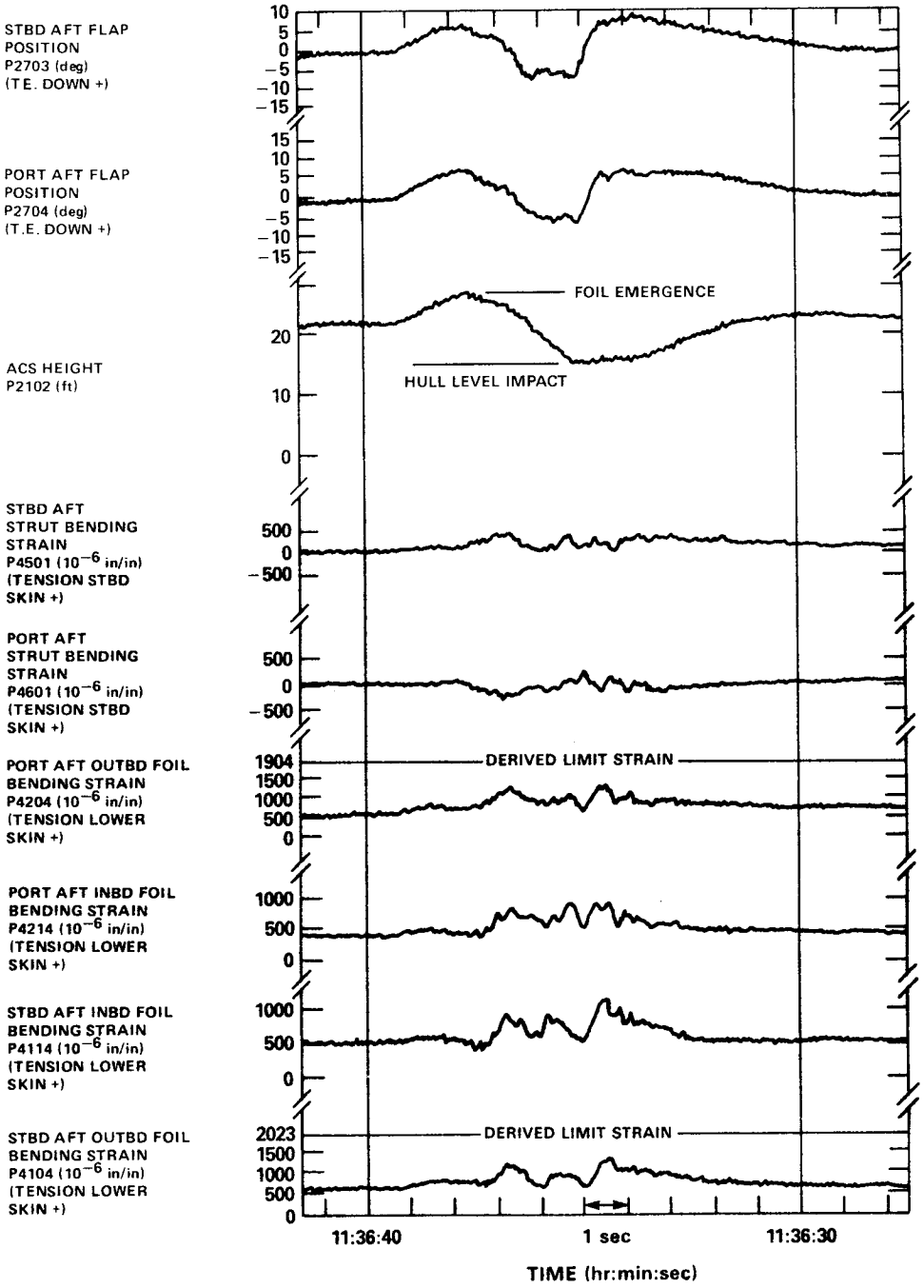

Figure 28 (Continued)

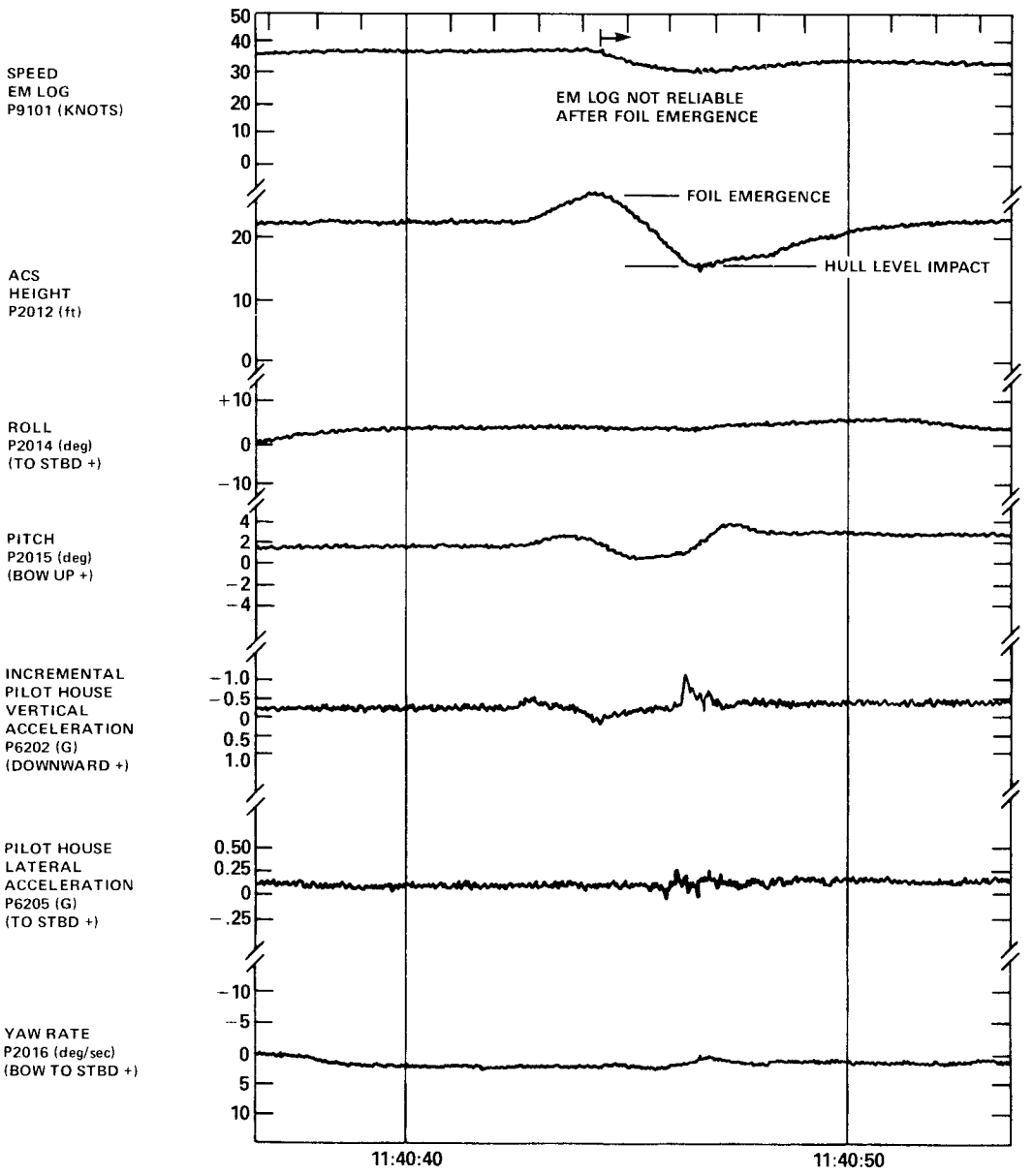

Figure 29 - Data Traces--Broach-in-Turn at 36 Knots, 30° Starboard Helm

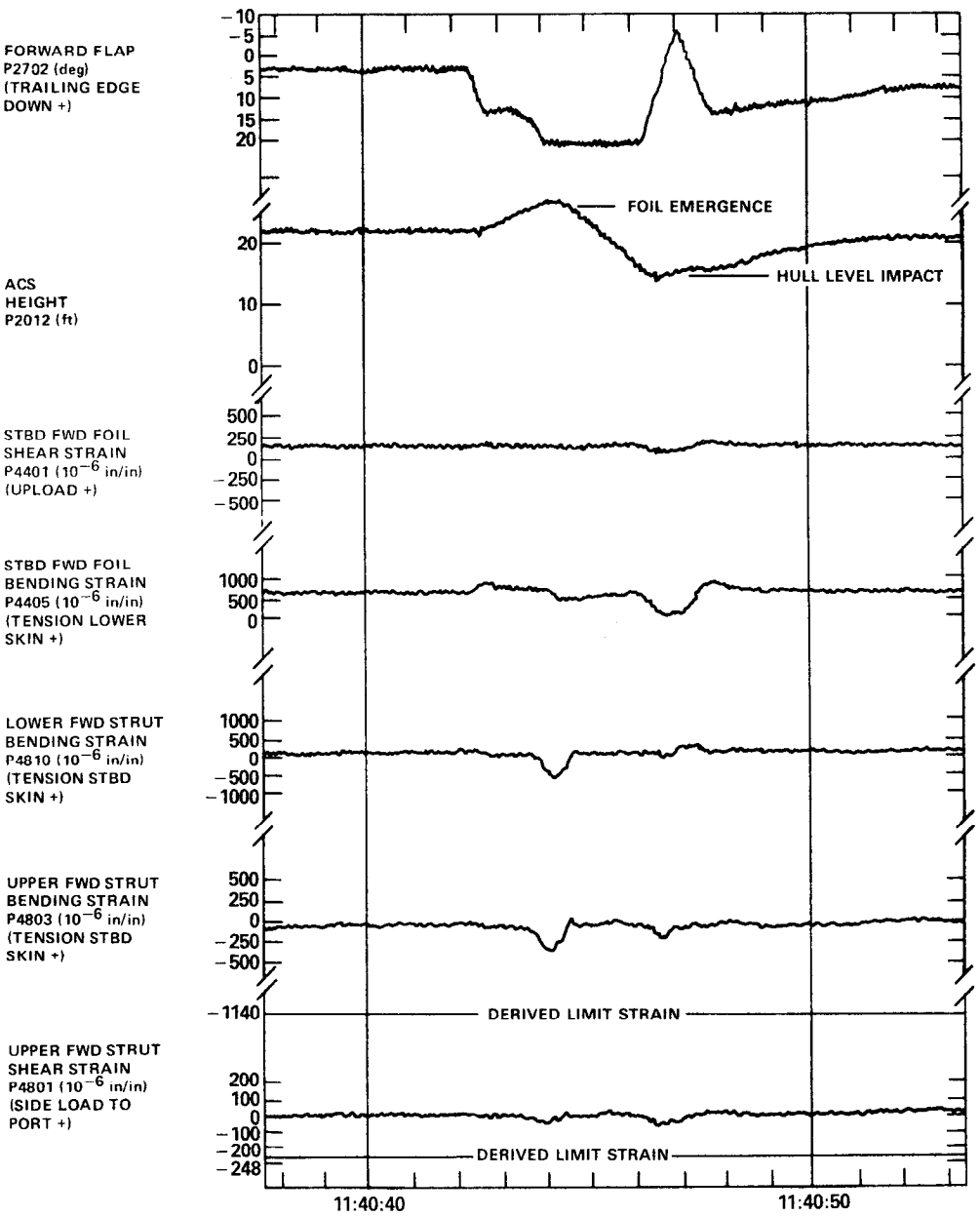

Figure 29 (Continued)

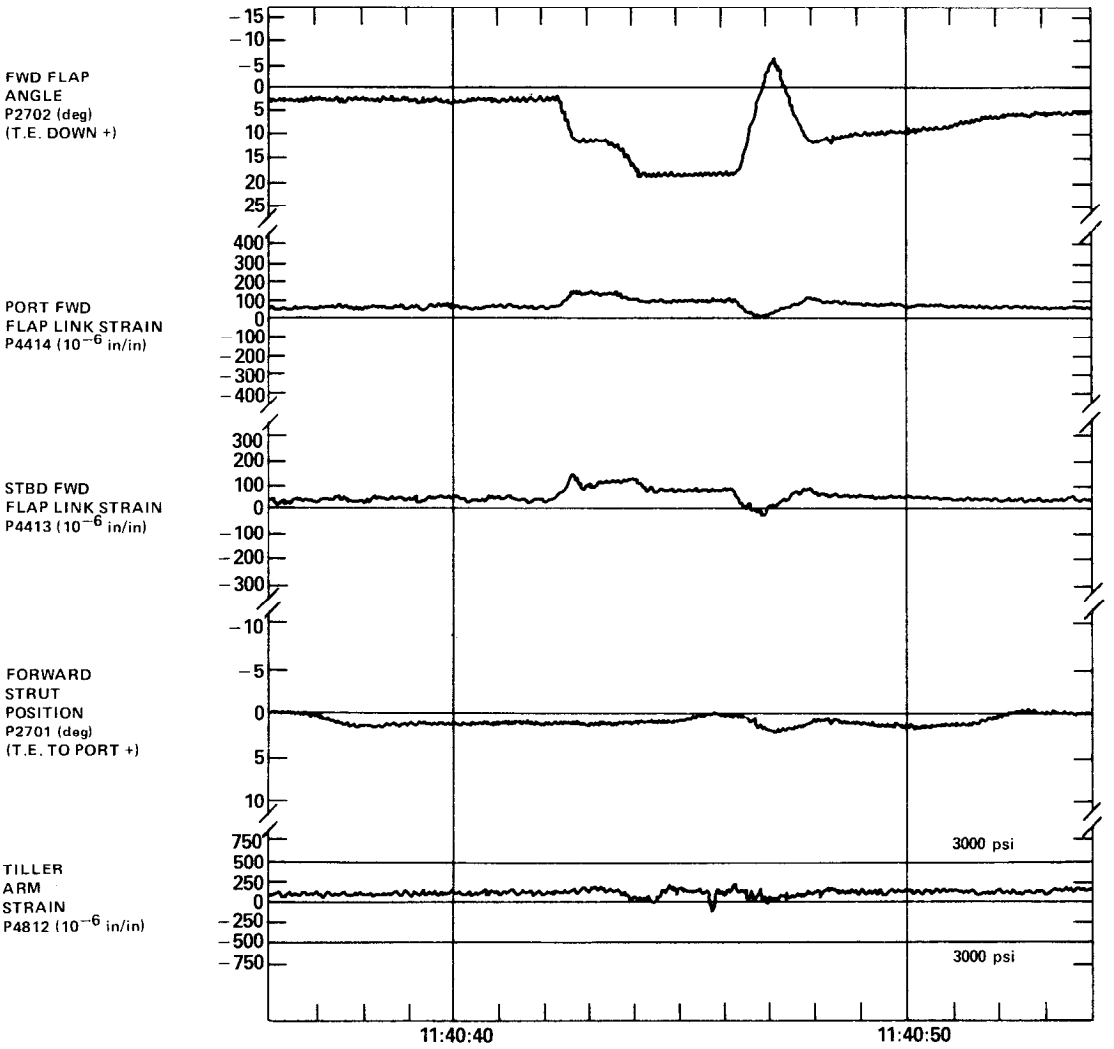

Figure 29 (Continued)

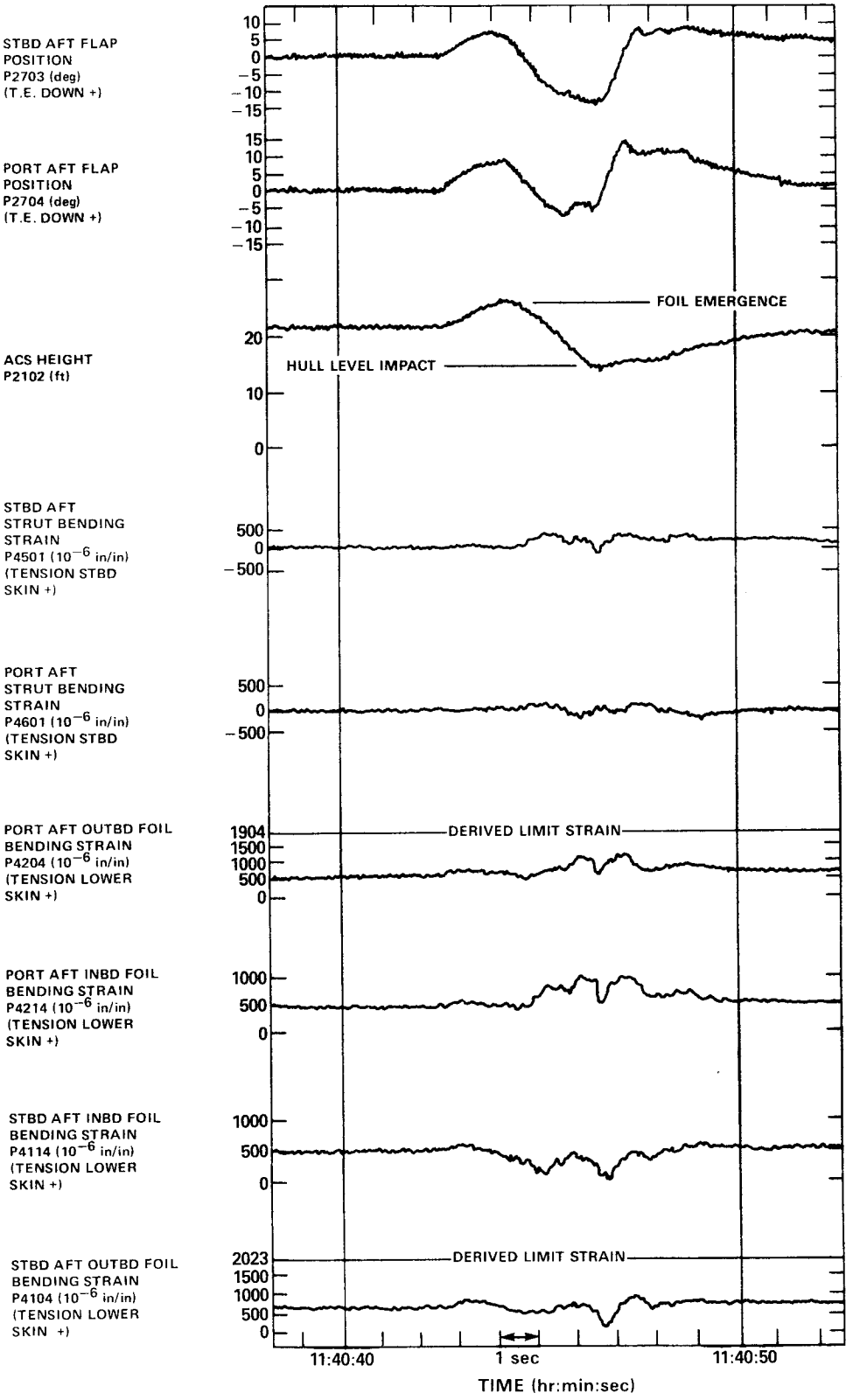

Figure 29 (Continued)

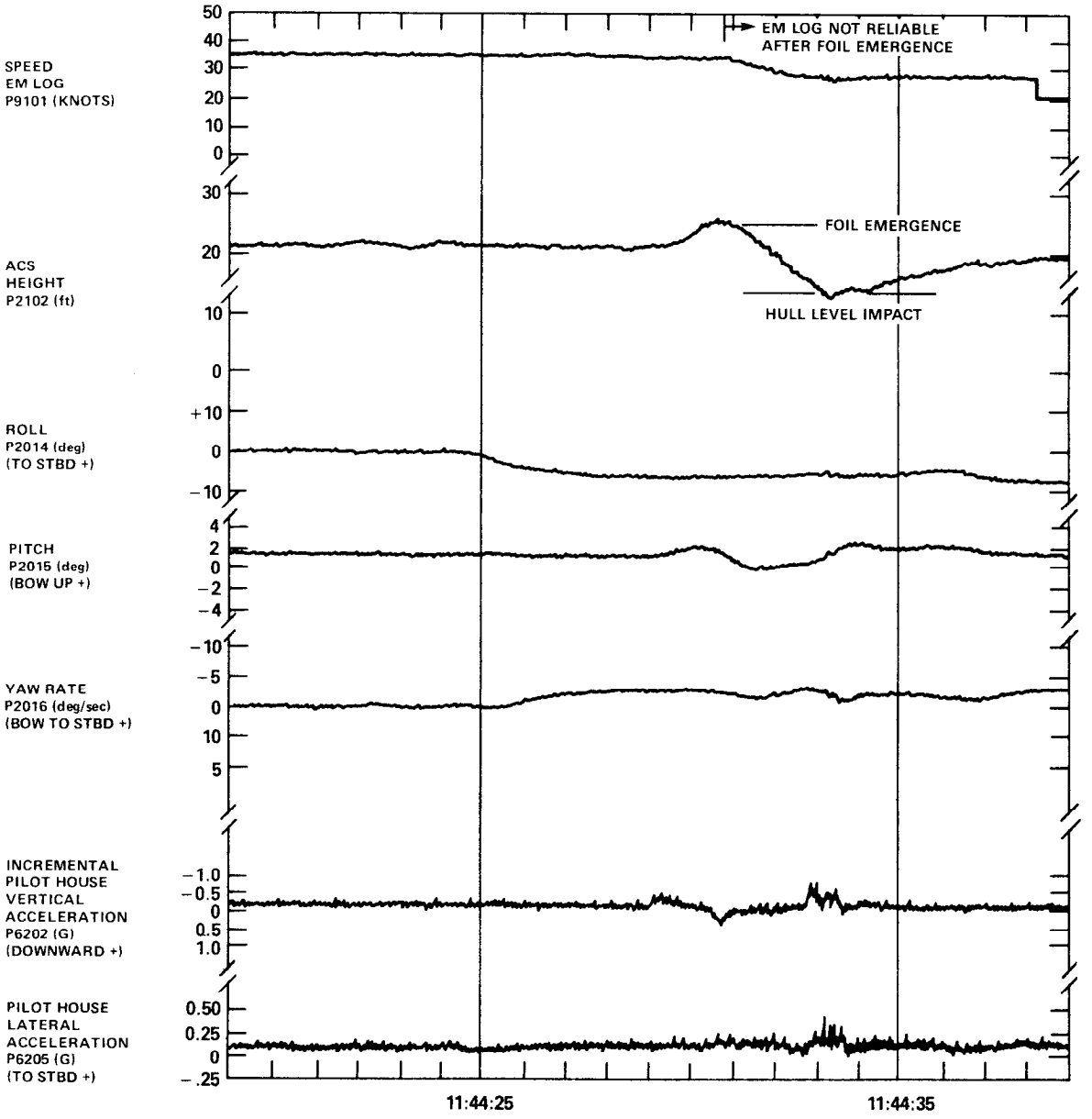

Figure 30 - Data Traces--Broach-in-Turn at 36 Knots, 60° Port Helm

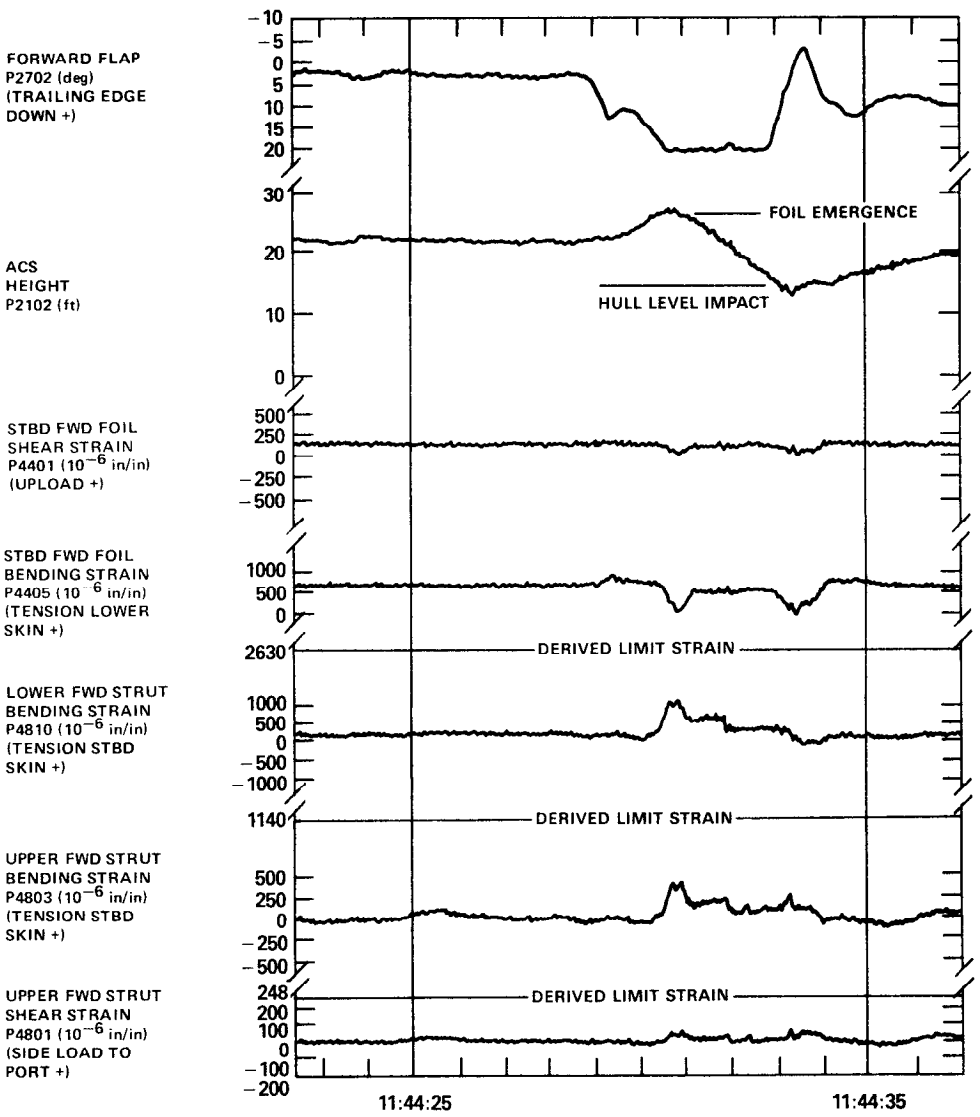

Figure 30 (Continued)

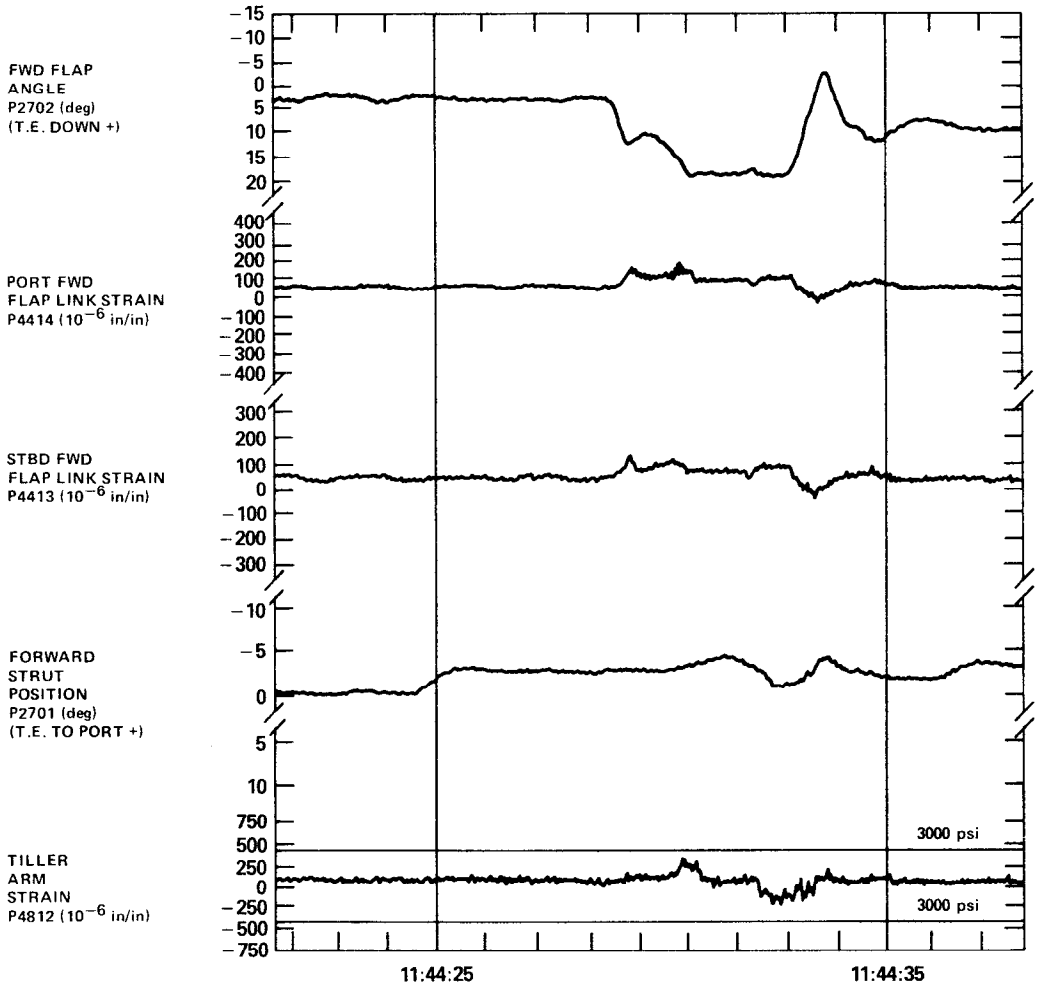

Figure 30 (Continued)

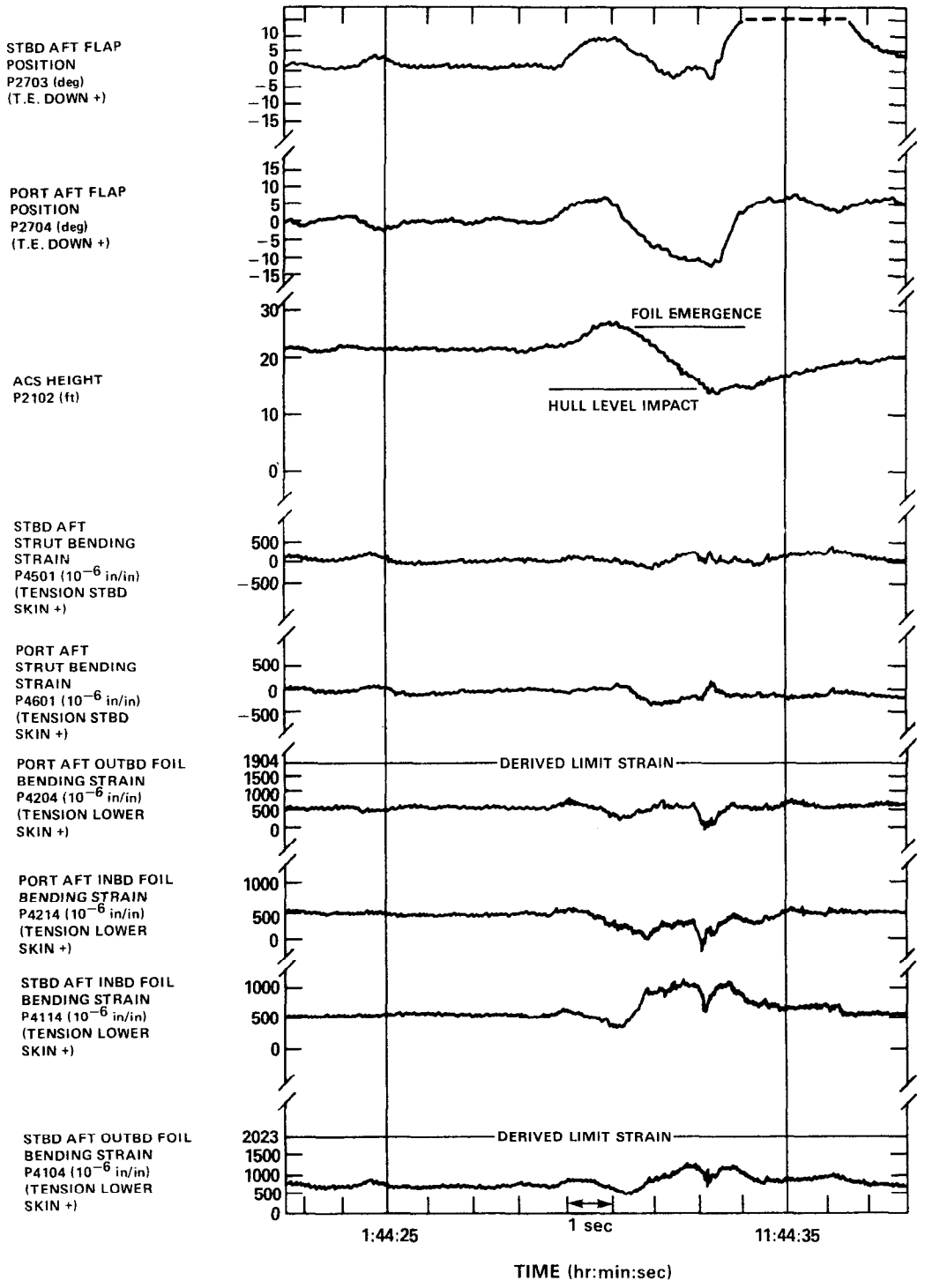

Figure 30 (Continued)

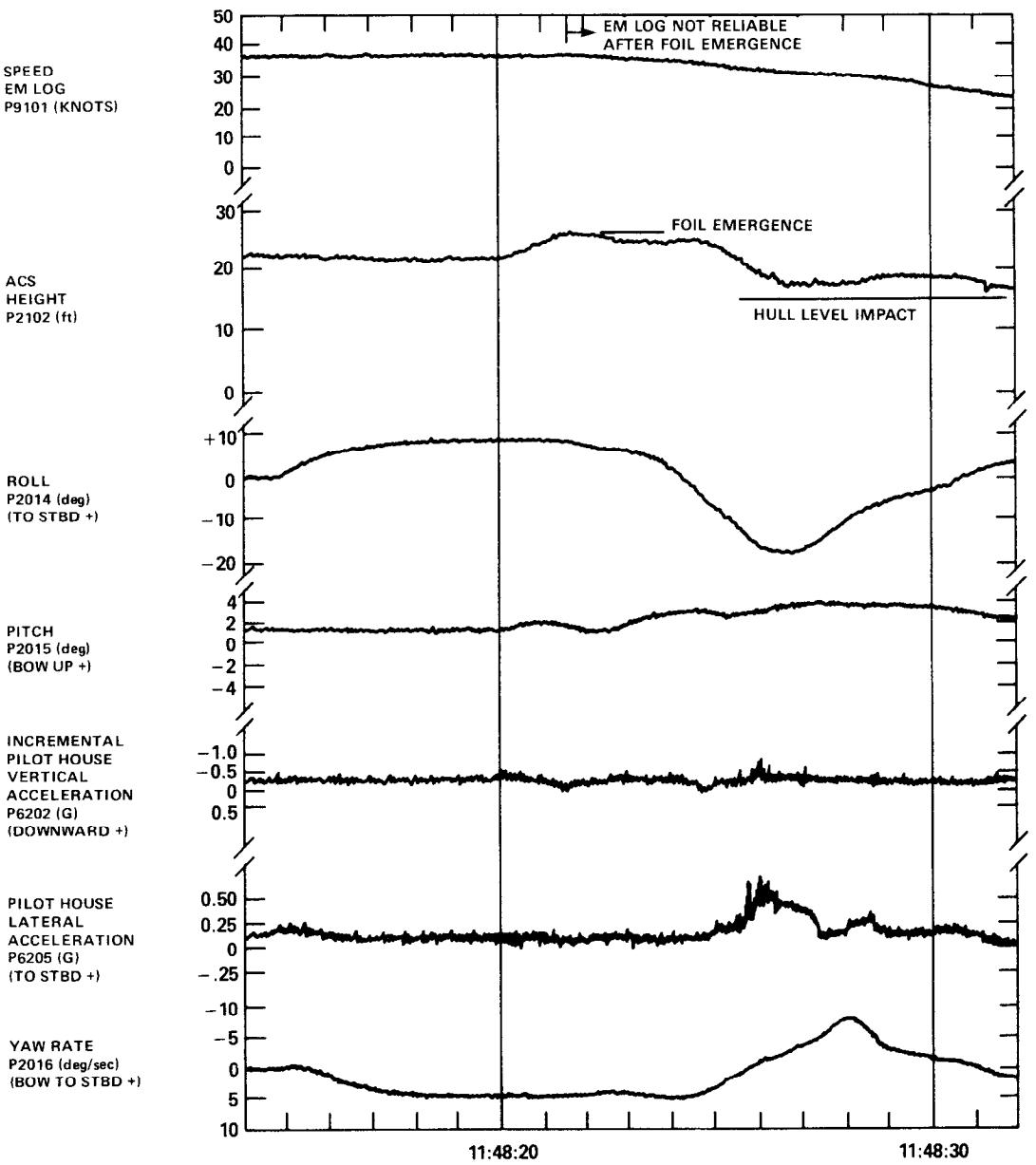

Figure 31 - Data Traces--Broach-in-Turn at 36 Knots, 90° Starboard Helm

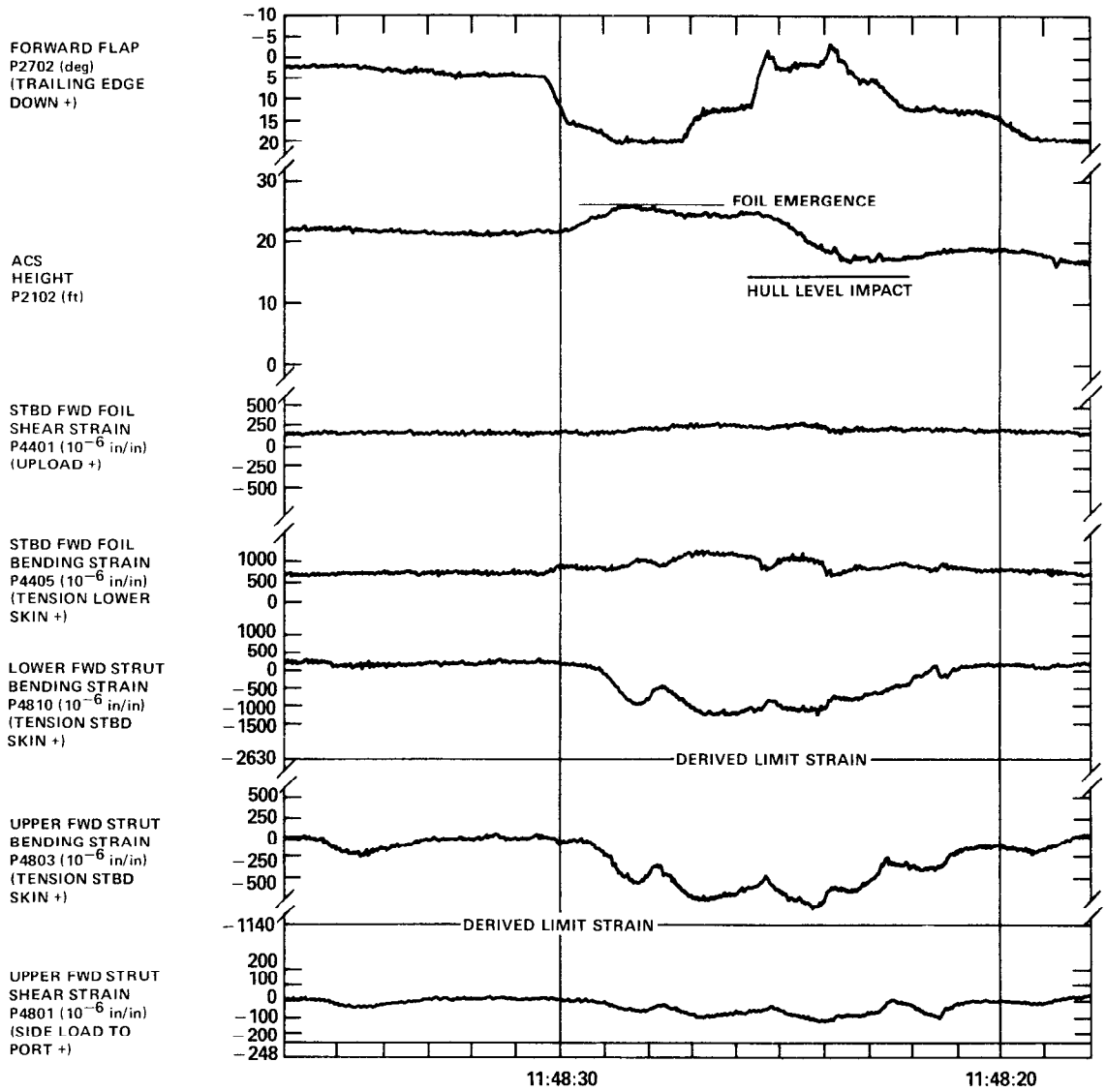

Figure 31 (Continued)

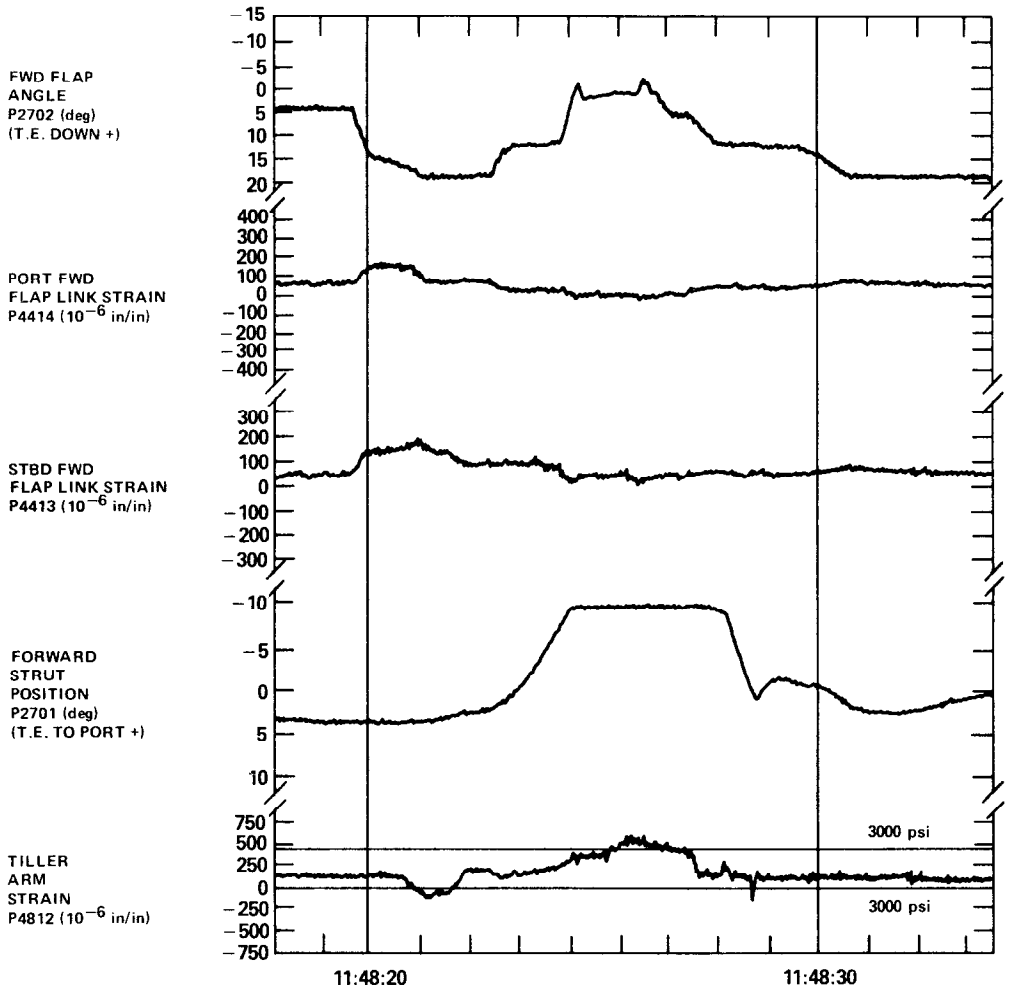

Figure 31 (Continued)

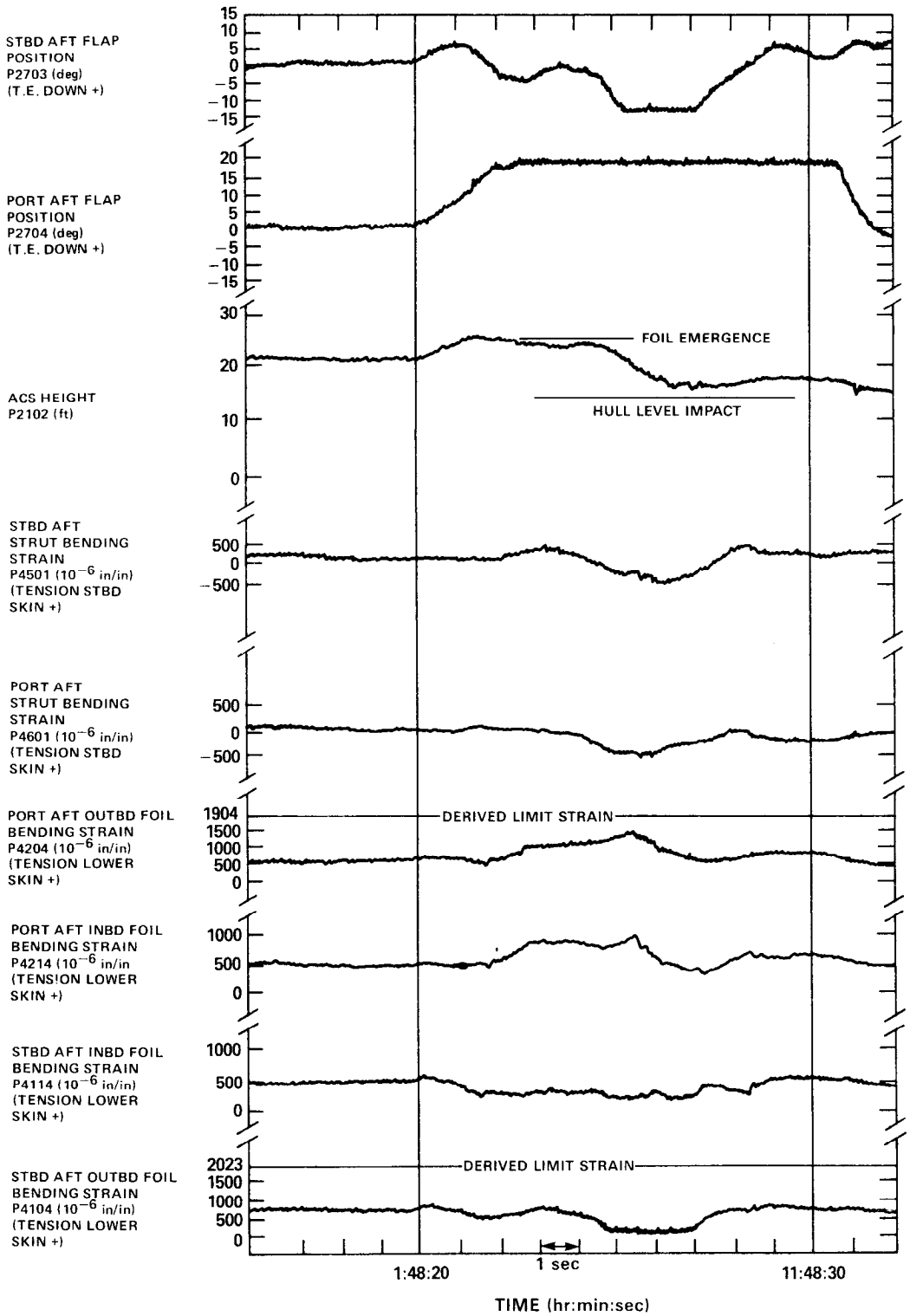

Figure 31 (Continued)

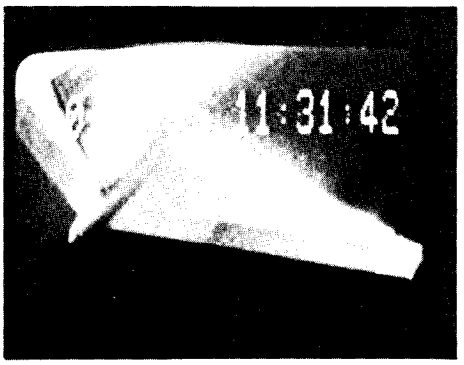

11:31:42.44
ROLL ANGLE = 0°
PITCH ANGLE = 2.35°
FLAP ANGLE = 13.6°

PORT SEMI SPAN
SPEED = 36.4 KNOTS
SUBMERGENCE = 2.1 FT.

11:31:42.84
ROLL ANGLE = 0°
PITCH ANGLE = 1.59°
FLAP ANGLE = 17.4°

PORT SEMI SPAN
SPEED = 36.4 KNOTS
SUBMERGENCE = 1.1 FT

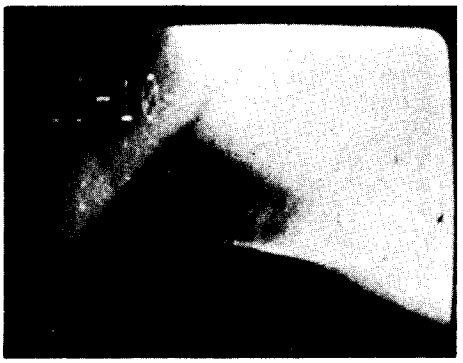

11:31:42.96
ROLL ANGLE = 0°
PITCH ANGLE = 1.24°
FLAP ANGLE = 18.6°

PORT SEMI SPAN
SPEED = N/A
SUBMERGENCE = 0.7 FT

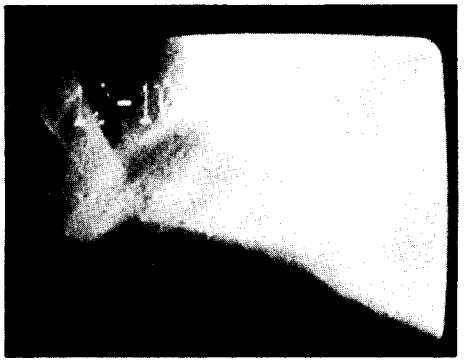

11:31:43.0
ROLL ANGLE = 0°
PITCH ANGLE = 1.18°
FLAP ANGLE = 18.7°

PORT SEMI SPAN
SPEED = N/A
SUBMERGENCE = 0.8 FT

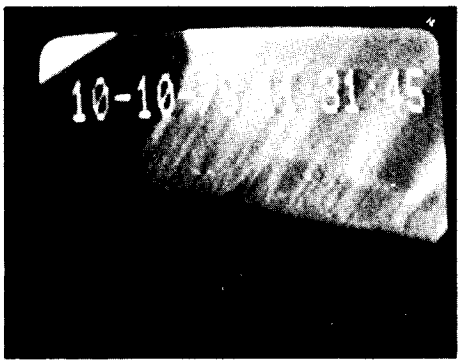

11:31:45.0
ROLL ANGLE = 0°
PITCH ANGLE = 0.82°
FLAP ANGLE = 21.2°

PORT SEMI SPAN
SPEED = N/A
SUBMERGENCE = 7.8 FT

11:31:45.46
ROLL ANGLE = 0°
PITCH ANGLE = 1.06°
FLAP ANGLE = 21.0°

PORT SEMI SPAN
SPEED = N/A
SUBMERGENCE = 10.8 FT

Figure 32 - Forward Foil Flow--36-Knot Straightaway Broach

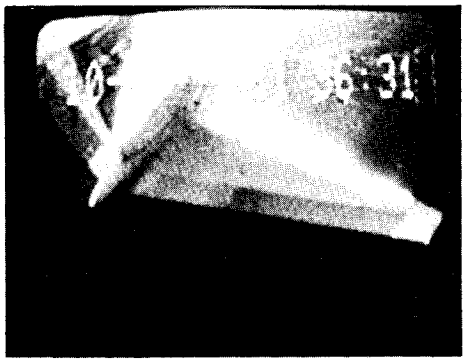

11:36:31.83
ROLL ANGLE = 0°
PITCH ANGLE = 1.41°
FLAP ANGLE = 13.5°

PORT SEMI SPAN
SPEED = 45.3 KNOTS
SUBMERGENCE = 1.8 FT

11:36:32.12
ROLL ANGLE = 0°
PITCH ANGLE = 1.41°
FLAP ANGLE = 14.2°

PORT SEMI SPAN
SPEED = 45.2 KNOTS
SUBMERGENCE = 1.6 FT

11:36:32.21
ROLL ANGLE = 0°
PITCH ANGLE = 1.38°
FLAP ANGLE = 14.9°

PORT SEMI SPAN
SPEED = 44.8 KNOTS
SUBMERGENCE = 0.8 FT

11:36:32.58
ROLL ANGLE = 0°
PITCH ANGLE = 0.24°
FLAP ANGLE = 20.9°

PORT SEMI SPAN
SPEED = N/A
SUBMERGENCE = 1.4 FT

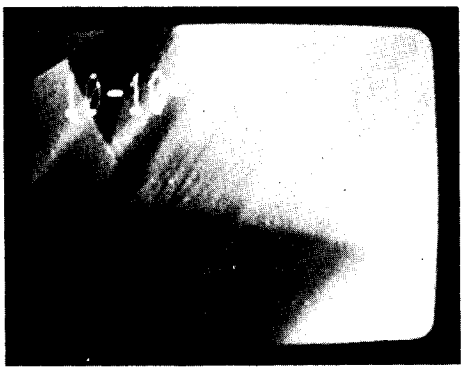

11:36:33.0
ROLL ANGLE = 0°
PITCH ANGLE = 0°
FLAP ANGLE = 21.4°

PORT SEMI SPAN
SPEED = N/A
SUBMERGENCE = 1.8 FT

11:36:33.30
ROLL ANGLE = 0°
PITCH ANGLE = 0.12°
FLAP ANGLE = 13.6°

PORT SEMI SPAN
SPEED = N/A
SUBMERGENCE = 2.6 FT

Figure 33 - Forward Foil Flow--45-Knot Straightaway Broach

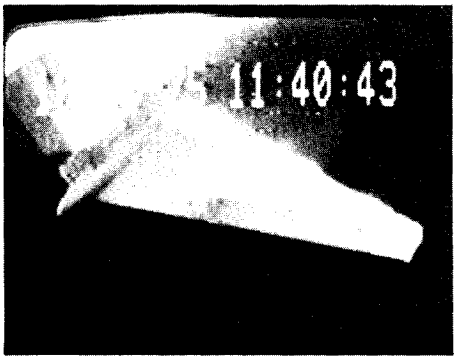

11:40:43.0
ROLL ANGLE = 3.1°
PITCH ANGLE = 2.12°
FLAP ANGLE = 13.0°

PORT SEMI SPAN
SPEED = 36.1 KNOTS
SUBMERGENCE = 4.1 FT

11:40:43.71
ROLL ANGLE = 3.1°
PITCH ANGLE = 2.59°
FLAP ANGLE = 15.6°

PORT SEMI SPAN
SPEED = 36.1 KNOTS
SUBMERGENCE = 1.6 FT

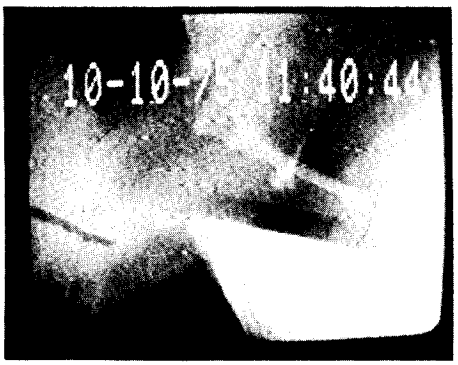

11:40:44.44
ROLL ANGLE = 3.1°
PITCH ANGLE = 1.59°
FLAP ANGLE = 21.2°

PORT SEMI SPAN
SPEED = N/A
SUBMERGENCE = 0.8 FT

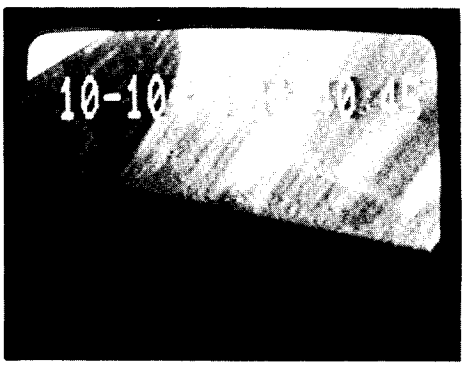

11:40:45.68
ROLL ANGLE = 2.5°
PITCH ANGLE = 0.47°
FLAP ANGLE = 21.2°

PORT SEMI SPAN
SPEED = N/A
SUBMERGENCE = 6.9 FT

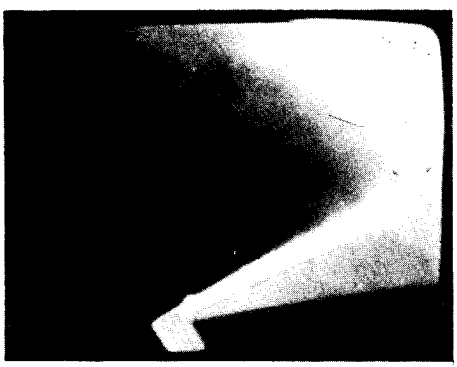

11:40:42.74
ROLL ANGLE = 3.1°
PITCH ANGLE = 1.71°
FLAP ANGLE = 13.6°

STARBOARD SEMI SPAN
SPEED = 36.1 KNOTS
SUBMERGENCE = 5.0 FT

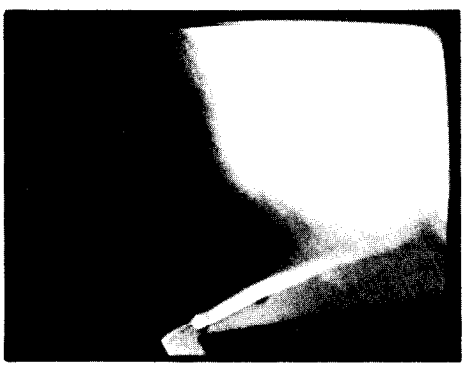

11:40:43.74
ROLL ANGLE = 3.1°
PITCH ANGLE = 2.59°
FLAP ANGLE = 16.1°

STARBOARD SEMI SPAN
SPEED = 36.1 KNOTS
SUBMERGENCE = 1.7 FT

Figure 34 - Forward Foil Flow--36-Knot Broach with 30° Starboard Helm

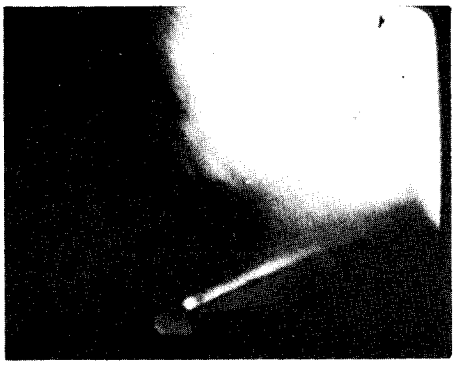

11:40:43.82
ROLL ANGLE = 3.1°
PITCH ANGLE = 2.47°
FLAP ANGLE = 16.9°

STARBOARD SEMI SPAN
SPEED = 35.9 KNOTS
SUBMERGENCE = 1.6 FT

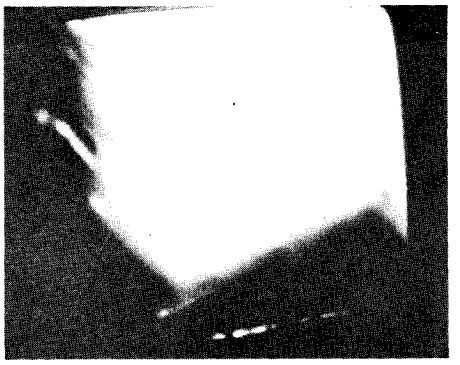

11:40:43.98
ROLL ANGLE = 3.1°
PITCH ANGLE = 2.35°
FLAP ANGLE = 19.5°

STARBOARD SEMI SPAN
SPEED = 35.9 KNOTS
SUBMERGENCE = 1.0 FT

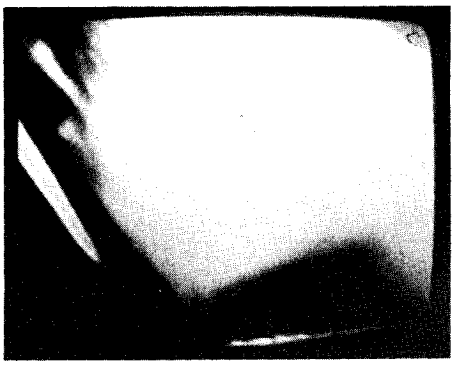

11:40:44.07
ROLL ANGLE = 3.1°
PITCH ANGLE = 2.41°
FLAP ANGLE = 20.8°

STARBOARD SEMI SPAN
SPEED = 35.7 KNOTS
SUBMERGENCE = 0.8 FT

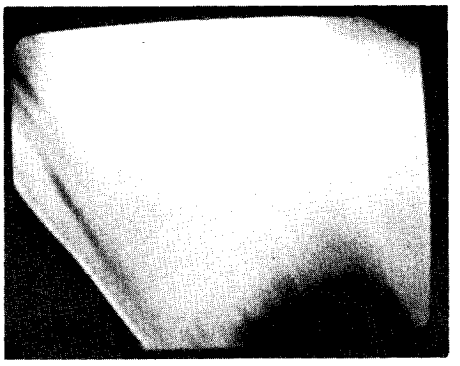

11:40:44.19
ROLL ANGLE = 3.1°
PITCH ANGLE = 2.18°
FLAP ANGLE = 21.0°

STARBOARD SEMI SPAN
SPEED = 35.7 KNOTS
SUBMERGENCE = 0.5 FT

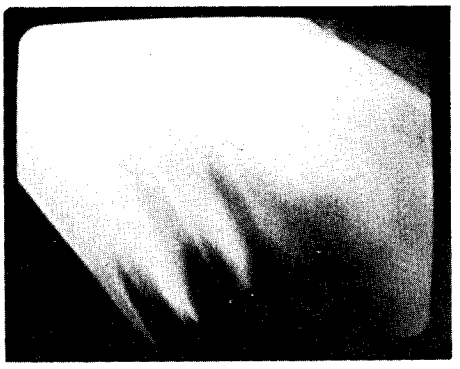

11:40:44.44
ROLL ANGLE = 3.1°
PITCH ANGLE = 1.59°
FLAP ANGLE = 21.2°

STARBOARD SEMI SPAN
SPEED = N/A
SUBMERGENCE = 0.8 FT

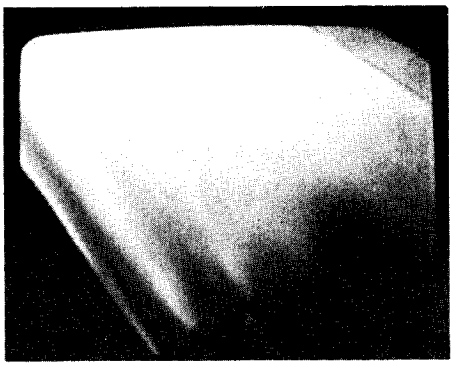

11:40:44.74
ROLL ANGLE = 2.4°
PITCH ANGLE = 0.8°
FLAP ANGLE = 21.2°

STARBOARD SEMI SPAN
SPEED = N/A
SUBMERGENCE = 2.1 FT

Figure 34 (Continued)

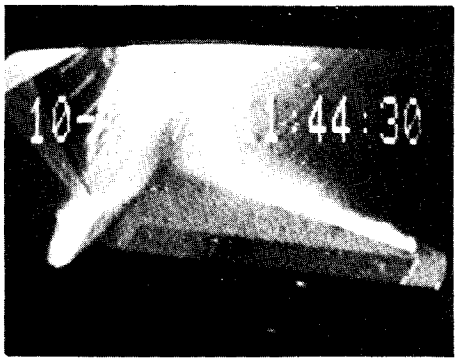

11:44:30.42
ROLL ANGLE =-5.9°
PITCH ANGLE = 2.59°
FLAP ANGLE = 17.2°

PORT SEMI SPAN
SPEED = 35.6 KNOTS
SUBMERGENCE = 1.6 FT

11:44:30.54
ROLL ANGLE =-5.9°
PITCH ANGLE = 2.59°
FLAP ANGLE = 19.5°

PORT SEMI SPAN
SPEED = 35.5 KNOTS
SUBMERGENCE = 0.8 FT

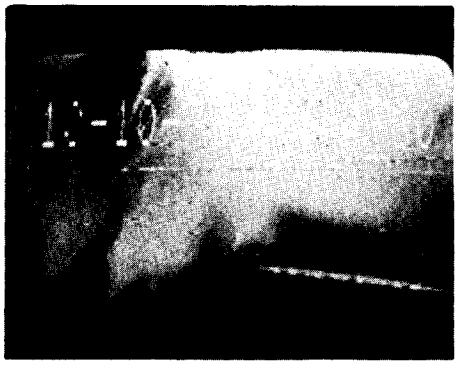

11:44:30.63
ROLL ANGLE =-5.9°
PITCH ANGLE = 2.35°
FLAP ANGLE = 20.8°

PORT SEMI SPAN
SPEED = 35.5 KNOTS
SUBMERGENCE = 0.7 FT

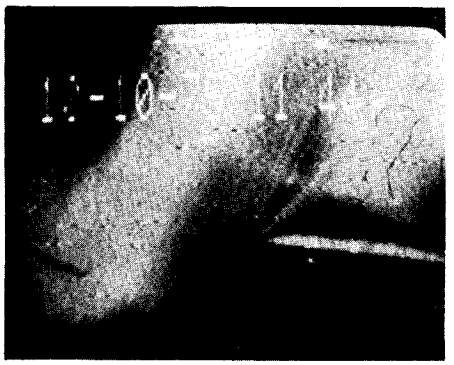

11:44:30.79
ROLL ANGLE =-5.9°
PITCH ANGLE= 2.12°
FLAP ANGLE = 20.5°

PORT SEMI SPAN
SPEED = 35.5 KNOTS
SUBMERGENCE = 0.8 FT

11:44:30.96
ROLL ANGLE =-5.9°
PITCH ANGLE = 1.65°
FLAP ANGLE = 21.0°

PORT SEMI SPAN
SPEED = N/A
SUBMERGENCE = 0.6 FT

11:44:31.12
ROLL ANGLE =-5.8°
PITCH ANGLE = 1.06°
FLAP ANGLE = 20.9°

PORT SEMI SPAN
SPEED = N/A
SUBMERGENCE = 1.6 FT

Figure 35 - Forward Foil Flow--36-Knot Broach with 60° Port Helm

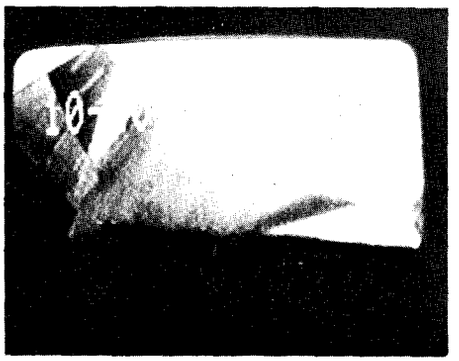

11:44:31.38
ROLL ANGLE = -5.8°
PITCH ANGLE = 0.47°
FLAP ANGLE = 20.5°

PORT SEMI SPAN
SPEED = N/A
SUBMERGENCE = 2.6 FT

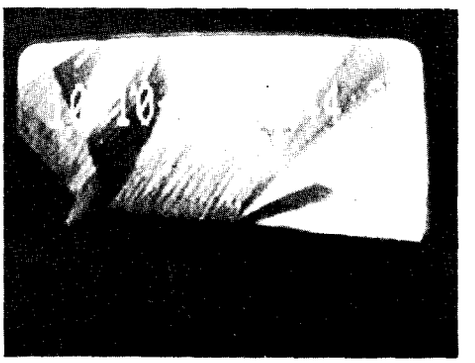

11:44:31.67
ROLL ANGLE = -5.8°
PITCH ANGLE = 0.32°
FLAP ANGLE = 21.0°

PORT SEMI SPAN
SPEED = N/A
SUBMERGENCE = 3.9 FT

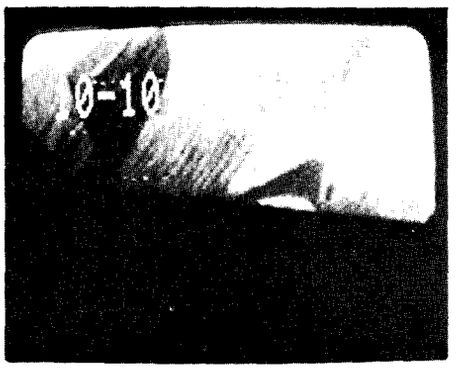

11:44:32.0
ROLL ANGLE = -5.8°
PITCH ANGLE = 0.59°
FLAP ANGLE = 19.4°

PORT SEMI SPAN
SPEED = N/A
SUBMERGENCE = 5.9 FT

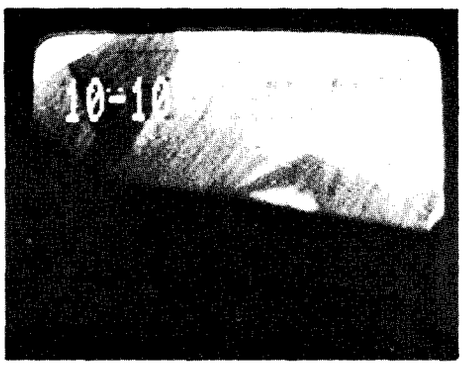

11:44:32.33
ROLL ANGLE = -5.5°
PITCH ANGLE = 0.94°
FLAP ANGLE = 20.8°

PORT SEMI SPAN
SPEED = N/A
SUBMERGENCE = 7.8 FT

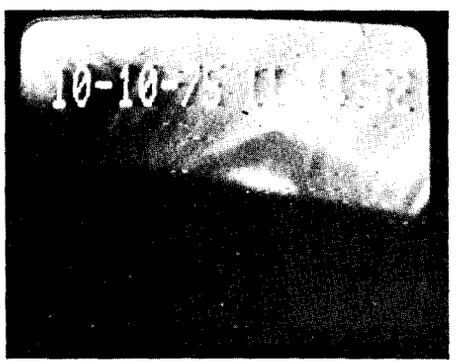

11:44:32.75
ROLL ANGLE = -5.2°
PITCH ANGLE = 1.06°
FLAP ANGLE = 20.9°

PORT SEMI SPAN
SPEED = N/A
SUBMERGENCE = 9.9 FT

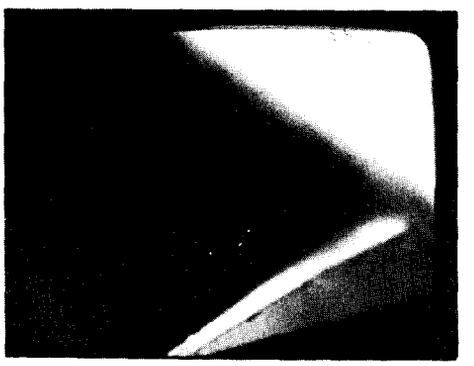

11:44:30.69
ROLL ANGLE = -5.9°
PITCH ANGLE = 2.12°
FLAP ANGLE = 21.1°

STARBOARD SEMI SPAN
SPEED = 35.5 KNOTS
SUBMERGENCE = 0.8 FT

Figure 35 (Continued)

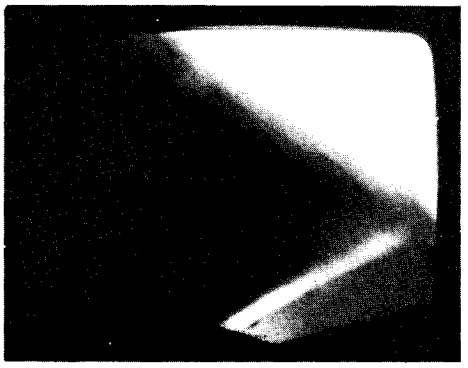

11:44:30.90
ROLL ANGLE =-5.9°
PITCH ANGLE = 1.88°
FLAP ANGLE = 21.0°

STARBOARD SEMI SPAN
SPEED = 35.6 KNOTS
SUBMERGENCE = 0.7 FT

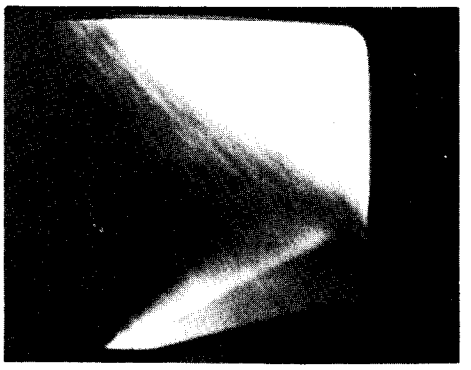

11:44:30.98
ROLL ANGLE =-5.9°
PITCH ANGLE = 1.53°
FLAP ANGLE = 21.0

STARBOARD SEMI SPAN
SPEED = 34.9 KNOTS
SUBMERGENCE = 1.2 FT

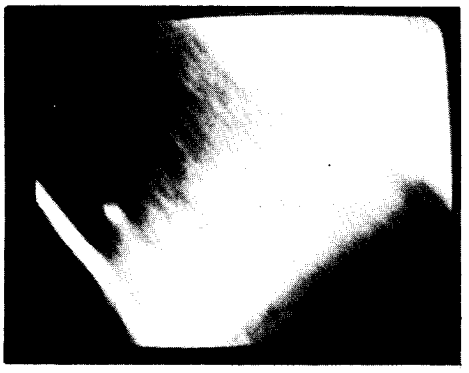

11:44:31.06
ROLL ANGLE =-5.9°
PITCH ANGLE = 1.15°
FLAP ANGLE = 20.6°

STARBOARD SEMI SPAN
SPEED = N/A
SUBMERGENCE = 1.5 FT

11:44:31.56
ROLL ANGLE =-5.8°
PITCH ANGLE = 0.47°
FLAP ANGLE = 21.0°

STARBOARD SEMI SPAN
SPEED = N/A
SUBMERGENCE = 3.0 FT

11:44:31.94
ROLL ANGLE =-5.8°
PITCH ANGLE = 0.59°
FLAP ANGLE = 19.5°

STARBOARD SEMI SPAN
SPEED = N/A
SUBMERGENCE = 5.6 FT

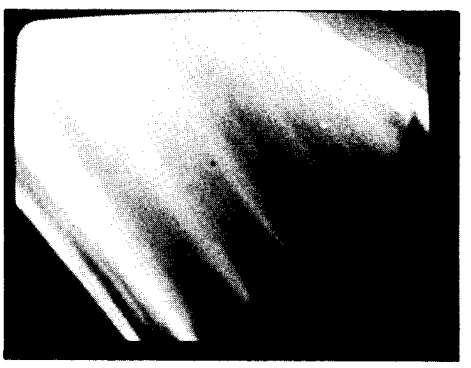

11:44:32.19
ROLL ANGLE =-5.8°
PITCH ANGLE = 0.82°
FLAP ANGLE = 20.5°

STARBOARD SEMI SPAN
SPEED = N/A
SUBMERGENCE = 7.2 FT

Figure 35 (Continued)

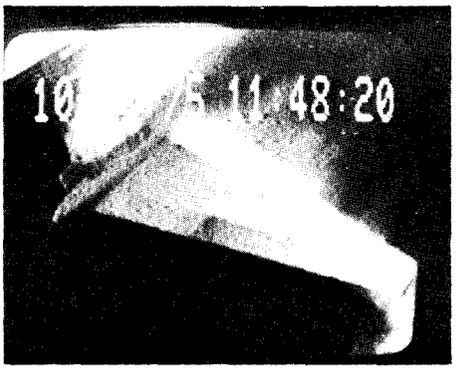

11:48:20.67
ROLL ANGLE = +9.1°
PITCH ANGLE = 2.47°
FLAP ANGLE = 17.4°

PORT SEMI SPAN
SPEED = 35.9 KNOTS
SUBMERGENCE = 3.7 Ft

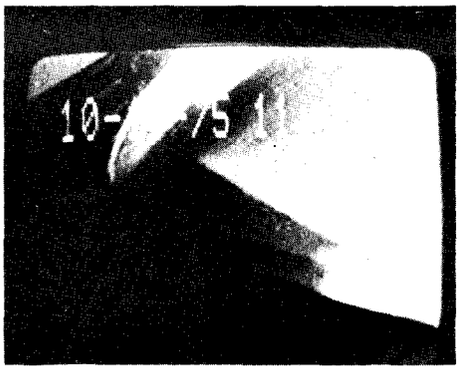

11:48:21.12
ROLL ANGLE = +8.9°
PITCH ANGLE = 2.47°
FLAP ANGLE = 20.0°

PORT SEMI SPAN
SPEED = 36.0 KNOTS
SUBMERGENCE = 3.4 Ft

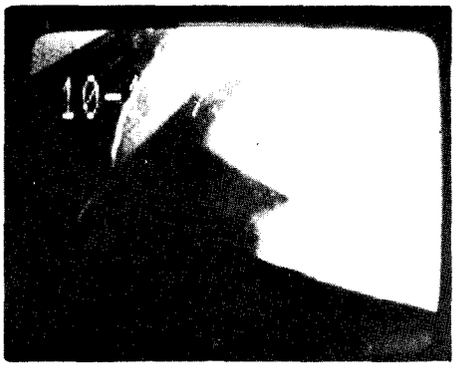

11:48:21.25
ROLL ANGLE = +8.8°
PITCH ANGLE = 2.35°
FLAP ANGLE =20.6°

PORT SEMI SPAN
SPEED = 36.0 KNOTS
SUBMERGENCE = 3.3 Ft

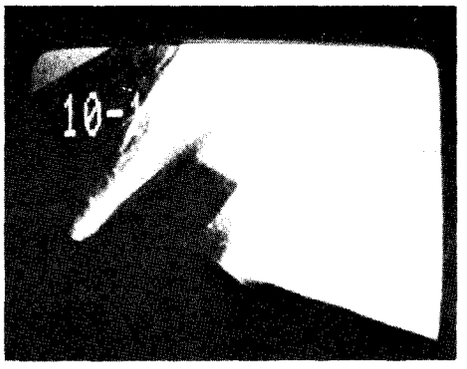

11:48:21.38
ROLL ANGLE = +8.8°
PITCH ANGLE = 2.23°
FLAP ANGLE = 21.0°

PORT SEMI SPAN
SPEED = 35.9 KNOTS
SUBMERGENCE = 2.2 Ft

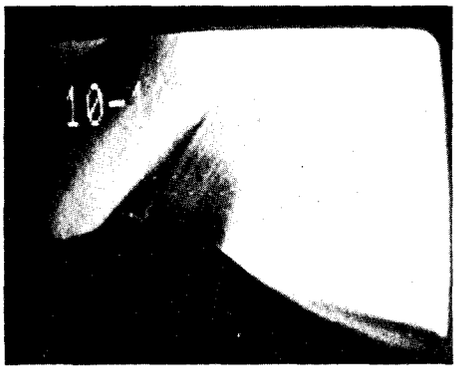

11:48:21.62
ROLL ANGLE = +8.7°
PITCH ANGLE = 1.88°
FLAP ANGLE = 21.0°

PORT SEMI SPAN
SPEED = N/A
SUBMERGENCE = 1.5 Ft

11:48:21.88
ROLL ANGLE = +8.5°
PITCH ANGLE = 1.75°
FLAP ANGLE = 20.8°

PORT SEMI SPAN
SPEED = N/A
SUBMERGENCE = 1.6 Ft

Figure 36 - Forward Foil Flow--36-Knot Broach With 90° Starboard Helm

11:48:22.17
ROLL ANGLE = + 7.5°
PITCH ANGLE = 1.65°
FLAP ANGLE = 21.0°

PORT SEMI SPAN
SPEED = N/A
SUBMERGENCE = 1.6 FT

11:48:23.04
ROLL ANGLE = +6.5°
PITCH ANGLE = 2.41°
FLAP ANGLE = 16.6°

PORT SEMI SPAN
SPEED = N/A
SUBMERGENCE = 2.7 FT

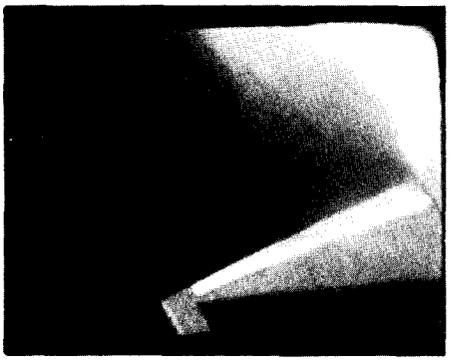

11:48:19.72
ROLL ANGLE = 9.1°
PITCH ANGLE = 1.63°
FLAP ANGLE = 4.7°

STARBOARD SEMI SPAN
SPEED = 35.9 KNOTS
SUBMERGENCE = 5.0 FT

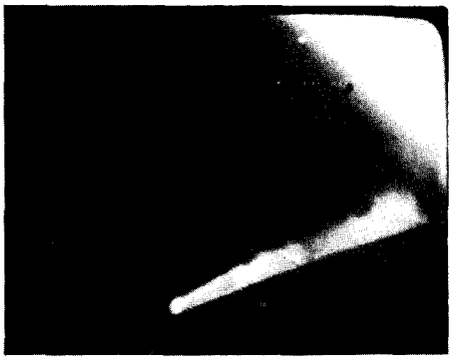

11:48:20.55
ROLL ANGLE = 9.1°
PITCH ANGLE = 2.41°
FLAP ANGLE = 17.2°

STARBOARD SEMI SPAN
SPEED = 35.9 KNOTS
SUBMERGENCE = 3.9 FT

11:48:20.97
ROLL ANGLE = 9.0°
PITCH ANGLE = 2.65°
FLAP ANGLE = 17.5°

STARBOARD SEMI SPAN
SPEED = 35.9 KNOTS
SUBMERGENCE = 2.8 FT

11:48:21.30
ROLL ANGLE = 8.8°
PITCH ANGLE = 2.36°
FLAP ANGLE = 20.5°

STARBOARD SEMI SPAN
SPEED = 35.9 KNOTS
SUBMERGENCE = 1.4 FT

Figure 36 (Continued)

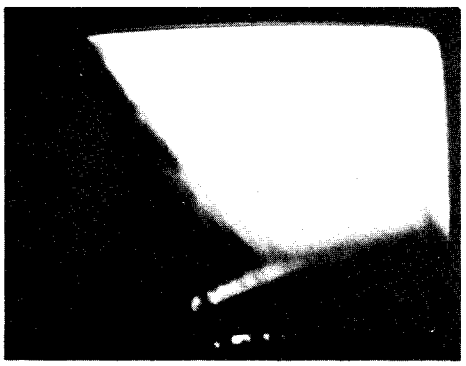

11:48:21.64
ROLL ANGLE = 8.7°
PITCH ANGLE = 1.99°
FLAP ANGLE = 20.6°

STARBOARD SEMI SPAN
SPEED = N/A
SUBMERGENCE = 1.3 FT

11:48:21.85
ROLL ANGLE = 8.5°
PITCH ANGLE = 1.75°
FLAP ANGLE = 20.6°

STARBOARD SEMI SPAN
SPEED = N/A
SUBMERGENCE = 1.6 FT

11:48:21.97
ROLL ANGLE = 7.9°
PITCH ANGLE = 1.63°
FLAP ANGLE = 20.6

STARBOARD SEMI SPAN
SPEED = N/A
SUBMERGENCE = 1.9 FT

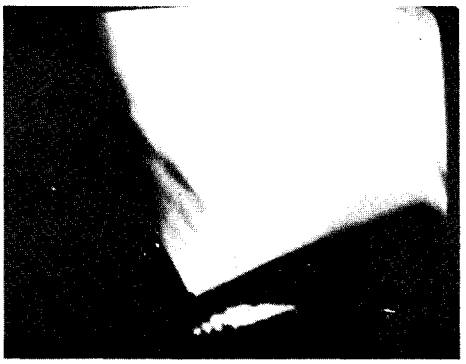

11:48:22.14
ROLL ANGLE = 7.5°
PITCH ANGLE = 1.57°
FLAP ANGLE = 20.6°

STARBOARD SEMI SPAN
SPEED = N/A
SUBMERGENCE = 1.6 FT

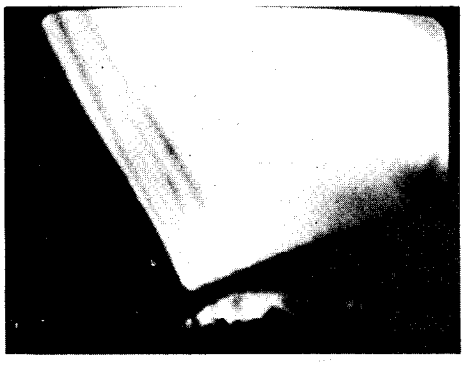

11:48:22.47
ROLL ANGLE = 7.2°
PITCH ANGLE = 1.45°
FLAP ANGLE = 20.6°

STARBOARD SEMI SPAN
SPEED = N/A
SUBMERGENCE = 2.1 FT

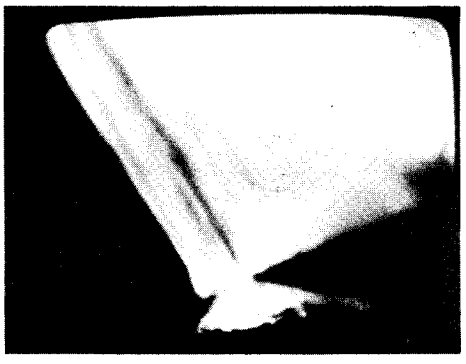

11:48:22.68
ROLL ANGLE = 6.9°
PITCH ANGLE = 1.75°
FLAP ANGLE = 20.6°

STARBOARD SEMI SPAN
SPEED = N/A
SUBMERGENCE = 2.6 FT

Figure 36 (Continued)

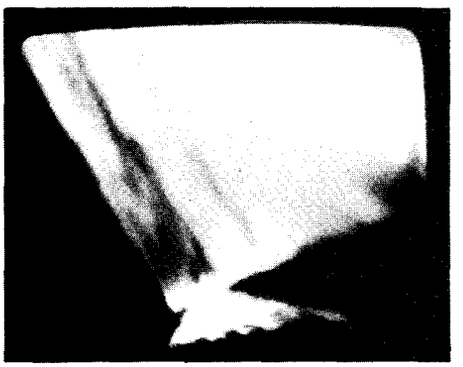

11:48:22.80
ROLL ANGLE = 6.7°
PITCH ANGLE = 2.05°
FLAP ANGLE = 20.6°

STARBOARD SEMI SPAN
SPEED = N/A
SUBMERGENCE = 2.5 FT

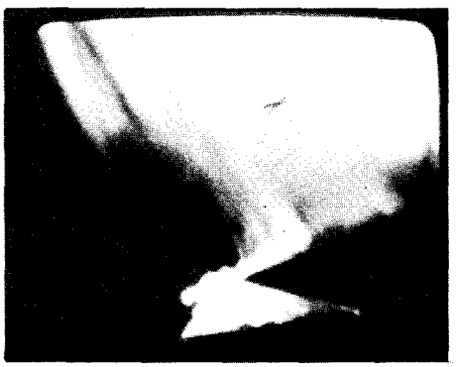

11:48:22.89
ROLL ANGLE = 6.4°
PITCH ANGLE = 2.12°
FLAP ANGLE = 19.4°

STARBOARD SEMI SPAN
SPEED = N/A
SUBMERGENCE = 3.0 FT

11:48:23.01
ROLL ANGLE = 6.3°
PITCH ANGLE = 2.36°
FLAP ANGLE = 17.5°

STARBOARD SEMI SPAN
SPEED = N/A
SUBMERGENCE = 2.7 FT

11:48:23.14
ROLL ANGLE = 6.1°
PITCH ANGLE = 2.77°
FLAP ANGLE = 15.4°

STARBOARD SEMI SPAN
SPEED = N/A
SUBMERGENCE = 2.7 FT

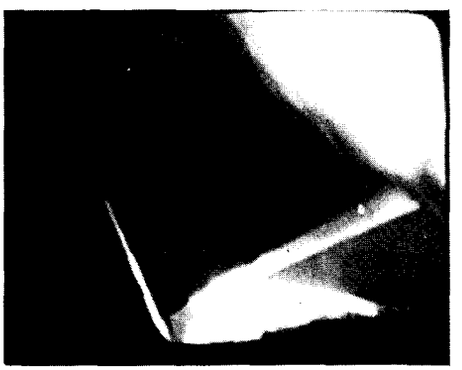

11:48:23.26
ROLL ANGLE = 5.9°
PITCH ANGLE = 2.95°
FLAP ANGLE = 13.9°

STARBOARD SEMI SPAN
SPEED = N/A
SUBMERGENCE = 2.7 FT

11:48:23.43
ROLL ANGLE = 5.3°
PITCH ANGLE = 2.95°
FLAP ANGLE = 13.8°

STARBOARD SEMI SPAN
SPEED = N/A
SUBMERGENCE = 3.0 FT

Figure 36 (Continued)

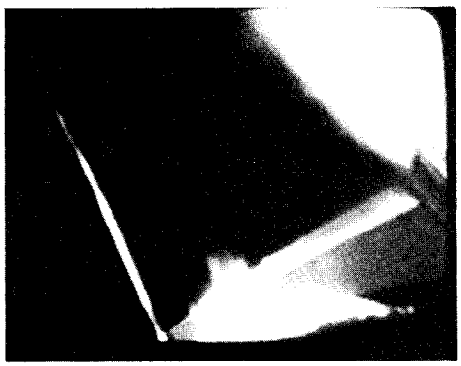

11:48:23.60
ROLL ANGLE = 4.9°
PITCH ANGLE = 3.20°
FLAP ANGLE = 13.8°

STARBOARD SEMI SPAN
SPEED = N/A
SUBMERGENCE = 3.0 FT

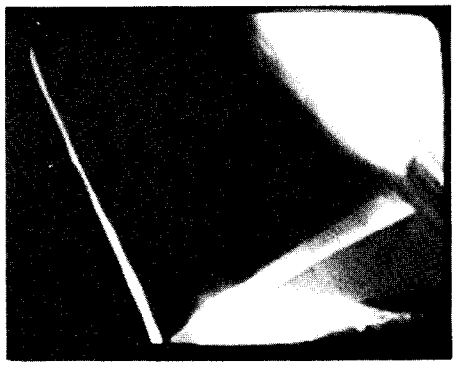

11:48:23.76
ROLL ANGLE = 4.3°
PITCH ANGLE = 3.65°
FLAP ANGLE = 13.6°

STARBOARD SEMI SPAN
SPEED = N/A
SUBMERGENCE = 3.0 FT

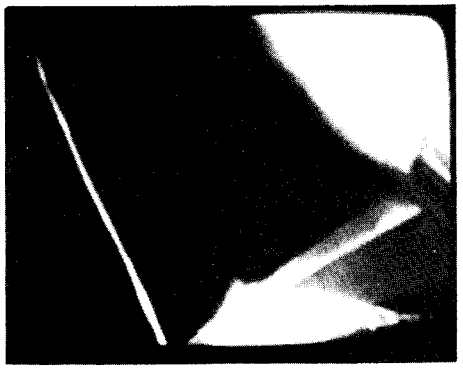

11:48:23.93
ROLL ANGLE = 3.6°
PITCH ANGLE = 3.71°
FLAP ANGLE = 13.3°

STARBOARD SEMI SPAN
SPEED = N/A
SUBMERGENCE = 2.9 FT

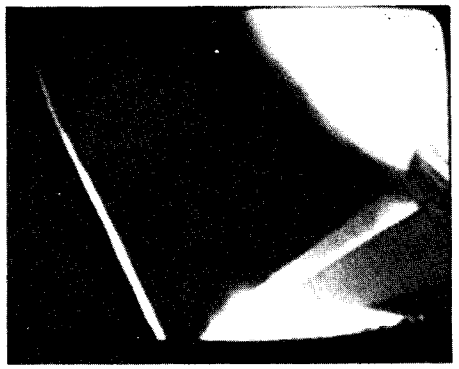

11:48:24.10
ROLL ANGLE = 2.3°
PITCH ANGLE = 3.90°
FLAP ANGLE = 12.5°

STARBOARD SEMI SPAN
SPEED = N/A
SUBMERGENCE = 3.0 FT

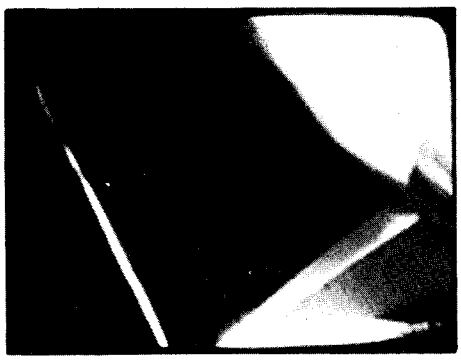

11:48:24.26
ROLL ANGLE = 0
PITCH ANGLE = 4.03°
FLAP ANGLE = 12.2°

STARBOARD SEMI SPAN
SPEED = N/A
SUBMERGENCE = 2.6 FT

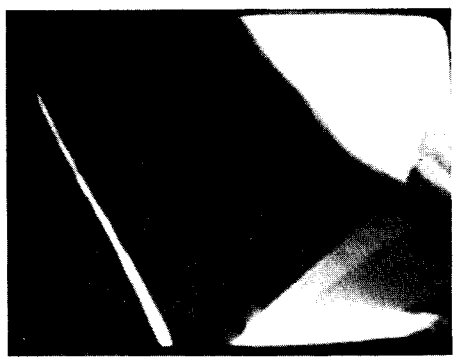

11:48:24.43
ROLL ANGLE = -1.3°
PITCH ANGLE = 4.05°
FLAP ANGLE = 11.1°

STARBOARD SEMI SPAN
SPEED = N/A
SUBMERGENCE = 2.6 FT

Figure 36 (Continued)

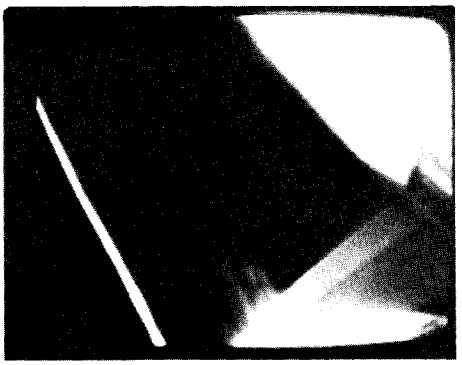

11:48:24.60
ROLL ANGLE =-3.46°
PITCH ANGLE = 3.97°
FLAP ANGLE = 4.4°

STARBOARD SEMI SPAN
SPEED = N/A
SUBMERGENCE = 2.8 FT

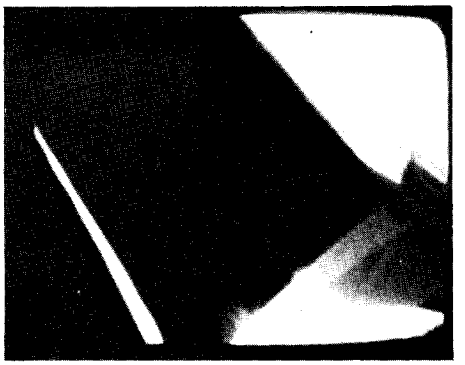

11:48:24.76
ROLL ANGLE =-5.3°
PITCH ANGLE = 3.84°
FLAP ANGLE = 0.8°

STARBOARD SEMI SPAN
SPEED = N/A
SUBMERGENCE = 3.0 FT

11:48:24.93
ROLL ANGLE =-6.2°
PITCH ANGLE = 3.77°
FLAP ANGLE = 1.4°

STARBOARD SEMI SPAN
SPEED = N/A
SUBMERGENCE = 3.5 FT

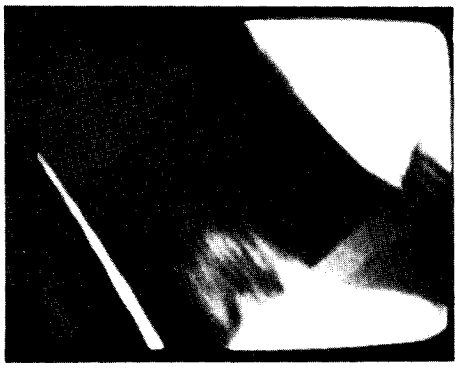

11:48:25.10
ROLL ANGLE =-8.1°
PITCH ANGLE = 3.72°
FLAP ANGLE = 3.3°

STARBOARD SEMI SPAN
SPEED = N/A
SUBMERGENCE = 4.1 FT

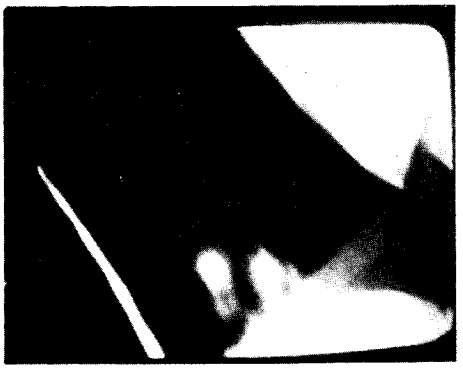

11:48:25.18
ROLL ANGLE =-9.3°
PITCH ANGLE = 3.40°
FLAP ANGLE = 3.6°

STARBOARD SEMI SPAN
SPEED = N/A
SUBMERGENCE = 4.8 FT

11:48:25.26
ROLL ANGLE =-10.2°
PITCH ANGLE = 3.46°
FLAP ANGLE = 2.65°

STARBOARD SEMI SPAN
SPEED = N/A
SUBMERGENCE = 5.0 FT.

Figure 36 (Continued)

11:48:25.35
ROLL ANGLE =-10.8°
PITCH ANGLE = 3.52°
FLAP ANGLE = 2.2°

STARBOARD SEMI SPAN
SPEED = N/A
SUBMERGENCE = 5.6 FT

11:48:25.43
ROLL ANGLE =-11.4°
PITCH ANGLE = 3.52°
FLAP ANGLE = 2.1°

STARBOARD SEMI SPAN
SPEED = N/A
SUBMERGENCE = 5.8 FT

11:48:25.55
ROLL ANGLE =-12.5°
PITCH ANGLE = 3.52°
FLAP ANGLE = 2.08°

STARBOARD SEMI SPAN
SPEED = N/A
SUBMERGENCE = 6.5 FT

11:48:25.68
ROLL ANGLE =-13.8°
PITCH ANGLE = 3.58°
FLAP ANGLE = 1.94°

STARBOARD SEMI SPAN
SPEED = N/A
SUBMERGENCE = 7.0 FT

11:48:25.80
ROLL ANGLE =-15.0°
PITCH ANGLE = 3.77°
FLAP ANGLE = 2.2°

STARBOARD SEMI SPAN
SPEED = N/A
SUBMERGENCE = 7.8 FT

11:48:25.93
ROLL ANGLE =-15.4°
PITCH ANGLE = 3.84°
FLAP ANGLE = 2.1°

STARBOARD SEMI SPAN
SPEED = N/A
SUBMERGENCE = 8.1 FT

Figure 36 (Continued)

11:48:26.05
ROLL ANGLE =-16.7°
PITCH ANGLE = 3.96°
FLAP ANGLE = 1.1°

STARBOARD SEMI SPAN
SPEED = N/A
SUBMERGENCE = 8.5 FT

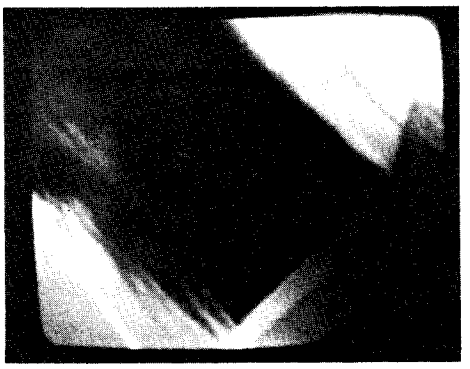

11:48:26.18
ROLL ANGLE =-17.2°
PITCH ANGLE = 4.02°
FLAP ANGLE =-2.2°

STARBOARD SEMI SPAN
SPEED = N/A
SUBMERGENCE = 9.0 FT

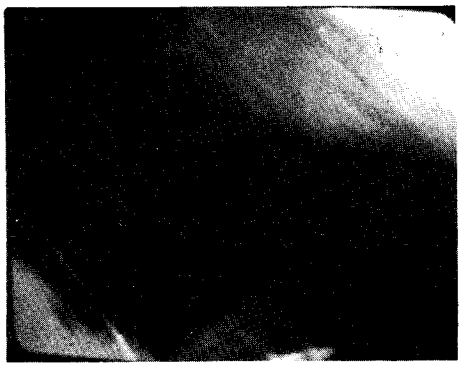

11:48:28.05
ROLL ANGLE =-9.0°
PITCH ANGLE = 4.78°
FLAP ANGLE = 13.2°

STARBOARD SEMI SPAN
SPEED = N/A
SUBMERGENCE = 9.9 FT

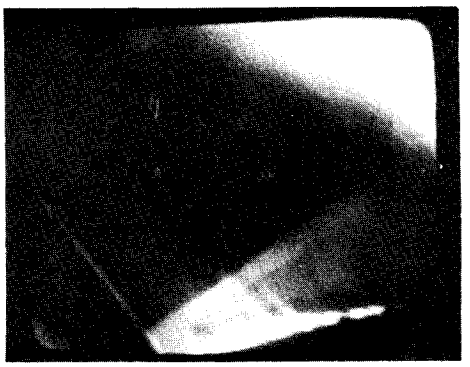

11:48:28.30
ROLL ANGLE =-8.1°
PITCH ANGLE = 4.72°
FLAP ANGLE = 13.3°

STARBOARD SEMI SPAN
SPEED = N/A
SUBMERGENCE = 9.7 FT

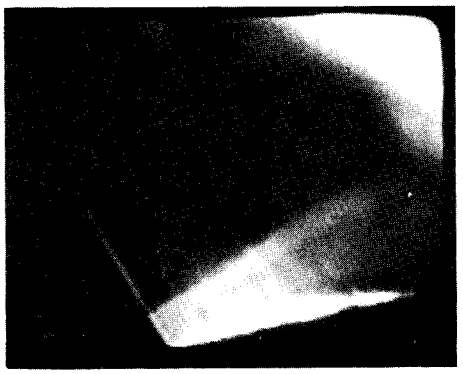

11:48:29.72
ROLL ANGLE =-2.7°
PITCH ANGLE = 4.47°
FLAP ANGLE = 14.3°

STARBOARD SEMI SPAN
SPEED = N/A
SUBMERGENCE = 8.7 FT

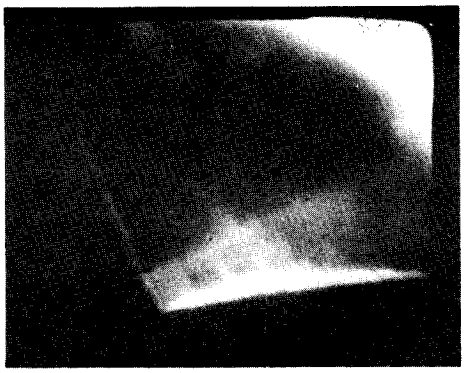

11:48:30.35
ROLL ANGLE =-1.3°
PITCH ANGLE = 4.24°
FLAP ANGLE = 18.3°

STARBOARD SEMI SPAN
SPEED = N/A
SUBMERGENCE = 8.8 FT

Figure 36 (Continued)

11:48:31.22
ROLL ANGLE = 2.96°
PITCH ANGLE = 3.76°
FLAP ANGLE = 20.8°

STARBOARD SEMI SPAN
SPEED = N/A
SUBMERGENCE = 9.6 FT

Figure 36 (Continued)

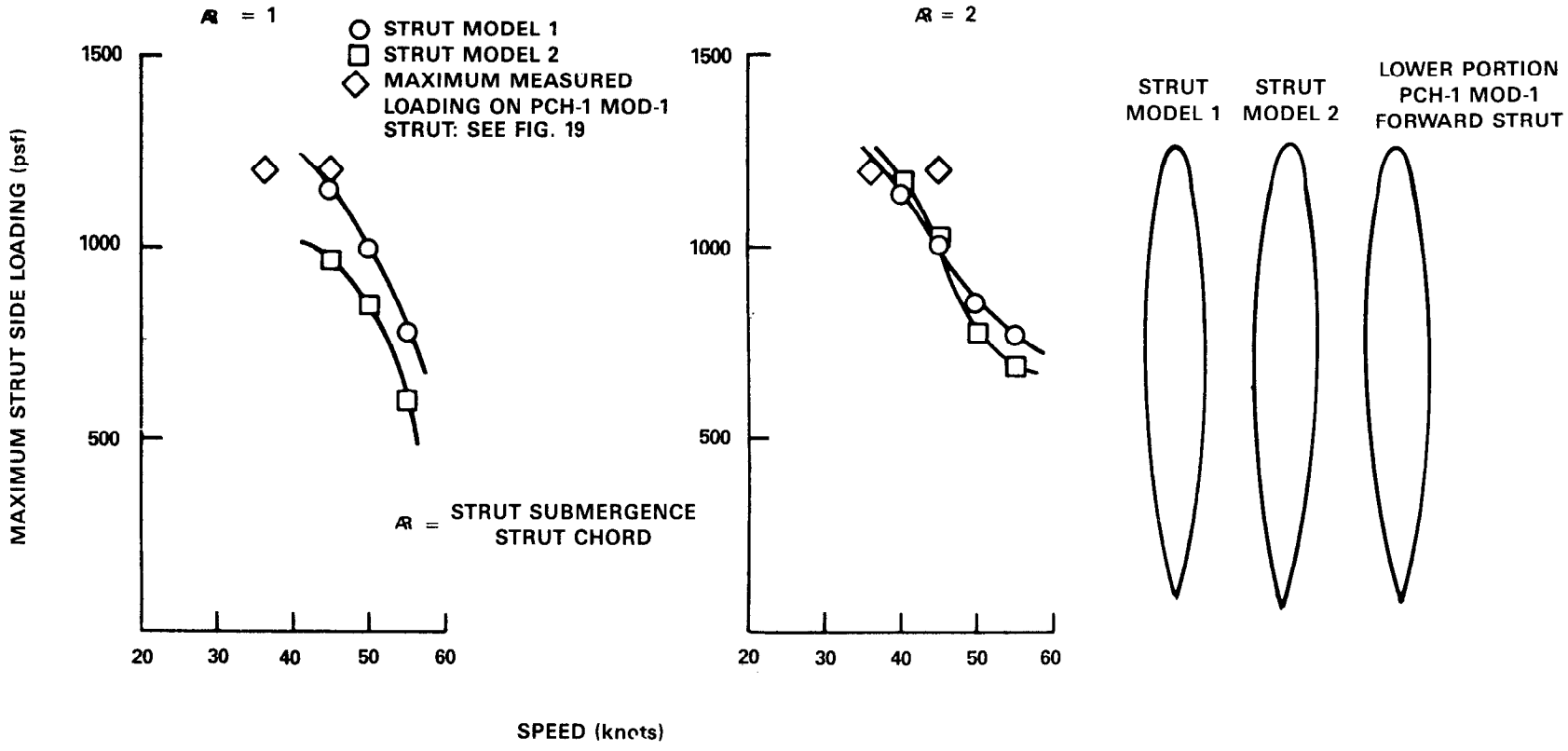

Figure 37 - Correlation of Maximum Model and Full-Scale Strut Hydrodynamic Loadings. (Model Data from Rothblum et al., NSRDC Report 3023, July 1969)

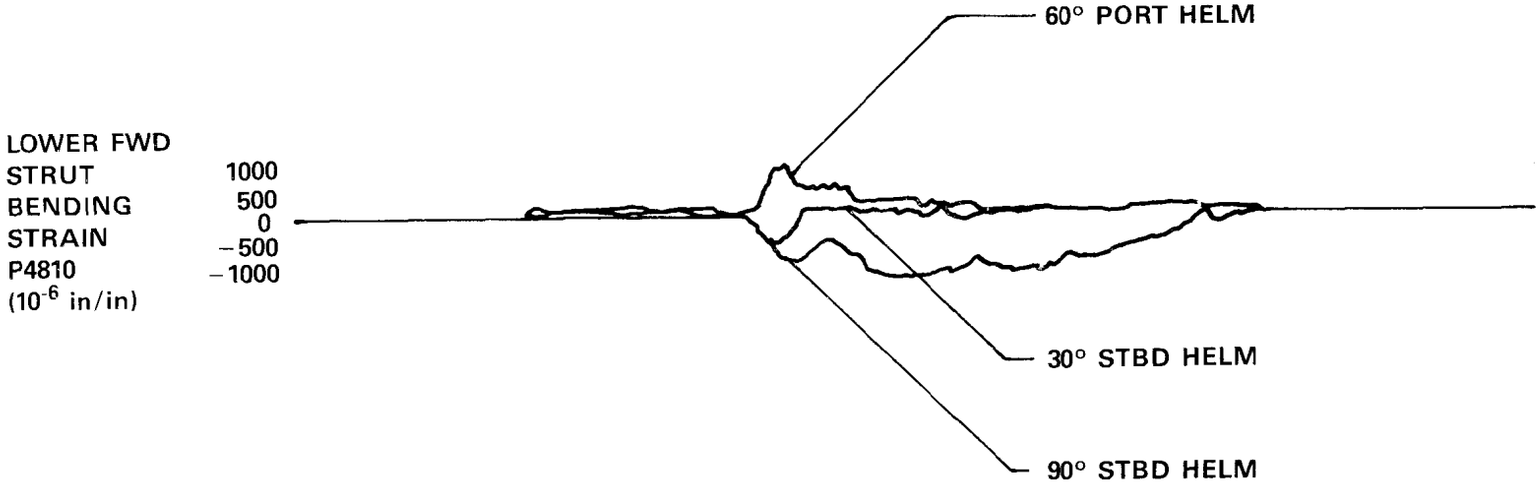

Figure 38 - Comparison of Lower Forward Strut Bending Strains for Broaches in Turns

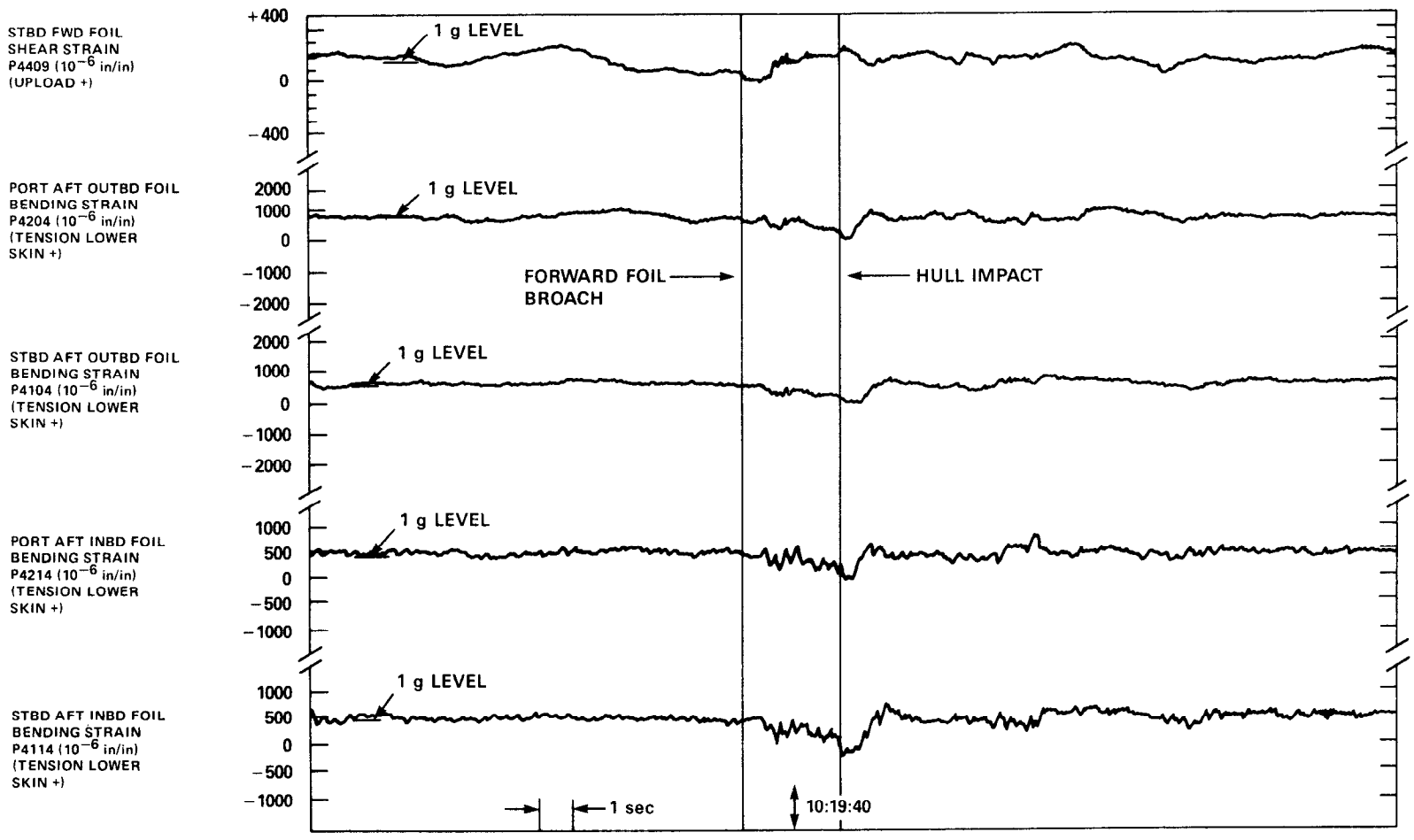

Figure 39 - Foil System Bending Strains During a Rough Water Broach: 6 April 1975

APPENDIX A

AUTOMATIC CONTROL SYSTEMS CHARACTERISTICS

A schematic of the Automatic Control System (ACS) is presented in Figure A.1, and associated control gains are in Table A.1. The foil system loadings experienced during these trials, especially the debris avoidance maneuvers, are influenced by the design characteristics of the ACS. In particular it can be seen that helm commands drive the aft control surfaces differentially to produce roll, and that the forward strut is positioned by roll angle and yaw rate sensor outputs only. The output of the helm position sensor that drives the aft flaps differentially is attenuated at frequencies above 1 rad/s, which is well under the maximum helm displacement rate of $\pi/0.3 = 10.5$ rad/s employed in the trials. Despite the attenuation, forward strut hydrodynamic loadings approaching maximum attainable values were experienced during debris avoidance maneuvers.

In order to perform forward foil broaches with the ship in an initial bow-up attitude (for safety reasons), a "Test Box" was temporarily inserted into the pitch angle circuit. The test box is not shown in Figure A.1.

TABLE A.1 - AUTOMATIC CONTROL SYSTEM GAINS

Channel	Gain Symbol	Gain Value
Acceleration	K_{aF}	1.5 deg/ft/s^2
	K_{aP}	1.5 deg/ft/s^2
	K_{aS}	1.5 deg/ft/s^2
Height	K_{HF}	3.5 deg/ft
Pitch	$K_{\theta F}$	- 1.3 deg/deg at ω = 0 -13.0 deg/deg at ω = 0.75 rad/s
	$K_{\theta F2}$	5.0 deg/deg
	$K_{\theta P}$	1.3 deg/deg at ω = 0 13.0 deg/deg at ω = 0.75 rad/s
	$K_{\theta S}$	1.3 deg/deg at ω = 0 13.0 deg/deg at ω = 0.75 rad/s
Roll	$K_{\phi S}$	4.5 deg/deg
	$K_{\phi P}$	- 4.5 deg/deg
	$K_{\phi R}$	1.45 deg/deg
	$K_{\phi F}$	0.015 ft/s^2/deg^2
Turn	K_{hP}	0.40 deg/deg
	K_{hS}	- 0.40 deg/deg
Yaw Rate	K_{RR}	- 2.0 deg/deg/s

APPENDIX A

AUTOMATIC CONTROL SYSTEMS CHARACTERISTICS

A schematic of the Automatic Control System (ACS) is presented in Figure A.1, and associated control gains are in Table A.1. The foil system loadings experienced during these trials, especially the debris avoidance maneuvers, are influenced by the design characteristics of the ACS. In particular it can be seen that helm commands drive the aft control surfaces differentially to produce roll, and that the forward strut is positioned by roll angle and yaw rate sensor outputs only. The output of the helm position sensor that drives the aft flaps differentially is attenuated at frequencies above 1 rad/s, which is well under the maximum helm displacement rate of $\pi/0.3 = 10.5$ rad/s employed in the trials. Despite the attenuation, forward strut hydrodynamic loadings approaching maximum attainable values were experienced during debris avoidance maneuvers.

In order to perform forward foil broaches with the ship in an initial bow-up attitude (for safety reasons), a "Test Box" was temporarily inserted into the pitch angle circuit. The test box is not shown in Figure A.1.

TABLE A.1 - AUTOMATIC CONTROL SYSTEM GAINS

Channel	Gain Symbol	Gain Value
Acceleration	K_{aF}	1.5 deg/ft/s^2
	K_{aP}	1.5 deg/ft/s^2
	K_{aS}	1.5 deg/ft/s^2
Height	K_{HF}	3.5 deg/ft
Pitch	K_{0F}	- 1.3 deg/deg at ω = 0 -13.0 deg/deg at ω = 0.75 rad/s
	$K_{\theta F2}$	5.0 deg/deg
	$K_{\theta P}$	1.3 deg/deg at ω = 0 13.0 deg/deg at ω = 0.75 rad/s
	$K_{\theta S}$	1.3 deg/deg at ω = 0 13.0 deg/deg at ω = 0.75 rad/s
Roll	$K_{\phi S}$	4.5 deg/deg
	$K_{\phi P}$	- 4.5 deg/deg
	$K_{\phi R}$	1.45 deg/deg
	$K_{\phi F}$	0.015 ft/s^2/deg^2
Turn	K_{hP}	0.40 deg/deg
	K_{hS}	- 0.40 deg/deg
Yaw Rate	K_{RR}	- 2.0 deg/deg/s

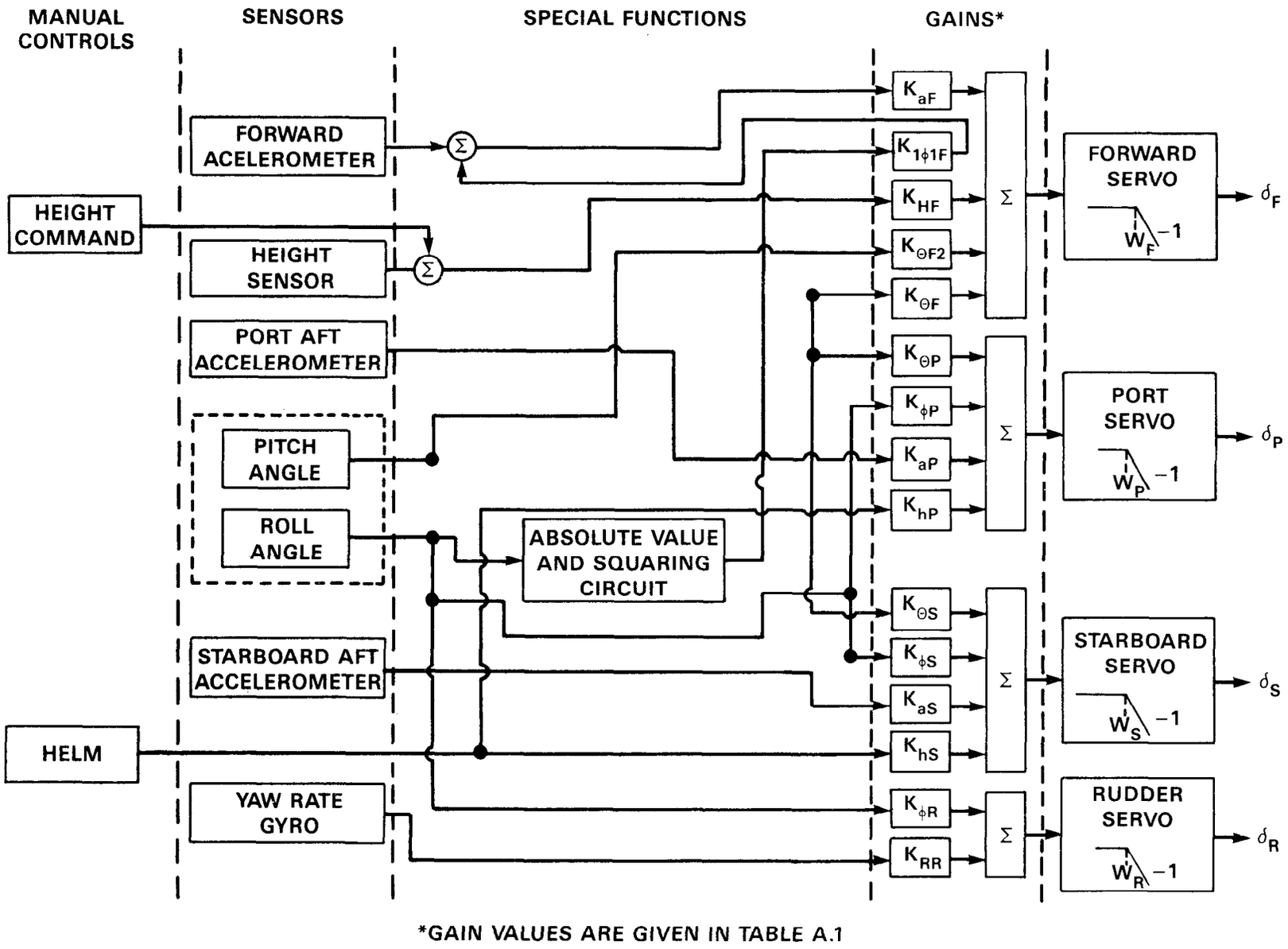

Figure A.1 - Block Diagram of HIGH POINT PCH 1 MOD 1 Automatic Control System
(Symbols used are defined in Table A.1)

APPENDIX B

CALIBRATION OF LATERAL SHEAR LOAD ON THE FORWARD STRUT

The estimates of forward strut lateral load associated with Figure 18 were obtained using a load calibration equation different from that originally recommended by the PCH 1 MOD 1 contractor.* The revised calibration equations resulted from the subsequent addition of a calibrated strain gage bridge (P4812) to the tiller arm at the top of the strut, which permitted the derivation of a calibration equation that corrected for the effects of strut torsion on the basic lateral shear and bending strain gage bridges (P4801, P4803, and P4804).

The original equation, which was derived by the methods of NACA Report 1178,** is:

$$V = 0.3201(P4801) - 0.0245(P4803) + 0.0092(P4804)$$

where V is in kips (1000 lb units) and the output of the strain gage bridges is in micro-inches per inch. The revised equation is:

$$V = 0.3008(P4801) - 0.0250(P4803) + 0.01196(P4804) - 0.0107(P4812)$$

For a 1000 lb load applied independently at each of the calibration load points shown in Figure B.1, the respective calibrations estimate the known loading to be as follows:

1000 lb Applied at Load Calibration Point	Original Calibration (lb)	Revised Calibration (lb)
(1)	1073	992
(2)	953	1012
(3)	1056	1006
(4)	896	989

For the load calibration points of Figure B.1, the error with the revised calibration equations is less than 2%.

*Boeing letter H-7308-1000-1778, "Contract N00600-75-C-1107 (Phase I) PCH 1 Work and Analysis Plan for Hydrofoil Loads Criteria Support - HIGH POINT (PCH 1) MOD 1, Report No. 4" (17 May 1976).

**NACA Report 1178, "Calibration of Strain Gage Installations in Aircraft Structures for the Measurement of Flight Loads" (1954).

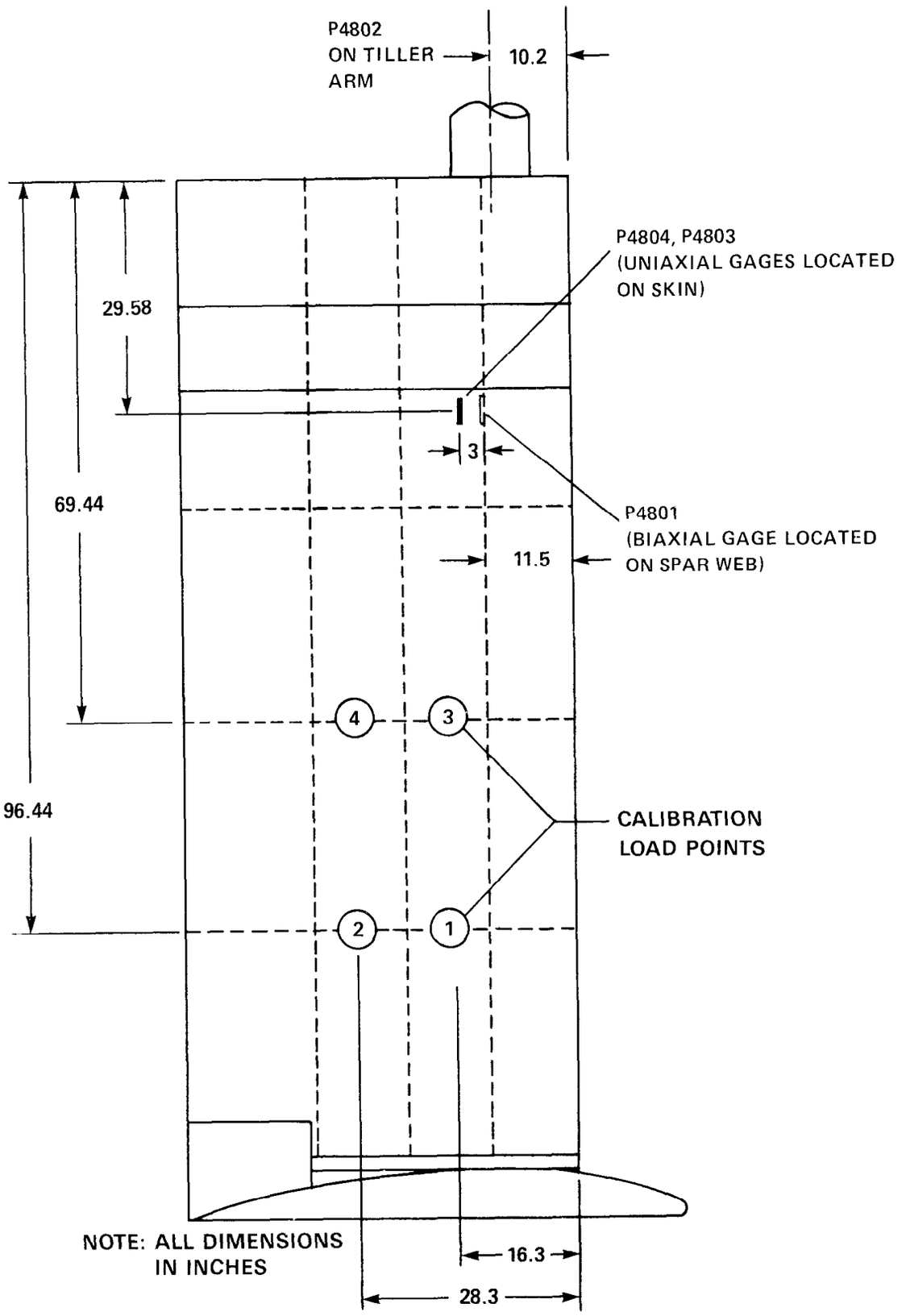

Figure B-1 - Forward Strut Strain Gage and Calibration Load Locations

APPENDIX C

DERIVED LIMIT STRAIN FOR FOIL SYSTEM

Derived limit strains have been used as a measure of the severity of loadings encountered during the calm water trials reported here. The following describes the basis on which individual values were determined as well as the meaning of the term "derived limit strain" as used in this report.

The structural design of PCH 1 MOD 1 defined various extreme loading conditions which were intended to identify potentially critical hydrodynamic loading conditions for the foil system. These component loadings were identified as limit loads and presumably corresponded to values unlikely to be exceeded in service. For structural design purposes limit loads were multiplied by a factor of 1.5 and designated "critical" loads. The foil system structure was required not to yield or collapse under these "critical" loads.

This basis of structural design is at variance with the load criteria currently recommended for U.S. Navy hydrofoil ship structural design. The recommended load criteria define yield loads as limit loads multiplied by a factor of 1.20 and ultimate loads as limit loads multiplied by a factor of 1.50. Under yield loads the structure is required to be free from deformations that will interfere with the normal operation of the ship as well as from any residual deformations following application of yield loads. Under ultimate loads the structure is required not to collapse.

The limit loads employed in the design of PCH 1 MOD 1 were also at variance with the presumption that they represented maximum loadings likely to be encountered in service, since, for strain monitoring purposes in calm and rough water trials, "redline" strains were established by dividing strain levels associated with "critical" loads by a factor of 1.25 rather than 1.50.

These differences were resolved by the rationale outlined in Figure C.1. Since the original "critical" loads and the current yield loads both require that the foil system not yield when they are applied to the structure, and since redline and (current) limit strains would be almost identical if critical loads were assumed to correspond to yield loads this assumption was made as shown in Figure C.1. Strain levels associated with critical loads were then divided by a factor of 1.20 to obtain derived limit strains, which are only slightly larger than the redline strains defined for trials monitoring. Individual values of derived limit strains for the foil system were then determined as summarized in Table C.1.

TABLE C.1 - DETERMINATION OF DERIVED LIMIT STRAINS FOR FOIL SYSTEM STRAIN GAGES

Component/ Location	Strain Gage Bridge	Critical Bending Moment (in-lb)	Critical Shear (lb)	Calibration Strain Response*	Critical Strain** (10^{-6} in/in)	Derived Limit Strain*** (10^{-6} in/in)	Origin of Calibration
Stbd Fwd Foil	P4401	-	123×10^3	2861	352	293	†
Stbd Fwd Foil	P4405	5.9×10^6	-	397	2342	1952	†
Lower Fwd Strut	P4810	6.0×10^6	-	526	3156	2630	††
Upper Fwd Strut	P4803	6.0×10^6	-	228	1368	1140	†
Upper Fwd Strut	P4801	-	62×10^3	4802	298	248	†
Port Fwd Flap Link	P4414	0.33×10^6	-	8970	2960	2467	††
Stbd Fwd Flap Link	P4413	0.33×10^6	-	8970	2960	2467	††
Tiller Arm	P4812	1.203×10^6	-	980	1176	980	††
Port or Stbd Aft Strut	P4601/ P4501	7.4×10^6	-	341	2523	2103	Calculated Based on Section Property
Port Aft Outbd Foil	P4202	6.8×10^6	-	336	2285	1904	†
Port or Stbd Aft Inbd Foil	P4214/ P4114	4.3×10^6	-	1005	4322	3601	Calculated Based on Section Property
Stbd Aft Outbd Foil	P4104	6.8×10^6	-	357	2428	2023	†

*10^{-6} in/in per in-lb or per lb.
**Strain corresponding to critical bending moment or shear.
***Critical strain divided by 1.2.

†Boeing Document No. D311-60001-1, "Strain Gage Calibration of Foils and Forward Strut," 21 Mar 1973.
††Boeing Letter 2-1524-1000-1451, Strain Gage Calibration Procedures and Data, Transmittal of, 25 Mar 1975.

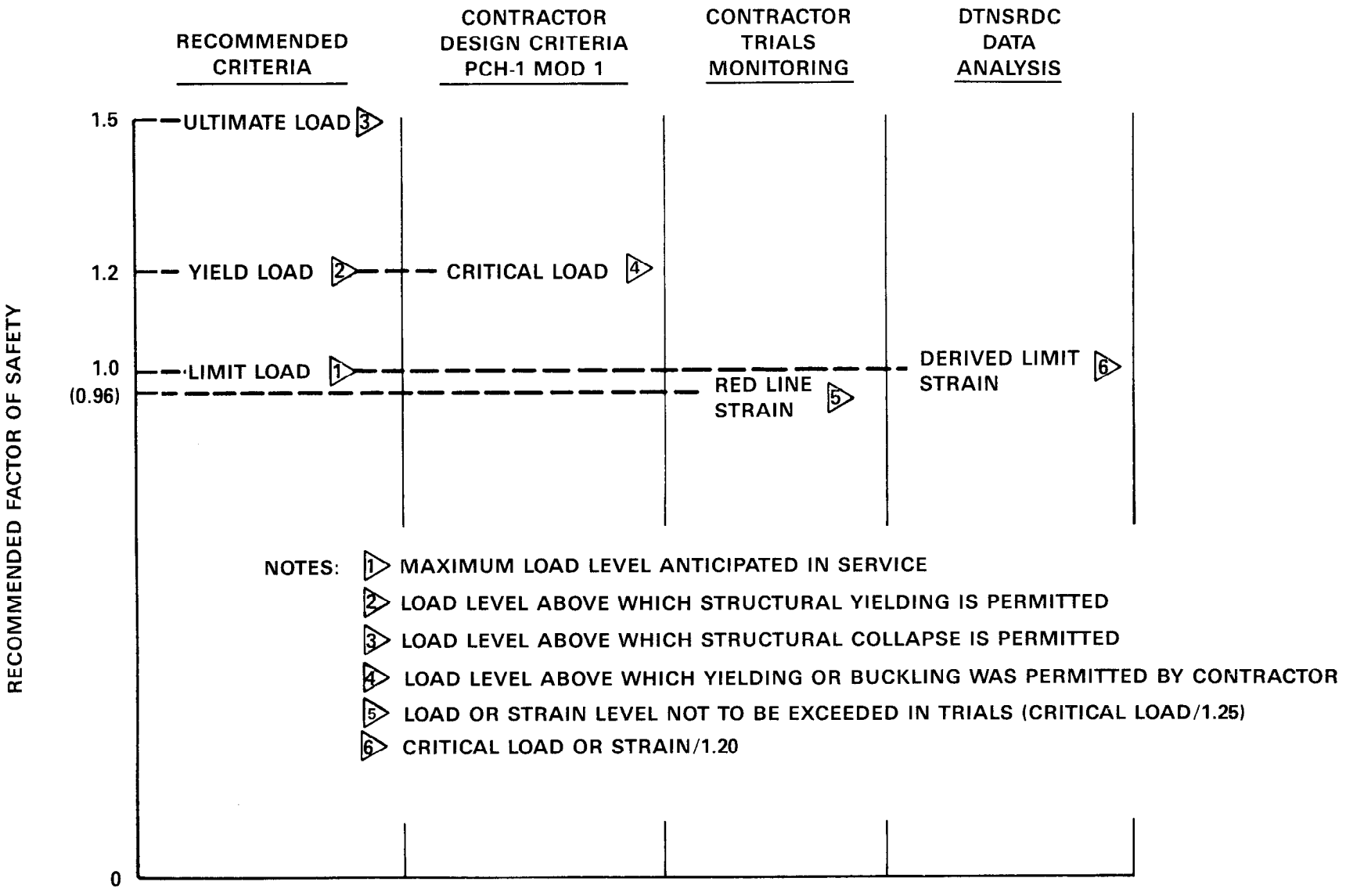

Figure C.1 - Definition of Derived Limit Strain

INITIAL DISTRIBUTION

Copies	
1	NRL
	1 5820/Johnson
5	NAVSEA
	1 05R12/Schuler
	1 05DC5/Jones
	1 50151/Bebar
	1 55W33/Sandberg
	1 55Y13/Gallagher
1	USNA/Library
1	NOSC/Library
12	DTIC
1	NASA Langley Res. Center/Library
1	UCAL Name
	1 J. Paulling
1	U. Iowa OJR
	1 Landweber
1	MIT Ocean Ener.
	1 Ogilvie
1	U. Michigan Name
	1 Couch
1	Penn. State U.
	1 Parkin
1	SWRI
	1 Abramson
1	SIT Davidson Lab.
	1 Savitsky
7	Boeing Marine Systems
	1 R. Dixon
	1 R. Merritt
	1 D. Olling
	1 A. Rand
	1 D. Round
	1 D. Stark
	1 F. Watson

Copies	
2	Tracor/Hydronautics
	1 Tulin
	1 Barr

CENTER DISTRIBUTION

Copies	Code	Name
1	012.3	D. Moram
1	12	W. Dietz
1	123	T. Sherman
3	1233	J. Meyer
1	1204	Data Bank
1	1233	P. Yarnall
1	1234	HYSTU
1	1234	D. Rieg
1	15	W. Morgan
1	1503	R. Rothblum
1	1522	M. Wilson
1	154.1	B. Yim
1	1542	Y. Shen
1	1543	G. Santore
1	1543	P. Besh
1	156	D. Cieslowski
1	1562	M. Davis
1	1563	J. Russ
1	16	H. Chaplin
1	17	W. Murray
1	173	A. Stavovy
1	1730.6	J. Beach
10	1730.6	W. Buckley
10	5211	Reports Distribution
1	522.1	TIC (C)
1	522.2	TIC (A)

DTNSRDC ISSUES THREE TYPES OF REPORTS

1. DTNSRDC REPORTS, A FORMAL SERIES, CONTAIN INFORMATION OF PERMANENT TECHNICAL VALUE. THEY CARRY A CONSECUTIVE NUMERICAL IDENTIFICATION REGARDLESS OF THEIR CLASSIFICATION OR THE ORIGINATING DEPARTMENT.

2. DEPARTMENTAL REPORTS, A SEMIFORMAL SERIES, CONTAIN INFORMATION OF A PRELIMINARY, TEMPORARY, OR PROPRIETARY NATURE OR OF LIMITED INTEREST OR SIGNIFICANCE. THEY CARRY A DEPARTMENTAL ALPHANUMERICAL IDENTIFICATION.

3. TECHNICAL MEMORANDA, AN INFORMAL SERIES, CONTAIN TECHNICAL DOCUMENTATION OF LIMITED USE AND INTEREST. THEY ARE PRIMARILY WORKING PAPERS INTENDED FOR INTERNAL USE. THEY CARRY AN IDENTIFYING NUMBER WHICH INDICATES THEIR TYPE AND THE NUMERICAL CODE OF THE ORIGINATING DEPARTMENT. ANY DISTRIBUTION OUTSIDE DTNSRDC MUST BE APPROVED BY THE HEAD OF THE ORIGINATING DEPARTMENT ON A CASE-BY-CASE BASIS.